SYNTHESIS AND IN VITRO STUDIES OF SELENOPHENE CONTAINING BODIPY DERIVATIVES AS MITOCHONDRIA TARGETED PHOTODYNAMIC THERAPY AGENTS

A THESIS SUBMITTED TO
THE GRADUATE SCHOOL OF NATURAL AND APPLIED SCIENCES
OF
MIDDLE EAST TECHNICAL UNIVERSITY

BY

OSMAN KARAMAN

IN PARTIAL FULFILLMENT OF THE REQUIREMENTS
FOR
THE DEGREE OF MASTER OF SCIENCE
IN
CHEMISTRY

JANUARY 2019

Approval of the thesis:

SYNTHESIS AND IN VITRO STUDIES OF SELENOPHENE CONTAINING BODIPY DERIVATIVES AS MITOCHONDRIA TARGETED PHOTODYNAMIC THERAPY AGENTS

submitted by **OSMAN KARAMAN** in partial fulfillment of the requirements for the degree of **Master of Science in Chemistry Department, Middle East Technical University** by,

Prof. Dr. Halil Kalıpçılar
Dean, Graduate School of **Natural and Applied Sciences** _____

Prof. Dr. Cihangir Tanyeli
Head of Department, **Chemistry** _____

Assoc. Prof. Dr. Görkem Günbaş
Supervisor, **Chemistry, METU** _____

Examining Committee Members:

Prof. Dr. Cihangir Tanyeli
Chemistry, METU _____

Assoc. Prof. Dr. Görkem Günbaş
Chemistry, METU _____

Assist. Prof. Dr. Özgül Persil Çetinkol
Chemistry, METU _____

Assist. Prof. Dr. Salih Özçubukçu
Chemistry, METU _____

Assist. Prof. Dr. Safacan Kölemen
Chemistry, Koç University _____

Date: 24.01.2019

I hereby declare that all information in this document has been obtained and presented in accordance with academic rules and ethical conduct. I also declare that, as required by these rules and conduct, I have fully cited and referenced all material and results that are not original to this work.

Name, Surname: Osman Karaman

Signature:

ABSTRACT

SYNTHESIS AND IN VITRO STUDIES OF SELENOPHENE CONTAINING BODIPY DERIVATIVES AS MITOCHONDRIA TARGETED PHOTODYNAMIC THERAPY AGENTS

Karaman, Osman
Master of Science, Chemistry
Supervisor: Assoc. Prof. Dr. Görkem Günbaş

January 2019, 123 pages

Photodynamic therapy (PDT) is an effective and clinically approved modality for various cancer types. It started to attract attention during the last decade, since it is minimally invasive and has fewer side effects compared to current treatment methods. Although several photodynamic therapy agents got approval for the treatment of various malignant diseases, their influence depth is quite shallow due to the lack of tissue penetration of the light that required to active these agents. In addition, their high photocytotoxicity, solubility-based distribution problems and lack of selectivity of tumor cells lead researchers to design and synthesize new generation photosensitizers to overcome these issues. BODIPY (4, 4-difluoro-4-bora-3a, 4a-diaza-s-indacene) derivatives has emerged as an attractive core owing to their remarkable properties such as high singlet oxygen quantum yields when modified with heavy atoms, ease of functionalization, tunable photophysical characteristics, perfect photostability and rapid cellular uptake. However, in order to show drastic PDT effect, fluorescence quenching should be achieved and the absorption maxima must be carried into therapeutic window where light can penetrate to body in appreciable amounts. Furthermore, subcellular localization, hydrophilicity and many other factors are effective on PDT mechanism. In this study, two red-absorbing, water-soluble and

mitochondria-targeted photosensitizers bearing either selenophene (BOD-Se) or 2-iodoselenophene (BOD-Se-I) units on 2,6-positions of BODIPY core were designed and synthesized. BOD-Br was synthesized as a control to compare its performance to selenium containing derivatives (BOD-Se, BOD-Se-I). Due to low fluorescence quantum efficiencies of BOD-Br, BOD-Se, BOD-Se-I, no heavy atom containing derivative BOD-H was synthesized in order to perform localization studies. Trap experiments proved that selenium containing derivatives have a higher singlet oxygen generation than the bromo analogue in aqueous media. Also, the in vitro PDT effect of BOD-Se-I was tested in different cell cultures. Results revealed that BOD-Se-I successfully kills tumor cells by apoptotic cell death mechanism and leaves healthy cells mostly unaffected. Furthermore, impact of BOD-Se-I on tumor cells was tested at hypoxic conditions and cell death was observed. This marks the first mitochondria targeted BODIPY-based photosensitizer, which can function under hypoxic conditions. In addition to target molecules, 2-ethynylselenophene substituted derivative was also synthesized to further push the absorption in the NIR region and its absorption maxima was compared with former target photosensitizers.

Keywords: Photodynamic Therapy, Hypoxia, Singlet Oxygen, BODIPY, Mitochondria Targeting

ÖZ

SELENOFEN İÇEREN BODIPY TÜREVLERİNİN MİTOKONDRİ HEDEFLİ FOTODİNAMİK TERAPİ AJANI OLARAK SENTEZİ VE HÜCRE DIŞI ÇALIŞMALARI

Karaman, Osman
Yüksek Lisans, Kimya
Tez Danışmanı: Doç. Dr. Görkem Günbaş

Ocak 2019, 123 sayfa

Fotodinamik terapi (PDT), çeşitli kanser türleri için etkili ve klinik olarak onaylanmış bir yöntemdir. Minimal invaziv oluşu ve mevcut tedavi yöntemlerine göre daha az yan etkisi olması son on yılda dikkat çekmesini sağlamıştır. Her ne kadar çeşitli fotodinamik terapi ajanları, çeşitli kötü huylu tümörlerin tedavisi için onay almış olsa da, ışığın bu ajanları aktifleştirmek için yeteri kadar dokuya penetre edememisinden dolayı vücuda nüfuzu oldukça sığdır. Buna ek olarak, yüksek fotositotoksisite, çözünürlüğe bağlı dağılım problemleri ve tümör hücrelerine seçicilik eksikliği, araştırmacıları bu sorunların üstesinden gelmek için yeni nesil ışığa duyarlılaştırıcıları tasarlamasına ve sentezlemesine yol açtı. Ağır atomlarla modifiye edilmiş BODIPY (4, 4-difloro-4-bora-3a, 4a-diaza-s-indacene) türevleri, yüksek singlet oksijen kuantum verimi, işlevselliği kolaylaştırıcılığı, ayarlanabilir fotofiziksel özellikleri, yüksek fotostabilite ve hızlı hücreye alımı gibi dikkat çekici avantajlar sağlaması nedeniyle cazip bir ışığa duyarlılaştırıcı yapı olarak ortaya çıkmıştır. BODIPY yapısının yüksek PDT etkisi göstermesi için floresan söndürmeye ulaşılmalı ve emilim maksiması ışığın vücuda yeterli miktarda penetre edebildiği terapötik pencereye taşınmalıdır. Ayrıca, hücre içi lokalizasyon, hidrofiliklik ve birçok faktör PDT mekanizması üzerinde etkisi vardır. Bu çalışmada, BODIPY çekirdeğinin 2,6-

pozisyonları üzerinde selenofen (BOD-Se) veya 2-iyodoselenofen (BOD-Se-I) birimleri taşıyan kırmızı ışık emici, suda çözünür ve mitokondri hedefli ışığa duyarlılaştırıcılar tasarlandı ve sentezlendi. BOD-Br, performansını selenyum içeren türevlerle (BOD-Se, BOD-Se-I) karşılaştırmak için sentezlendi. BOD-Br, BOD-Se, BOD-Se-I'nin düşük floresans kuantum verimlerinin olması sebebiyle, ağır atom içermeyen BOD-H türevi sentezlendi ve lokalizasyon çalışmalarında kullanıldı. Tuzak deneyleri, selenium türevlerinin bromo analogundan daha yüksek singlet oksijen ürettiğini gösterdi. Ayrıca; BOD-Se-I'in in vitro PDT etkisi, farklı hücre kültürlerinde test edildi. Sonuçlar, BOD-Se-I'in apoptotik hücre ölüm mekanizmasıyla tümör hücrelerini başarıyla öldürdüğünü ve sağlıklı hücreleri genel olarak etkilemediğini ortaya koydu. Ayrıca, BOD-Se-I'in tümör hücreleri üzerindeki etkisi hipoksik koşullarda da test edildi ve hücre ölümü gözlemlendi. Bu sonuçlar hipoksik koşullarda çalışabilen ilk mitokondri hedefli BODIPY türevi fotoduyarlaştırıcı olma özelliğini vurguluyor. Ayrıca, 2-etinilselenofen içeren türevler absorpsiyon maksimasını yakın kızıl ötesi bölgeye daha fazla kaydırabilmek için sentezlendi ve maksimum absorpsiyon değerleri önceki hedef fotoduyarlaştırıcılarla karşılaştırıldı.

Anahtar Kelimeler: Fotodinamik Terapi, Hipoksi, Singlet Oksijen, BODIPY, Mitokondri Hedefli

To my beloved family…

ACKNOWLEDGMENTS

First, I would like to express my deep gratitude to my supervisor, Assoc. Prof. Dr. Görkem Günbaş for the opportunity he gave to me, endless support, encourage and patience. He always motivated me to strive hard, even when I was tempted to give up. All the things that I have learnt from him and his guidance were invaluable.

I would like to thank to Assist. Prof. Dr. Safacan Kölemen, not only for collaboration in optical studies but also sharing his knowledge and treating me as one of his student.

I would also thank to my examining committee members, Prof. Dr. Cihangir Tanyeli, Assist. Prof. Dr. Özgül Persil Çetinkol, Assist Prof. Dr. Salih Özçubukçu and Assist Prof. Dr. Safacan Kölemen for accepting to evaluate my thesis and their valuable suggestions.

I thank to Assist. Prof. Dr. Gürcan Günaydın and his research group for their collaboration in vitro cell studies.

Also, I would like to thank to TÜBİTAK (216Z129) for financial support.

I am grateful to all technicians of our department for their help.

Special thanks to Cansu İğci for being such a good mentor and good friend during my undergraduate years. Without her guidance on lab skills, this thesis would not have been possible.

I would like to express my gratitude to Gizem Atakan, Figen Varlıoğlu, Ecem Aydan, Cevahir Ceren Akgül, Dilay Kepil, Aliekber Karabağ and Mustafa Yaşa for being my second family.

I am very grateful to Nihan Yılmazer, Hayriye Kocademirci, Selin Akpınar, Gülsüm Güneş, Cevahir Ceren Akgül, Sena Tarım, Esra Köprücüoğlu and Çağlayan Kızıleniş for their help and learning how to deal with science with me during their undergraduate research.

Also, I would like to thank to the Günbaş Lab members for their help, friendship and positive working environment.

I feel grateful to my housemates, Altuğ Özbeycan and Zübeyir Elmazoğlu for their patience during thesis writing process and help to escape from all scientific stuff with their friendship.

Last but not least, I would like to give special thanks to my family. Without their love, support and guidance in life I could not have become who I am today.

TABLE OF CONTENTS

LIST OF TABLES

TABLES

LIST OF FIGURES

FIGURES

LIST OF SCHEMES

SCHEMES

LIST OF ABBREVIATIONS

ABBREVIATIONS

AcOH	Acetic Acid
ADMDA	2,2’-(Anthracene-9,10-diyl)bis(methylene)Dimalonic Acid
ALA	1,5-Aminolevulinic Acid
Ar	Argon
BODIPY	4,4-Difluoro-4-bora-3a,4a-diaza-s-indacene
DBPF	1,3-Diphenylisobenzofuran
DCM	Dichloromethane
DDQ	5,6-Dicyanobenzoquinone
DMEM	Dulbecco's Modified Eagle Medium
DMF	Dimethylformamide
DMSO	Dimethyl Sulfoxide
FDA	Food and Drug Administration
HeLa	Henrietta Lacks (uterine cell variety; named for deceased patient)
HpD	Hematoporphyrin Derivative
HRMS	High Resolution Mass Spectroscopy
IC_{50}	the Half Maximal Inhibitory Concentration
ICT	Intramolecular Charge Transfer
ISC	Intersystem Crossing
LED	Light-Emitting Diode
LLLT	Low-Level Laser Therapy

MeOH	Methanol
MP	Methyl Pyridinium
MTT	3-(4, 5-Dimethylthiazolyl-2)-2,5-diphenyltetrazolium bromide
NBS	n-Bromosuccinimide
n-BuLi	n-Butyllithium
NIH/3T3	3-Day Transfer, Inoculum 3 x 10^5 Cells
NIR	Near Infrared
NIS	n-Iodosuccinimide
NMR	Nuclear Magnetic Resonance
PBS	Phosphate-Buffered Saline
PDT	Photodynamic Therapy
PS	Photosensitizer
ROS	Reactive Oxygen Species
rt	Room Temperature
THF	Tetrahydrofuran
TLC	Thin Layer Chromatography

LIST OF SYMBOLS

SYMBOLS

ϕ	Fluorescence Quantum Yield
$\lambda_{max\ abs}$	Maximum absorption wavelength
ςn	Spin Orbit Coupling Constant
ϕ_{Δ}	Singlet Oxygen Quantum Yield
ε_{max}	Absorption Coefficient

CHAPTER 1

INTRODUCTION

1.1. Photodynamic Therapy

Photodynamic therapy (PDT) is a clinically approved cancer treatment modality and minimally invasive compared to current methods. For PDT action, three basic components are needed. These are photosensitizer, light and oxygen. Photosensitizer accumulate in tumor tissue and mostly harmless unless activated by light. For light activation in deep tissues, red or near infrared light is needed. Light activated photosensitizers generate singlet oxygen from molecular oxygen, which is fatal for tissues. For an effective PDT several parameters should be considered such as, localization of photosensitizer, oxygen level of tissue, absorption maxima of photosensitizer, cellular signaling, cell metabolism and modes of cell death that operate on a cellular level, as well as photosensitizer pharmacokinetics, biodistribution, tumor localization and modes of tumor destruction. PDT is a promising treatment modality and has the potential to be a strong alternative to current treatment methods with the enhancements on the influence depth, cell death effectiveness and selectivity. (Luby, D., & Zheng, 2018).

1.2. History of the PDT

Light has been used for treatment of many diseases for several thousand years. (Hill, M. D. Daniell, 1991) In antic Egypt, China and India light was widely used to treat of various diseases such as psoriasis, rickets and skin cancer (Ackroyd *et al*. 2001). However, its full potential was not appreciated until the beginning of the 20^{th} century.

In 1900, Oscar Raab showed the effect of light when it is combined with a photosensitizer on paramecia cells (Paramecium caudatum). Paramecia cells were not affected when they were exposed to either light or acridine orange. However, when

they were exposed to both at the same time, cell death was observed within 2 hours. In that experiment, acridine orange (Figure 1.1) was used as a photosensitizer and Paramecia cells became sensitive for light. When the cells were exposed to light, the cytotoxic effect caused cell death (Raab, 1900). In the same year, J. Prime discovered that patients who were treated with Eosin (Figure 1.1) suffered from dermatitis when they were exposed to sunlight (Prime, 1900).

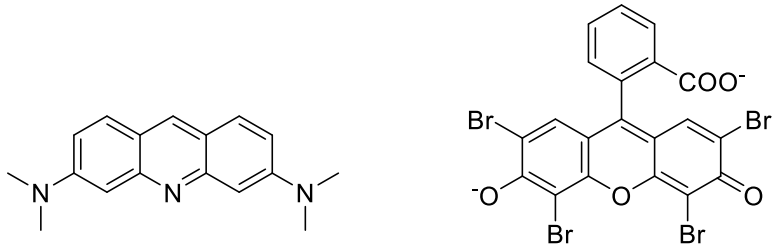

Acridine orange Eosin

Figure 1.1. Structure of Acridine orange and Eosin

In 1901, Niels Finsen found that formation and discharge of smallpox pustules could be prevented and even treated with red light exposure. He also treated cutaneous tuberculosis with ultraviolet sunlight. In 1903, he was awarded with a Nobel Prize as a result of his studies on the treatment of cutaneous tuberculosis (Finsen, 1901). This work opened a new era in modern light therapy.

In the same year, dermatologist Herman Von Tappeiner and A. Jesionek used Eosin and white light to treat skin cancer. This phenomenon was described as "photodynamic action" (Tappeiner & Jodlbauer, 1907).

In 1911, W. Hausmann performed studies on the treatment of red blood cells and paramecium by using light and hematoporphyrin - a porphyrin derivative.

Hematoporphyrin (Figure 1.2) is the most applied photosensitizer in PDT so far since it was reported in the beginning of the 20th century by Hausmann. He also reported that Hematoporphyrin could photosensitize the cells of guinea pigs and mice by light (Hausmann, 1911).

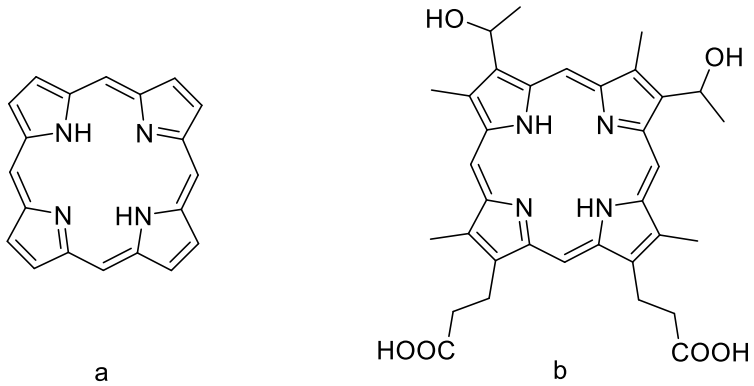

Figure 1.2. (a): Structure of porphyrin ring. (b): Structure of Hematoporphyrin.

In 1913, first human trial of photodynamic therapy was performed by German physicist Friedrich Meyer-Bertz. He injected 200 mg Hematoporphyrin into his hand to observe the effects of light-activated photosensitizer on human body. He suffered from swelling and pain, especially in the light-exposed parts of his body (Meyer–Betz, 1913).

In 1942, Auler discovered that Hematoporphyrin accumulates more in tumor cells than it does in the surrounding cells when it is activated with light source. This phenomenon ended up with necrotic cell death (Auler & Banzer, 1942).

In 1955, Dr. Samuel Schwartz developed Hematoporphyrin derivative (HpD). which is a mixture that was obtained by acetylation followed by hydrolysis of the product. HpD has twice the cytotoxic effect than its ancestor Hematoporphyrin (Schwartz *et al.* 1955).

In 1960, Lipton and coworkers illustrated that HpD could be useful for diagnosis (Lipson & Baldes, 1960).

In 1972, Diamond and coworkers carried out the first in vivo study. They implanted porphyrin to rats and they revealed that it delayed the growth of tumor by 10-20 days. Due to the lack of deep tumor tissue penetration, growth was observed to start again (Diamond, I. *et al*. 1972).

In 1975, Dougherty and coworkers reported that HpD completely destroyed mammary tumor growth in mice when it was activated with red light (Dougherty *et al.* 1975). In the same year, bladder carcinoma was eliminated with light activated HpD by J. F. Kelly and coworkers (Kelly *et al.* 1975).

In 1976, first human trials of HpD was initiated by Kelly and coworkers. They treated bladder cancer by using HpD on five patients. They also treated recurrent bladder cancer of one patient whose treatment had failed by radiotherapy and chemotherapy treatments. HpD slowed tumor growth and necrosis was observed on light received areas (Kelly & Snell, 1976). Following this study, 25 patients with various stage of skin tumors were treated with HpD by Dougherty *et al*. Only 2 tumors out of 113 showed resistance towards treatment (Dougherty *et al*., 1978). After successful treatments of bladder and skin cancers, Y. Hayata and coworkers failed in lung tumor removal. PDT action slowed tumor growth in many patients but only a few of the tumors were completely eliminated (Y. Hayata *et al.* 1982).

In 1984, J. S. Mc Caughan *et al*. treated patients with oesophageal cancer by using PDT modality (McCaughan, Hicks, Laufman, May, & Roach, 1984). After Caughan, O. J. Balchum and Y. Hayata reported successful lung (Balchum *et al.* 1984) and gastric cancer treatments (Yoshihiro Hayata *et al.* 1985) respectively.

Until the end of the 1980s many studies revealed promising results in the treatment of patients with various malignant tumors. Therefore, PDT started to be recommended for patients with breast cancer (Dimofte *et al.* 2002), head and neck tumors (Biel, 1998), brain tumors (Rosenthal *et al*., 2001), intraocular tumors (Landau *et al.* 2002), pancreatic cancer (Bown *et al.*, 2002) and many other types of cancer and it showed a great success at the early stages of cancers (Star *et al.*, 1986).

In 1990, Kennedy and coworkers reported a new porphyrin derivative, aminolevulinic acid (ALA) (Figure 1.3) which is the first topical porphyrin derivative. ALA, in fact, is a prodrug of a photosensitizing agent. When it is applied to the skin, it is absorbed and converted into its active form, Protoporphyrin IX (PpIX) (Figure 1.3) (Kennedy

et al. 1990). ALA is less cytotoxic than HpD. It takes a couple of days to remove ALA from the body whereas it takes months to remove HpD (Gold & Goldman, 2004).

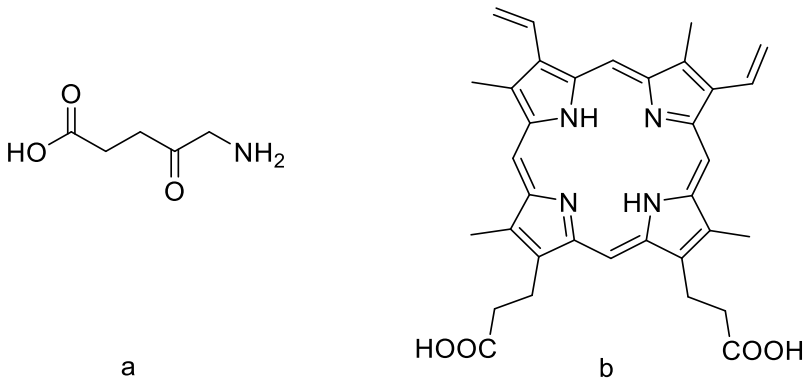

Figure 1.3. (a): Structure of ALA. (b): Structure of PpIX.

In 1993, further purified hematoporphyrin derivative, known as porfimer sodium (photofrin) (Figure 1.4), got a Food and Drug Administration (FDA) approval from Canadian Health Agency for its use in bladder cancer. After Canada, porfimer sodium got FDA approvals from some parts of Europe, USA, and Japan (Tian *et al.* 2008).

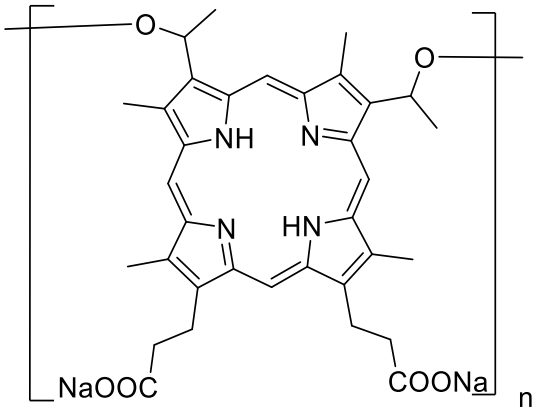

Figure 1.4. Structure of Porfimer Sodium.

After porfimer sodium, many other PDT agents got FDA approvals and they are still in use for the treatment of various malignant tumors. Many other next generation PDT agents are still being explored by researchers and clinical tests are in progress (Tian *et al.*, 2008).

1.3. Working principles of PDT

Photodynamic therapy needs three basic components: a photosensitizer, light and oxygen. Photosensitizers (PS) are dyes that are activated by light after being selectively localized in malignant tissue. Activated photosensitizers can generate reactive oxygen species (ROS), if they are modified properly (D.E.J.G.J. Dolmans *et al.* 2003).

After the absorption of light, photosensitizer is transformed from a singlet ground state to a singlet excited state. There are three possible pathways at this point (Figure 1.5). Fluorescence, intersystem crossing (ISC) to longer lived triplet excited state and thermal relaxation. Fluorescence ability of photosensitizers make them suitable for being used in photodetection and theranostic applications (Yoon, Li, & Shim, 2013), (Foote, 1991).

Energy transferred from excited photosensitizer to molecular oxygen results in ROS, mostly singlet oxygen (Figure 1.5). Singlet oxygen destroys tumor cells by giving direct damage to cellular membrane, indirect vascular shutdown and immune responses for activation of tumor cells. This damage can result in cell death in two ways; either apoptotic or non-apoptotic (necrosis and autophagy). Type of cell death mechanism depends on light intensity. Generally, low light intensity causes apoptosis whereas high intensity light results in necrosis (Agostinis *et al.*, 2011).

Phosphorescence is a spin-forbidden process for photosensitizer due to the loss of energy by emission of light. This causes photosensitizer to remain at triplet excited state for a longer time, producing an opportunity for more ROS generation (Atkins & Paula, 2008).

Making intersystem crossing to a triplet excited state from a singlet excited state is vital for photodynamic action because long-lived triplet state gives opportunity to generate more ROS. In order to make intersystem crossing, PS should be modified. Introducing heavy atoms allows PS to make intersystem crossing. High spin-orbit

coupling values of larger halogens (Br, I) make them a favorable option for enhanced intersystem crossing (Martin, 1971).

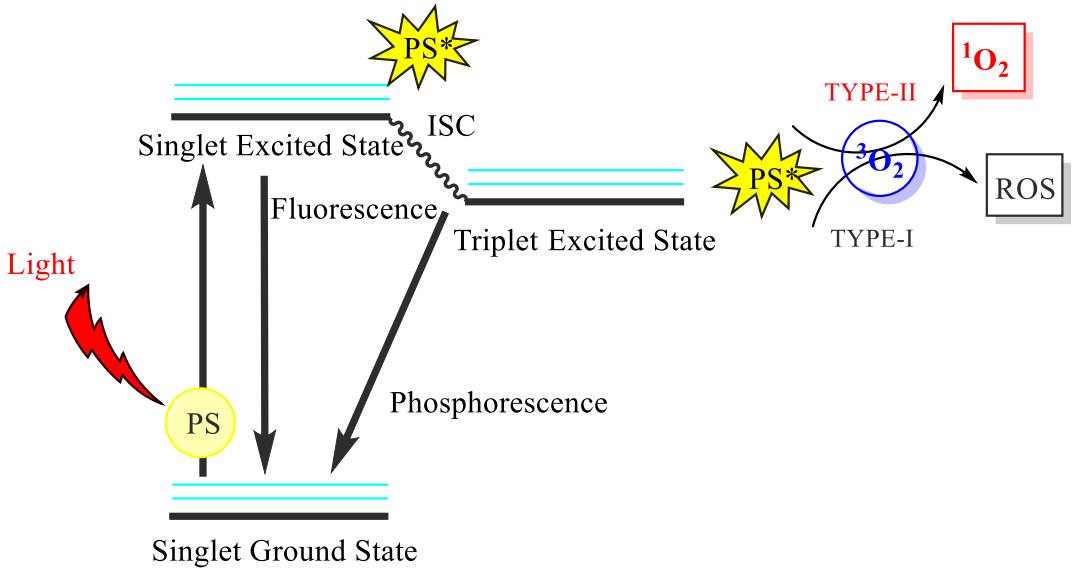

Figure 1.5. Schematic illustration of photodynamic therapy including the Jablonski diagram.

Reactive oxygen species could be generated in two ways: In Type-I reactions, molecular oxygen is converted to peroxides, superoxides and other ROS (Valko *et al.* 2005). In Type-II reaction molecular oxygen is converted into singlet oxygen. In the abundance of oxygen, the desirable Type – II mechanism predominates (Figure 1.6) (Leach & Houk, 2002).

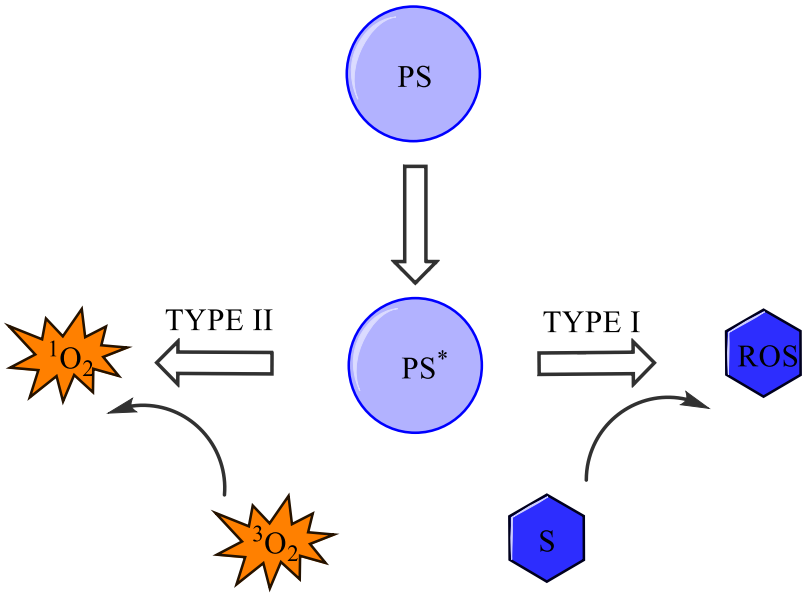

Figure 1.6. Type I vs. Type II photosensitization reactions. PS: photosensitizer, S: substrate in cell, ROS: reactive oxygen species.

Reactive oxygen species have high reactivity and short half-life. Due to this fact, they can affect only the tissues in which they are produced and the other tissues in close vicinity. Also, high dependence on oxygen causes effective PDT action to happen only at the oxygen-rich areas of the tissues (Moan & Berg, 1991).

Improving PDT action could be done with selective localization of PS in certain areas in the tissue. Different oxygen levels of organelles and their roles in cell death mechanisms make them possible targets in PDT based cell death mechanism. (D.E.J. Dolmans *et al.*, 2003)

Photodynamic therapy has some drawbacks such as prolonged skin photosensitization and patients should avoid direct sunlight exposure for a certain period of time (Cairnduff *et al.* 1994).

1.4. Cell Death Mechanisms

In PDT based treatment, singlet oxygen generation initiates cell death via three main mechanisms. First one is the direct tumor death with ROS which is generated with

PDT action secondly, tumor related vasculature damage and thirdly, activation of immune response toward tumor cells (Tayyaba Hasan *et al.* 2003).

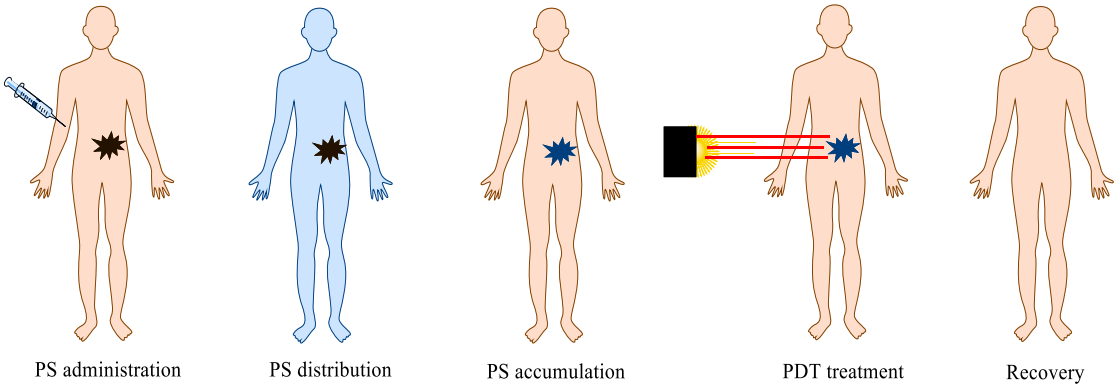

Figure 1.7. Schematic illustration of PDT mechanism in human cell.

All three of these mechanisms influence each other but an effective tumor control needs a combination of all three mechanisms (Tayyaba Hasan *et al.*, 2003). As a result of these three mechanisms, cell death is observed as apoptotic or non-apoptotic (Yoo & Ha, 2012). Apoptosis is a programmed cell death, and it is also known as type-I cell death. Apoptosis is controlled by diverse cellular and molecular signaling pathways (Danial & Korsmeyer, 2004). Non-apoptotic cell death includes necrosis and autophagy. Autophagy is a type-II cell death and it is a potential alternative cell death mechanism for PDT action. It eliminates long-lived proteins and organelles (Kessel *et al.* 2006). On the other hand, necrosis is an uncontrollable mechanism. It happens in response to hypoxic or ischemic injury. It is also known as type-III cell death mechanism (Galluzzi *et al.* 2011). Type of cell death depends on the location of the photosensitizer and the quantity of the singlet oxygen. When the photosensitizer is located in mitochondria or endoplasmic reticulum, cell death mostly ensues via apoptosis and/or autophagy. On the other hand, if photosensitizer is located in lysosomes or in the plasma membrane, cell death mostly ensues via necrosis (Figure 1.8) (Castano *et al.* 2006).

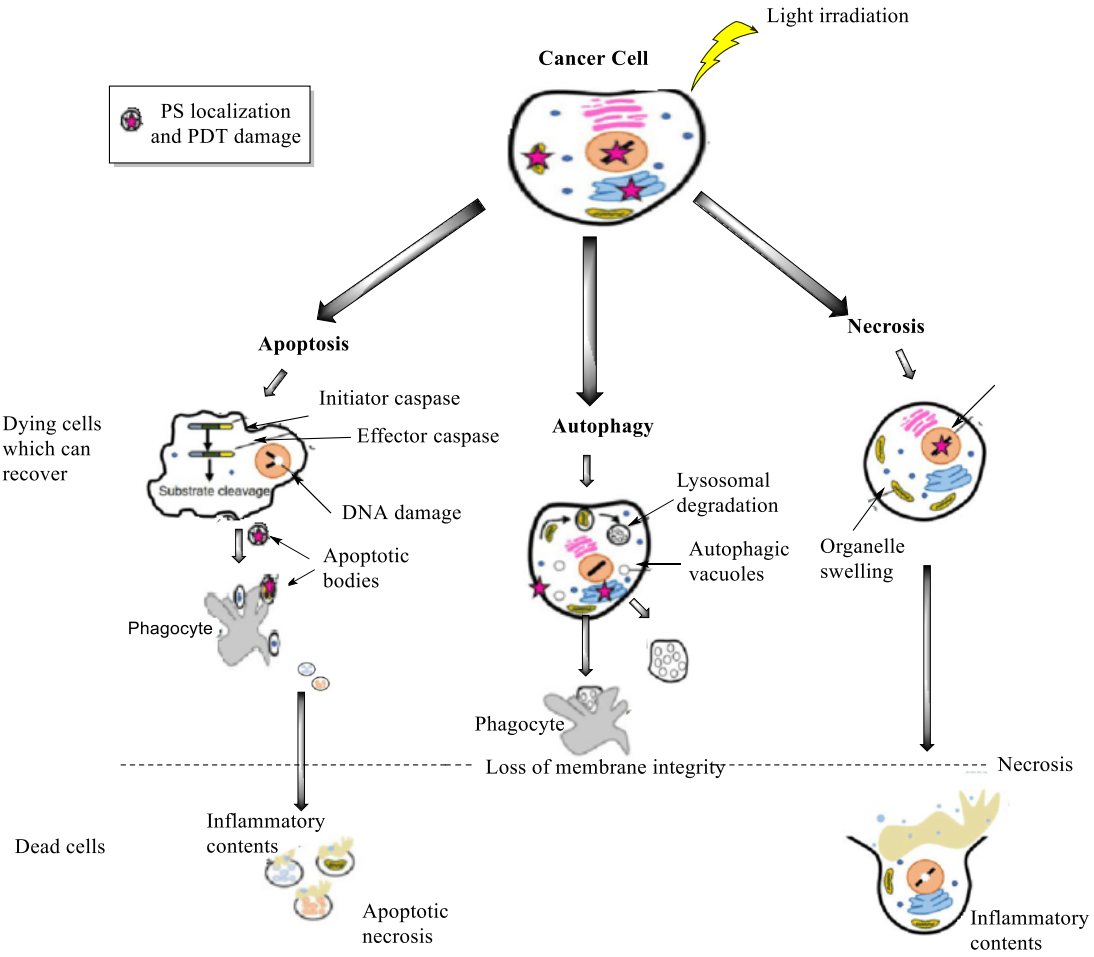

Figure 1.8. Cell death pathways in PDT.

1.5. Subcellular Localization

Subcellular localization control of the photosensitizer in cells is very important since it has an impact on PDT efficiency and selective cytotoxicity. Targeting the mitochondria rather than the nucleus increases the efficiency of PDT action even at low levels of singlet oxygen generation. Also, minimizing unwanted cytotoxic activity is possible by forming the PDT-active species at the target site. Another issue that should be tackled is keeping the photosensitizer in subcellular structure. It depends on photosensitizer solubility and local concentration gradient because it can diffuse out of cytoplasm (Rubio *et al.* 2009).

Table 1.1. *Examples for mitochondria and lysosome targeting photosensitizer.*

Photosensitizer Type	Sub-Cellular Localization
N-aspartyl chlorin E6 (NPe6)	Lysosome
Benzoporphyrin derivative (BPD)	Mitochondria
5-Ethylamino-9-diethylyaminobenzo-[a]-phenothiazinium chloride (EtBNS)	Lysosome
Galactose conjugate of 3-(1-hexyloxyethyl)-3-devinyl pyrophorbide-a (HPPHgal)	Lysosome
Porphyrin-rhodamine B cation	Mitochondria
Porphyrin-mono-triphenyl phosphonium cation	Mitochondria
Triphenylphosphonium (TPP) cation	Mitochondria
(E)-N-alkyl-4-[2-(ferrocenyl)vinyl] pyridinium cations	Mitochondria

There are several factors that affect cell uptake and selectivity. One of the factors is hydrophobicity of the photosensitizer. Hydrophobic photosensitizers can easily bind to membranes. Hydrophilic photosensitizers with hydrophobic side groups (amphiphilic) are also able to bind to the membrane. AIPcS2a which is good example for amphiphilic photosensitizers (Weyergang *et al.* 2009). Although hydrophobic photosensitizers have a higher tendency to accumulate on the cell membrane, they lack proper delivery method in aqueous media. Hydrophilic photosensitizers have several advantages over hydrophobic ones. Removing hydrophilic photosensitizers from body is faster, which results in less side effects (Sakamoto *et al.*, 2002). Also, inner mitochondrial membrane has negative transmembrane potential around 150-170mV (Ormond & Freeman, 2013) which allows cationic photosensitizers to accumulate in the mitochondria (Pavani *et al.* 2009). All these advantages make the hydrophilic photosensitizer more attractive in PDT studies.

Singlet oxygen generation is one of the key factors of PDT. To generate singlet oxygen, cell culture should contain molecular oxygen. Tumor cells are oxygen deficient which is known as hypoxia (Wilson & Hay, 2011). To overcome this problem, the photosensitizer should be modified to target appropriate organelles, such as mitochondria and lysosome, which play essential role in cell respiration and

digestion respectively. More importantly, both these organelles are closely related to the cell apoptosis (Kroemer & Jäättelä, 2005). During photo-activation, mitochondria-targeted PDT agent can damage biological functions of the organelle resulting in the death of tumor cells (Huang *et al.*, 2015).

1.6. Light in Photodynamic Therapy

Light is the one of the three key elements of PDT action. Activation of photosensitizer is performed with light. Absorption spectrum of the photosensitizer determines the required wavelength. Therapeutic window is in the range between 650 nm and 800 nm wavelengths for the use of PDT in cancer treatment. ROS is readily produced in this range. Higher wavelength, which means lower energy, decreases the singlet oxygen production capability. On the other hand, efficiency of photodynamic therapy depends on the depth of light penetration. Longer wavelengths penetrate tissues deeper than shorter ones (Figure 1.9). Also, total light dose, light delivery mode and fluence rate are the other parameters influencing the efficiency of PDT. All these factors should be considered when choosing the light source for PDT (Zhu & Finlay, 2008).

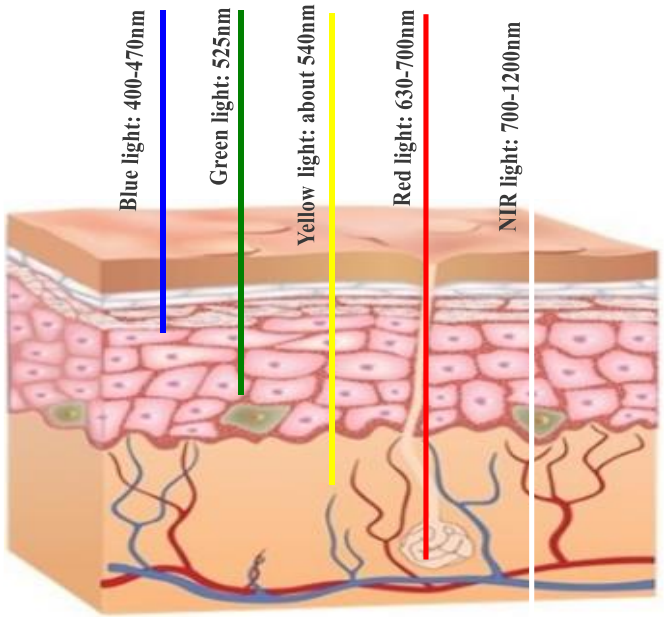

Figure 1.9. Penetration depth of different wavelength range to the skin.

Low-Level Laser Therapy (LLLT) dominated PDT for a long time. It provides monochromaticity and short time to reach the required light dose due to very powerful light source. However, these laser sources have limitations such as high cost, large size, complexity and narrow range due to monochromaticity (Brancaleon & Moseley, 2002). Light Emitting Diodes (LEDs) could overcame these limitations. Compared to laser sources, they are cheaper and more compact. Furthermore, they could extend their wavelength range when they combined with semiconductors. Although former laser sources are still dominant in PDT, LEDs have started to replace them. Also, incandescent lamps could be used as a light source in PDT because of their wide wavelength range, simplicity and low cost (Sorbellini *et al.* 2018).

1.7. Photosensitizers

1.7.1. Photosensitizers Based on BODIPY Dyes

Over the past decade, a new class of photosensitizer for PDT action has emerged. These are based on the 4,4-difluoro-4-bora-3a,4a-diaza-s-indacene (BODIPY) core (Figure 1.10). Many ideal photosensitizer characteristics are ensured by BODIPY based structures. It has higher extinction coefficients, environment insensitivity, photobleaching resistivity and higher light-dark toxicity ratios over old fashioned PDT agents (Awuah & You, 2012). Until several decades ago, many studies focused on BODIPY's role as fluorescence imaging probe rather than its PDT-based photosensitizer ability (Awuah *et al.* 2011), (Deniz *et al.*, 2008). Fluorescence occurs by relaxation from singlet excited state which is not desirable for PDT action. Enhancing singlet to triplet intersystem crossing and depressing fluorescence make BODIPY suitable for PDT action (Kamkaew *et al*., 2013).

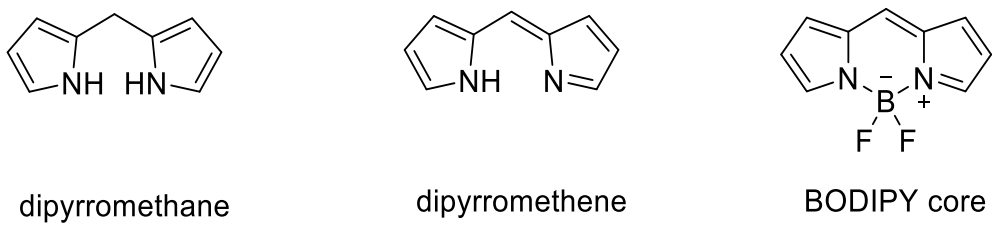

Figure 1.10. Structure of BODIPY core and its precursors.

4,4-difluoro-4-bora-3a,4a-diaza-s-indacene (BODIPY) core is suitable for modifications towards PDT. The design should aim to confer a long wavelength absorption property and intersystem crossing ability to the modified BODIPY. Absorbing at longer wavelength makes it possible to reach the therapeutic window and intersystem crossing gives the opportunity to generate singlet oxygen from molecular oxygen since this action happens at triplet excited state (Hinkeldey *et al.* 2008).

"Tetramethyl BODIPY" has low quantum yield for singlet oxygen generation (Figure 1.11). One of the concepts to increase the quantum yield is halogenation. Heavy atoms provide high population at triplet excited state, which is favorable for PDT action. 2- and 6- positions of BODIPY have a tendency to undergo electrophilic substitution due to the mesomeric structure of the BODIPY. This electron rich property provides an opportunity to make many chemical modifications such as electrophilic aromatic substitution with halogens (Br, I) (Figure 1.11). This substitution provides high intersystem crossing capacity on high spin-orbit coupling heavy atoms (Yogo *et al.* 2005).

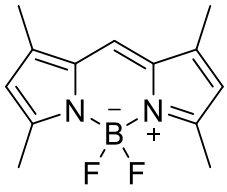

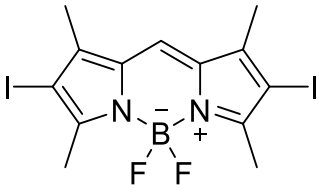

ϕ in MeOH: 0.7	ϕ in MeOH: 0.02
$\lambda_{max\ abs}$: 502nm	$\lambda_{max\ abs}$: 534nm
$^1O_2$ generation rel. rate: 0.48 (methylene blue)	$^1O_2$ generation rel. rate: 23.9 (methylene blue)

Figure 1.11. Fluoresecence quantum yield in MeOH, absorption maxima, singlet oxygen generation rate relative to methylene blue of tetramethyl BODIPY core and its di-iodo derivative.

Bromination of the BODIPY core is a highly efficient method for creating potential photosensitizer for PDT activity. Thus, many synthetic methods utilize bromine for

the halogenation of the BODIPY core (Scheme 1.1). For example, free radical type bromination with NBS and AIBN results in high yield. Regioselective bromination of BODIPY core is also possible with using proper equivalents of NBS at room temperature. Molecular bromine could also be effective on bromination (Deniz *et al.*, 2008), (Dost *et al.* 2006), (Hayashi *et al.* 2011), (Cihaner & Algi, 2009).

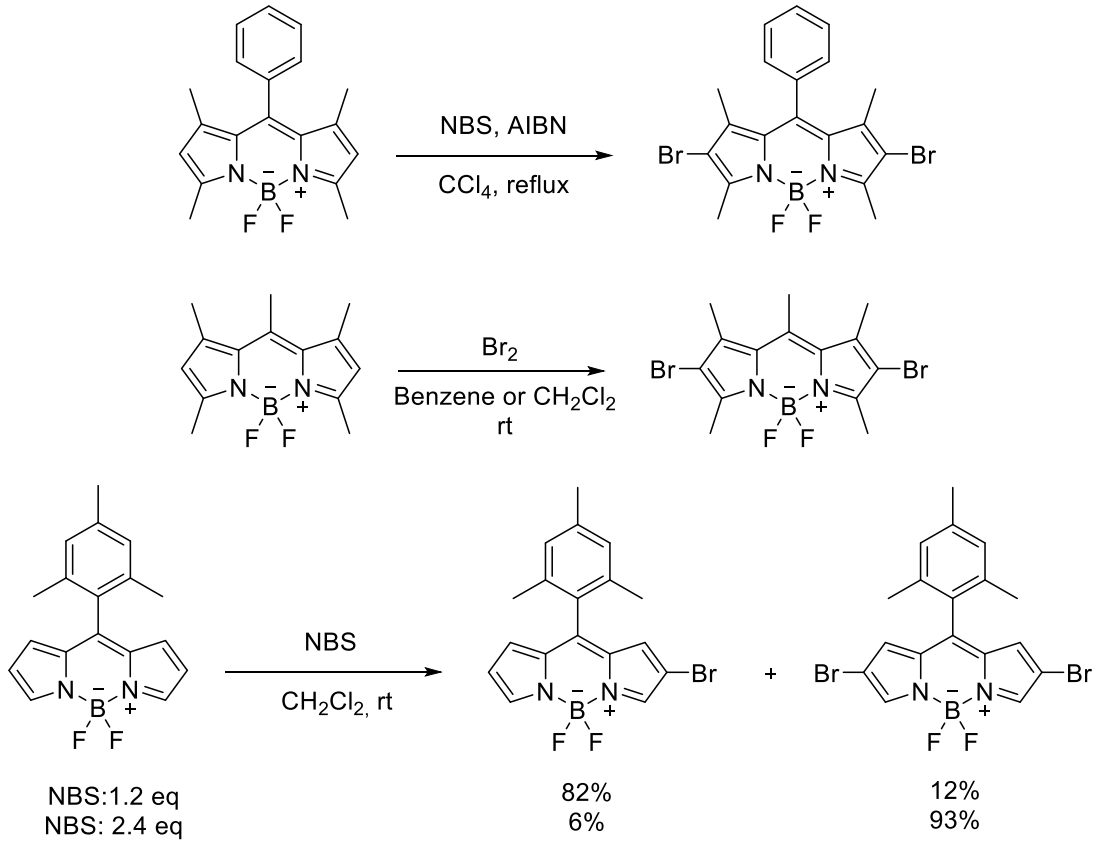

Scheme 1. 1. Examples for bromination reactions of BODIPY.

Iodine is a heavier atom than bromine. It is also effective on enhancing singlet to triplet intersystem crossing due to heavy atom effect. Nagona et al. pioneered the iodination of tetramethyl BODIPY and they showed high singlet oxygen generation efficiencies in both polar and apolar medium. To no surprise, diiodo analogue was shown to have high light-to-dark phototoxicity ratios. A 30 nm batochromic shift of absorption maxima in 30nm was achieved with iodination. Nagano et al. also suggested that diiodo analogue could also be used for PDT in membranes in lipophilic media (Yogo

et al., 2005). Polyiodinated derivatives revealed improvements on singlet oxygen generation by Ortiz *et al*. In 2012, 2-,6- diiodo substituted and 3-,5- diiodo substituted BODIPY derivatives were prepared by same group (Figure 1.12) (Ortiz *et al*., 2012).

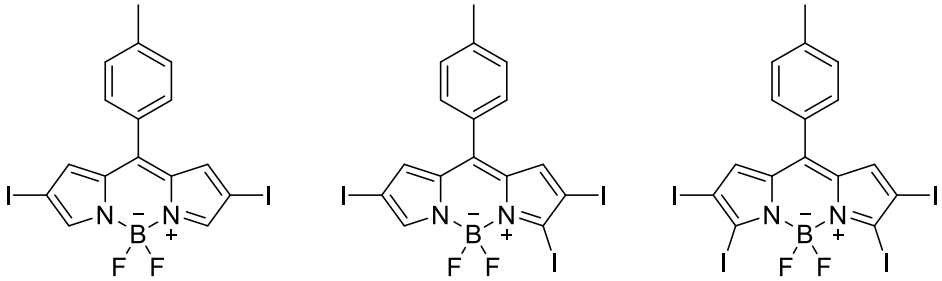

ϕ in c-Hexane: 0.012	ϕ in c-Hexane: 0.060	ϕ in c-Hexane: 0.099
$\lambda_{max\ abs}$: 548.5nm	$\lambda_{max\ abs}$: 563.5nm	$\lambda_{max\ abs}$: 581nm
$^1O_2$ QY: 0.83 ± 0.07	$^1O_2$ QY: 0.86 ± 0.09	$^1O_2$ QY: 0.87 ± 0.06

Figure 1.12. Fluoresecence quantum yield in c-Hexane, absorption maxima, and singlet oxygen quantum yield of iodinated BODIPY derivatives.

Thiophene substitution on BODIPY core gives the advantage to extend conjugation. Its HOMO-LUMO energy levels make thiophene suitable for conjugation with unsaturated fragments. Extended conjugation provides batochromic shift where one of the goals in PDT is reaching NIR region to make efficient treatment (K. Umezawa *et al.* 2008), (Umezawa *et al.* 2009). However, thiophene substitution on BODIPY core is not enough for PDT application. Spin-orbit coupling constant (ζn^{*3}) for $3p^3$ hybrid of sulfur is 288 cm^{-1} whereas for $4p^4$ bromine is 1780 cm^{-1} and for $4p^4$ iodine is 4690 cm^{-1} (Martin, 1971). These data revealed that, thiophene alone is not suitable for PDT action. Suzuki *et al*. constructed and synthesized fused-aryl ring thiophene-containing BODIPY derivatives. Results show that even halogenated derivatives have quite moderate quantum yields. On the other hand, these derivatives have longer wavelength maxima, a high molar extinction coefficient, and a higher photostability than m-THPC which is the clinically approved PDT drug (Figure 1.13) (K. Umezawa *et al.* 2008), (Umezawa *et al.*, 2009).

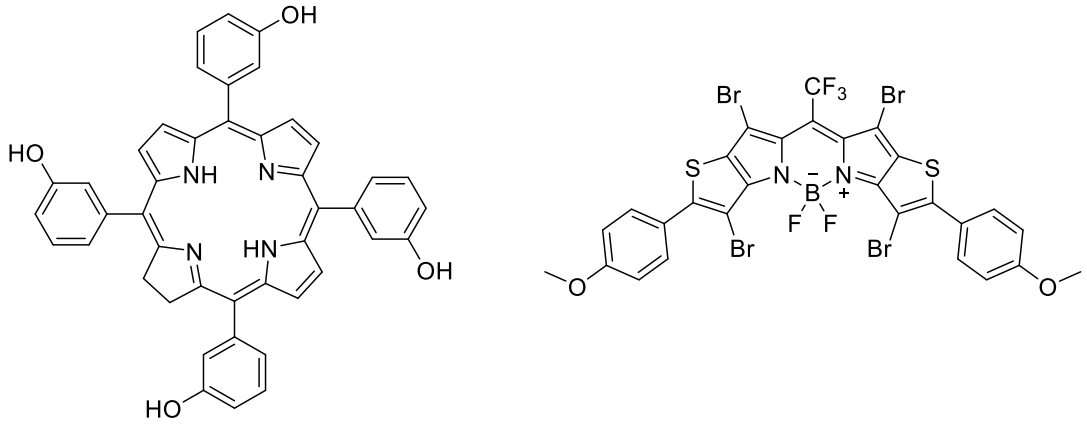

Figure 1.13. Structure of m-THPC (left) and structrure of fused-aryl ring thiophene-containing BODIPY derivative (right).

There is a new approach toward shifting absorption maxima of BODIPY core to NIR region while generating efficient singlet oxygen with selenophene substitution. The properties of selenophene are similar to those of thiophene. It has the ability to extend conjugation via its aromatic structure. Also, in comparison to sulfur in thiophene, selenium in selenophene has a higher spin-orbit coupling constant which is similar to that of bromine (1670 cm^{-1} for $4p^3$). These data indicate that selenophene-substituted BODIPY derivatives are good candidates of efficient photosensitizers for PDT.

Nabeshima *et al*. synthesized the first selenophene substituted BODIPY derivatives very recently. They synthesized several selenophene derivatives to examine the effect of substitution site with moderate yields. These derivatives reached batochromic shift to NIR more than thiophene derivatives did. Also, they revealed moderate quantum yields of singlet oxygen generation in organic media but research does not include in vitro studies due to lack of water solubility of the PSs (Figure 1.14) (Taguchi *et al.* 2018).

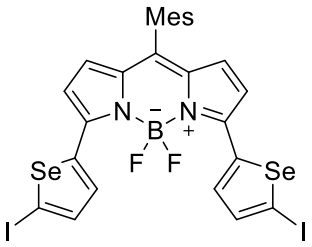

ϕ in $CHCl_3$: 0.51

$\lambda_{max\ abs}$: 651nm

$^1O_2$ QY: 0.30

Figure 1.14. Fluoresecence quantum yield in c-Hexane, absorption maxima, singlet oxygen quantum yield of selenophene containing BODIPY derivative.

Styryl substitution provides redshift around 100 nm and second substitution also provides further redshift. Styryl substitution achieved by Knoevanegel condensation from 1-, 7- methyl units which are relatively acidic. Introducing styryl groups with water soluble moieties enhance biocompatibility, cellular uptake and hydrophilicity. Akkaya *et al* (Atilgan *et al.* 2006). and Ng et al (He *et al.* 2011b) are pioneers of this methodology.

Akkaya et al. synthesized styryl BODIPY derivative with three bromine atoms to provide ISC and oligoethylene glycol substituent to enhance water solubility (Figure 1.15). This derivative has IC_{50} value around 200 nM and via fluorescence microscopy, cytotoxic damage on cell membrane was indicated (Atilgan *et al*., 2006).

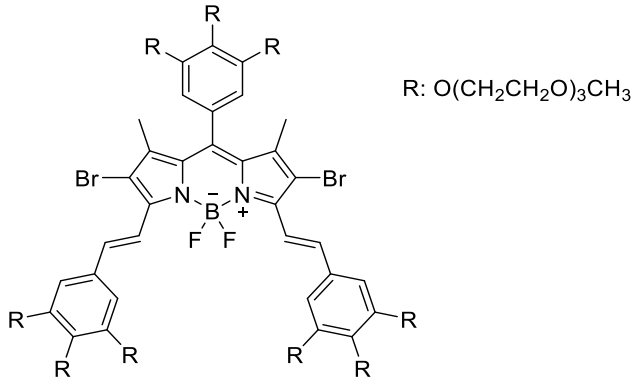

Figure 1.15. Styryl substituted brominated BODIPY derivative.

Ng et al. synthesized iodinated BODIPY derivative, which is similar to Akkaya's work (Figure 1.16). Results indicated that the iodinated derivative has lower IC value of 7nM. Fluorescence microscopy proved endoplasmic reticulum localization (He *et al.*, 2011b).

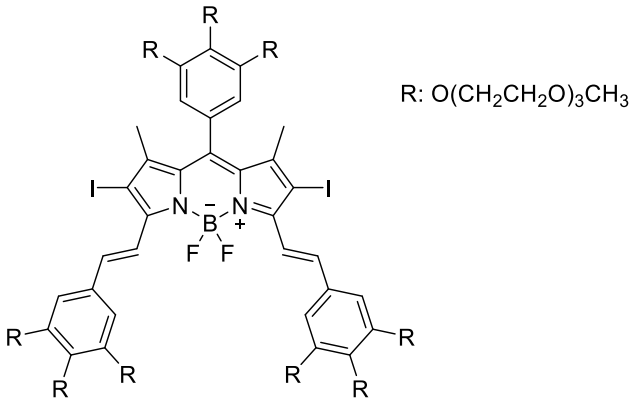

Figure 1.16. Styryl substituted iodinated BODIPY derivative.

Unsymmetrical styryl substitution promotes an amphiphilic character. Also, dimethyl amine which is the most studied one in this case, shows low IC value (17nM) (Figure 1.17) and accumulates in lysosome selectivity rather than endoplasmic reticulum organelle (He *et al.* 2011a).

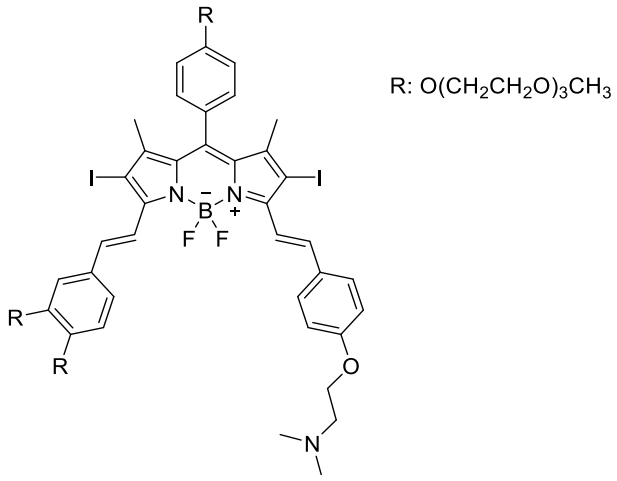

Figure 1.17. Unsymmetrical styryl substituted BODIPY derivative.

Introducing acetylene derivatives to BODIPY is another design principle to extend conjugation and get absorption and emission spectra shifted toward longer wavelength

(Rohand *et al.* 2006). BODIPY core functionalized with acetylene or arylacetylene using Sonogashira coupling. Jiao *et al*. introduced several arylacetylene derivatives to di-iodo BODIPY from 3- and 5- positions (Figure 1.18) and they showed different arylacetylene groups could cause batochromic shift on both absorption and emission maxima up to 110 nm and 116 nm respectively (Jiao *et al.*, 2010).

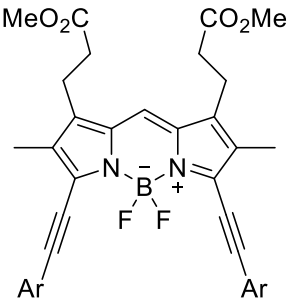

Figure 1.18. Arylacetylene subsitituted BODIPY derivative.

1.7.2. Photosensitizers Based on Other Dyes

1.7.2.1. First Generation Photosensitizers

Photophrin and hematoporphyrin derivatives (HpD) are in the family of first generation photosensitizers, because they have complex mixtures of monomeric, dimeric and oligomeric structures. Photophrin, which is the first FDA approved PDT agent, has low absorption maxima at 630 nm ~ 3000 M^{-1} cm^{-1}. Low absorption maxima limits the treatment attainability to a depth of 2-3 mm under the skin. Photophrin has long term photocytotoxicity. Patients should avoid direct sunlight and artificial light exposure for about six to ten weeks. However, it has high singlet oxygen quantum yield ϕ_{Δ} = 0.89. Although Photophrin has a high photocytotoxicity, it is a safe treatment method. It received its first FDA approval from Canadian Health Agency for treatment of bladder cancer in 1993. After Canada, it also received FDA approval from the USA for the treatment of esophageal cancer in 1995 and lung cancer in 1998. It's area of use extended to head, neck, abdominal, thoracic, brain, intestinal, skin, breast, and cervical cancer (Pushpan *et al*., 2002).

Photogem and Photosan-3 are other FDA approved hematoporphyrin derivatives where Photogem received approval from Russia and Brasil and Photosan-2 from the European Union (Hage *et al.* 2012).

1.7.2.2. Second Generation Photosensitizers

Due to short absorption maxima and undesirable skin photocytotoxicity of first generation photosensitizers, agents were developed with improved properties. (Ormond & Freeman, 2013).

1.7.2.2.1. Phorphyrins Based Photosensitizers

Meta-tetra(hydroxyphenyl)porphyrin (m-THPP) (Figure 1.19) is a second generation photosensitizer and it is around 30 times more effective than HpD in tumor photo-necrosis and it has a longer absorption maximum at 648nm. However, it has a high photocytotoxicity (Bonnett, 1995). On the other hand, 5,10,15,20-tetrakis(4-sulfanatophenyl)-21H,23H-porphyrin (TPPS4) (Figure 1.19) has a low photocytotoxicity and it has absorption maxima at 645nm (Santoro *et al.*, 1990).

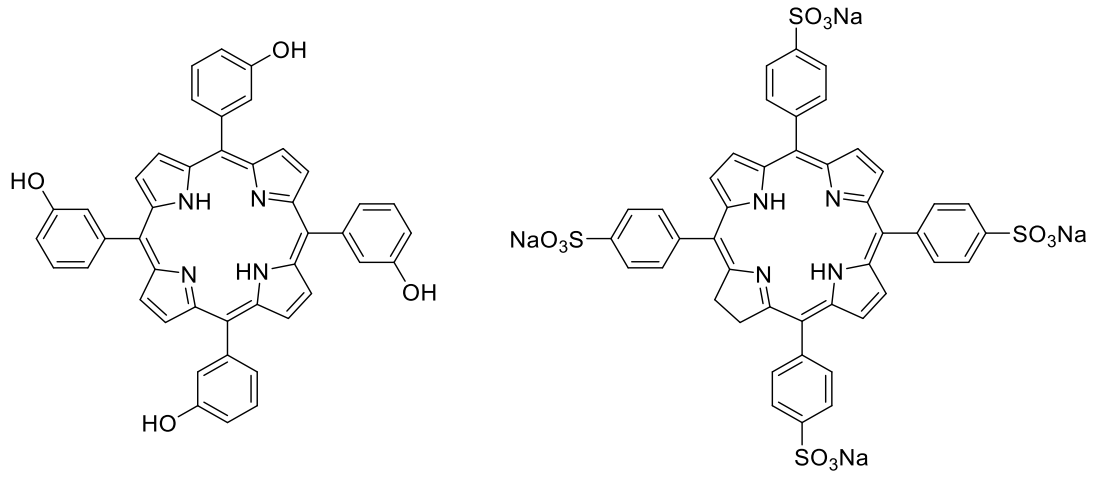

Figure 1.19. (a): Structure of m-THPP. (b): Structure of m-TPPS4.

1,5-aminolevulinic acid (ALA) is the first topical porphyrin derivative. In fact, it is a prodrug of the photosensitizing agent. When it is applied to skin, it is absorbed and is

converted to its active form Protoporphyrin IX (PpIX). It received a FDA approval from the USA in 1999 to be used for non-oncological PDT treatment of actinic keratosis. It has a short absorption maximum at 630 nm. On the other hand, it is metabolized in 48 hours, reducing skin sensitization (Morton *et al.*, 2002).

Methyl aminolevulinate got a FDA approval from the USA for the treatment of actinic keratosis in 2004 and it is still in use under the commercial name Metvixia, MAL. Light source of Metvixia provides a deeper tissue penetration even though it has emission at 630 nm. This ability confers an advantage over ALA (Gilchrest, 2010).

Chlorines differ from porphyrin only with two more hydrogens on one pyrrole ring (Figure 1.20). This modification provides bathochromic shift in absorption in between 640-700 nm and their ε_{max} around 40000 M^{-1} cm^{-1}. Well-known chlorines are BDP-MA (Visudyne) and m-THPC (Foscan). They have absorption maxima at 689 nm and 652 nm respectively. BDP-MA is useful for the treatment of age-related macular degeneration in ophthalmology and m-THPC is useful for the treatment of breast, prostate and pancreatic cancers (Ormond & Freeman, 2013).

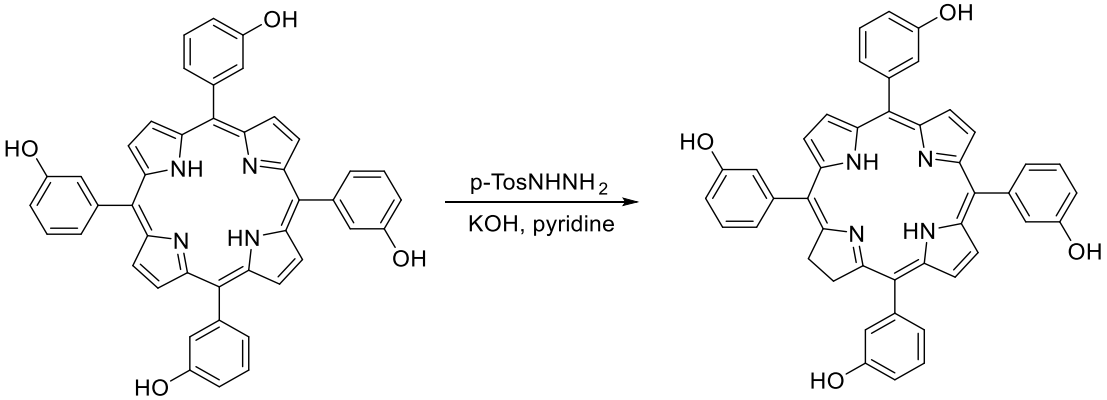

m-THPP m-THPC

Figure 1.20. Formation of m-THPC by tosylhydrazine reduction of m-THPP.

Texaphyrins are another derivative of phorphyrins. In 1988, they were introduced by Sessler *et al*. They predominantly absorb in the NIR region. Texaphyrins have five well-coordinated nitrogen atoms with a central Lanthanide atom. Lutetium (III)

derivative (Lu-Tex) has absorption maxima at 732 nm which gives better tissue penetration plus, it is water soluble. Lu-Tex has high singlet oxygen quantum yield and low dark toxicity (Figure 1.21). The Gadolinium (III) and Cadmium (II) derivatives are other texaphyrin derivatives with Cadmium (II) derivative having the highest absorption maxima at 864 nm (Sessler *et al.* 1988)

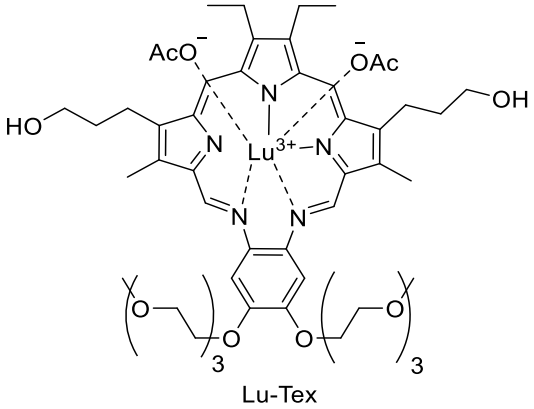

Figure 1.21. Structure of Lutetium Texaphyrin.

1.7.2.2.2. Non Porphyrin Based Photosensitizers

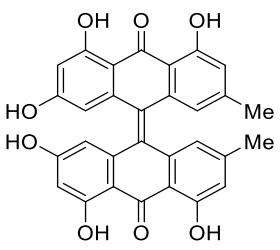

Hypericin

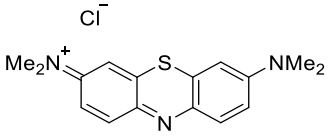

Methylene Blue

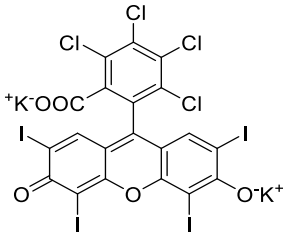

Rose Bengal

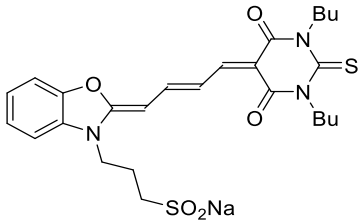

Merocyanine 540

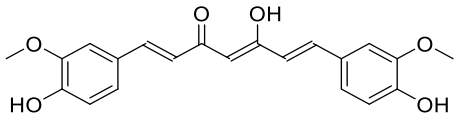

Curcumin

Figure 1.22. Examples for non-porphyrin PDT photosensitizers.

Although porphyrin derivatives dominate PDT, several chromophores exhibit photodynamic action. Non-porphyrin second generation photosensitizers for PDT activity can be classified as anthraquinones, phenothiazines, xanthenes, cyanines and curcuminoids (Figure 1.22). Their most known derivatives, absoption maxima, and application areas listed below (Table 1.2) (Ormond & Freeman, 2013):

Table 1.2. *Properties of selected non-porphyrin PDT candidates.*

Compound	λ_{max} (nm)	ε_{max} ($M^{-1}cm^{-1}$)	Application
Hypericin	590	44000	squamous cell carcinoma, basal cell carcinoma
Methylene Blue	666	82000	chronic periodontitis
Rose Bengal	549	100000	breast carcinoma, melanoma
Merocyanine 540	556	110000	leukemia, lymphoma
Curcumin	420	55000	oral disinfectant

Table 1.3. *Clinically approved PDT drugs.*

Photosensitizer	Trade Name	λ_{max} (nm)	Approved	Application (cancer type)
HpD-Porfimer sodium	Photophrin	630	Worldwide	Cervical, Endobroncial, Esophageal, Gastric, Bladder, Brain, Ovarian
5-ALA	Levulan	635	Worldwide	Skin, Head and Neck, Gynaecological
5-ALA-methylester	Metvix	635	Europe	Basal cell carcinoma, Bladder
5-ALA-hexylester	Hexvix	375-400	Europe	Bladder tumor diagnosis
5-ALA-benzylester	Benzvix	635	Europe	Gastrointestinal
Temoporphin	Foscan	652	Europe	Head and Neck, Lung, Skin, Brain
Verteporphyin	Visudyne	690	Worldwide	Pancreatic, Basal cell carcinoma
Talaporphyrin	Laserphyrin	664	Japan	Lung
$SnEt_2$	Photrex	664	the USA	Breast, Skin, Prostate
Lu-Tex	Lutrin, Optrin, Antrin	732	the USA	Breast
Padoporphyrin	TOOKAD	762	the USA	Prostate
Ce6-PVP	Fotolon	660	Belarus, Russia	Sarcoma, Brain, Nasopharyngeal

1.8. Aim of the Study

In this study, our aim was to introduce novel, selenophene-containing, mitochondria-targeted and water soluble BODIPY derivatives for efficient PDT activity. A selenophene containing BODIPY derivative was recently published during finalization of our work (Taguchi *et al.*, 2018). However this study does not contain any *in vivo* or *in vitro* studies. Additionally our patent application predates this publication. In the design phase, it was envisioned that the introduction of an aromatic

selenophene ring to BODIPY core would shift the absorption maxima to NIR more than the halogen introduced analogue does, and also it would provide efficient singlet oxygen generation due to high spin orbit coupling constant of selenium atom. In addition, with offering an extra site for halogenation, selenophene derivatives have the potential to enhance singlet oxygen generation. Besides high singlet oxygen generation at red/NIR region, proper drug delivery to tumor cells and organelle targeting were considered. Our aim was to overcome both issues with one single modification. Odeh *et al*. had converted zinc coordinated porphyrin derivatives to cationic alkyl pyridinium in order to localize them in mitochondria (Odeh *et al*., 2014). The findings in this work encouraged our study. It was anticipated that, simply converting selenophene containing photosensitizer to an alkyl pyridium salt could provide hydrophilicity and localization to mitochondria. Additionally for any drug candidate to be a viable alternative cost is of importance. Hence the design was made in the sense that all the targeted properties can be achieved by a molecule that can be synthesized in minimum number of steps. To assess the validity of our design, target photosensitizers were synthesized, characterized, and tested in vitro cell studies.

CHAPTER 2

RESULTS AND DISCUSSION

2.1. Design of Target Photosensitizers

BODIPY core has many desirable characteristics for PDT action. However, the core should be modified to enhance PDT action. In this study, we made two basic modifications. The presence of selenium as a heavy atom on the BODIPY favors spin-orbit coupling mediated inter-system crossing, resulting in effective singlet oxygen generation upon excitation. Hence a modification with selenophene ring was performed. Additionally selenophene ring offers additional sides for selective and high yielding iodination that leads to improved photocytotoxicity due to the enhanced heavy atom effect. Secondly, hydrophobic selenophene-containing BODIPY core is converted to water-soluble agents by modifying it with methyl pyridinium (MP) moieties (Hammerer *et al*., 2017). This conversion not only improves water solubility, but also allows photosensitizer to localize in mitochondria toward improving the performance of PDT action due to oxygen rich nature of this organelle (Wang *et al.* 2013), (Wallace, 2012). Additionally this modification results in significant red shift in the absorption maxima of the photosensitizer.

2.2. Retrosynthetic Analysis of Target Molecules

Figure 2.1 represents successful (blue) and failed (red) retrosynthetic approaches of target photosensitizers

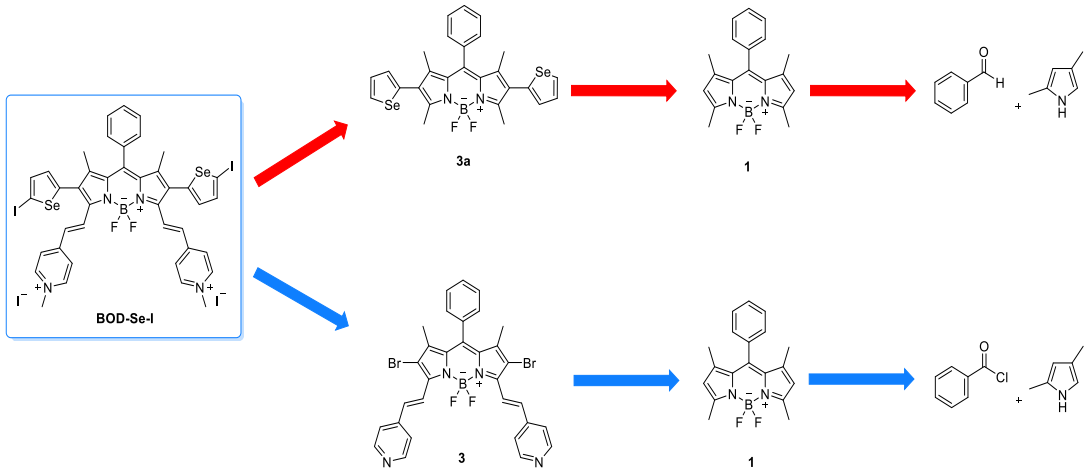

Figure 2.1. Successful (blue) and failed (red) retrosynthetic approaches of target photosensitizers.

During the synthesis of the target photosensitizers different pathways followed and different synthetic approaches applied. Some of the approaches were either failed or abandoned due to failure of forthcoming reactions. In this section both unsuccessful and successful approaches will be discussed.

2.2.1. Unsuccessful and Low Yielding Attempts for the Synthesis of Core Structural Parts of Target Photosensitizers

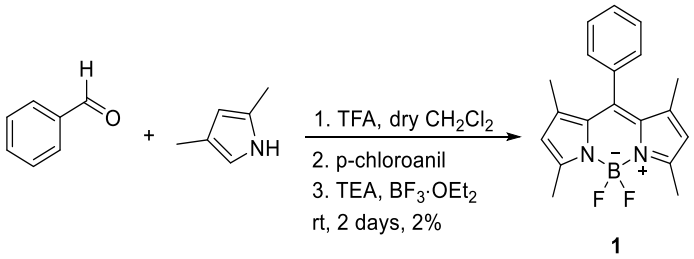

Figure 2.2. Synthesis of compound 1 from benzaldehyde and 2,4-dimethylpyrrole.

In order to synthesize compound **1**, we first used benzaldehyde and 2,4-dimethyl pyrrole. In case of aldehyde, we need an oxidizer such as p-chloloanil or 2,3-dichloro-5,6-dicyanobenzoquinone (DDQ). The reaction is difficult to control due to side

oxidation reactions that occur during this step. Furthermore, use of dated reagents especially, $BF_3.OEt_2$ had an important impact in the lower yields observed in this reaction.

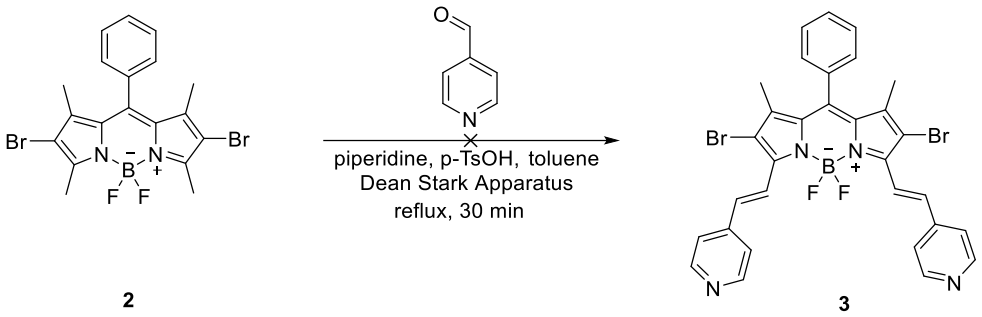

Figure 2.3. Synthesis of compound 3 from compound 2 under the Dean Stark conditions.

Double condensation reactions on BODIPY cores are generally performed with toluene as a solvent under Dean-Stark conditions. However, under these conditions controlling reaction is difficult and generally several number of side products are observed. The difficulty to control the reaction forced us to abandon this methodology.

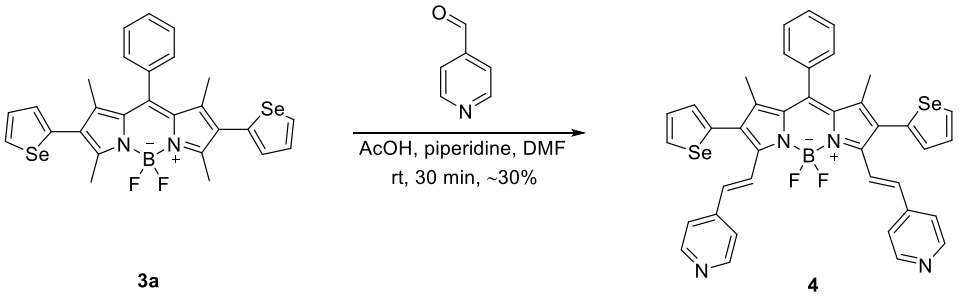

Figure 2.4. Synthesis of compound 4 from compound 3a.

Double condensation reaction was also done with selenophene introduced BODIPY core (compound **3a**). However, during the reaction TLC analysis showed several spots which were eluted closely to the product spot. Due to gruelling purification efforts and low yield, this methodology was abandoned.

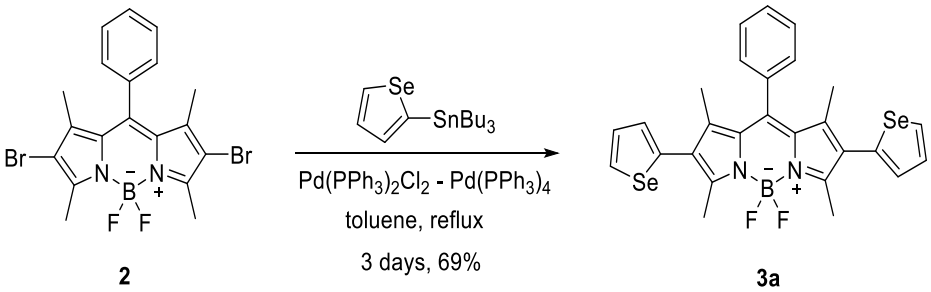

Figure 2.5. Synthesis of compound 3a from compound 2.

In this reaction, a quite acceptable yield was obtained but due to the low yield of the following reaction, which is double condensation reaction, this route was not used.

2.2.2. Succesful Approach for the Synthesis of Core Structural Part of Target Photosensitizers

Scheme 2.1 represents the synthetic pathway for core structural part of the target photosensitizers:

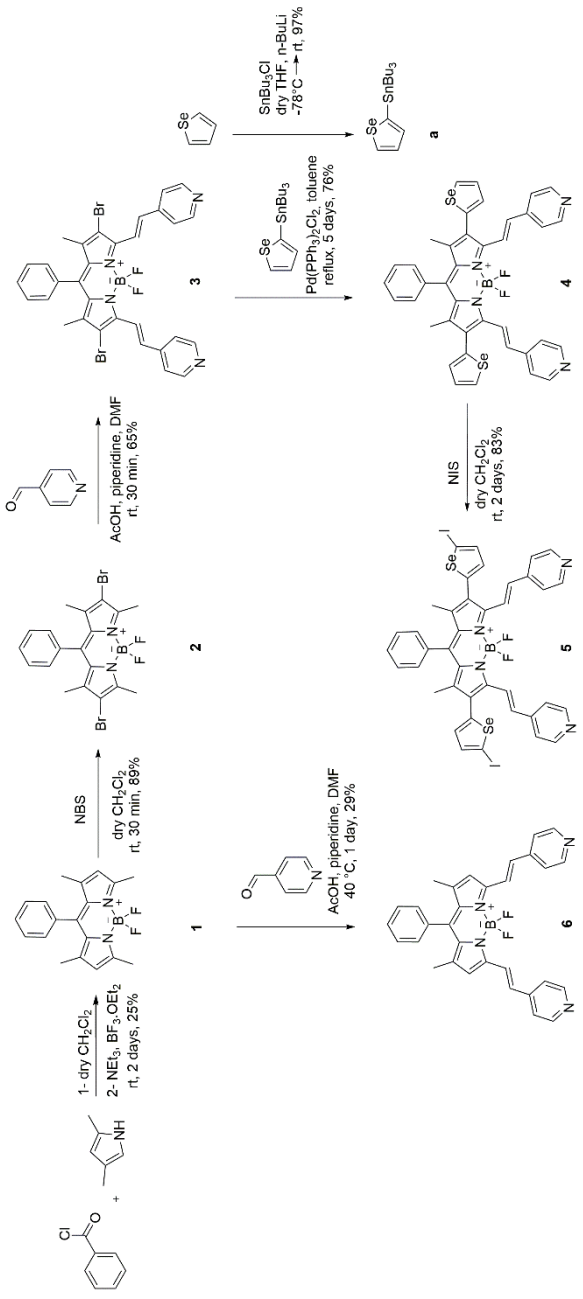

Scheme 2. 1. The synthetic pathway for core structural parts of target photosensitizers.

Synthesis of the target molecules starts with BOD core (**1**) synthesis. Tetra methyl substituted phenyl BODIPY core was synthesized in the presence of benzoyl chloride and 2,4-dimethyl pyrrole. In this synthesis, the yield of the product depends on the purity of the reagents. Changing $BF_3.OEt_2$ with fresh one increased the yield from 6% to 25%. Also, we struggled at the purification step. Excess base and Lewis acid used for BODIPY formation resulting in a complex formation and this complex co-eluted with the product and could not have been monitored with TLC unless oxidized with $KMnO_4$ stain. To purify our product, we applied two column chromatography. First, with eluent system 6:1 hexane:ethyl acetate to separate the complex, then with the eluent system 2:1 DCM: hexane to obtain pure target product. Eventually, we obtained pure compound **1** with reasonable yield (25%) (Chen *et al.* 2012). In the second step, we brominated compound **1** from -2 and -6 positions. First, we used DCM and DMF mixture as a solvent. But removing DMF needs higher temperature and more time. During at that time, we observed some new side-products. After that we used only DCM as a solvent and addition of NBS solution dropwise to reaction medium eliminated the most of the side-products. All in all, compound **2** was synthesized with a high yield (89%) (Bartelmess *et al.,* 2014). Compound **3** was synthesized according to a recently published study where a double condensation on a BODIPY core with benzaldehyde was performed in DMF in good yields (Rio *et al*., 2016). This method was used in our system. However, optimization of the reaction was the most challenging part of the whole synthetic pathway. Product formed just after the addition of AcOH and piperidine and decomposition started before consumption of all starting material. To stop reaction at an optimum point, quenching with water and extraction was tried, however, an emulsion was formed with the presence of insoluble side products. Several workup techniques such as addition of NaCI was tried to increase the ionic strength of the aqueous layer and addition of a few milliliters of isopropanol was tried . Neither of these methods worked and emulsion did not break down. Then we decided to skip workup procedure and DMF was evaporated and column chromatography applied immediately. After optimization of AcOH and piperidine amounts compound **3** was obtained with a sufficient yield (65%). The same

methodology was also applied in the synthesis of compound **6**. The reason for low yield is attributed to the lowered acidity of the methyl protons due to the diminished inductive effect asserted by halogen atoms. The next step of the synthesis was the Stille coupling of compound **3** with the formerly synthesized tributyl(selenophen-2-yl)stannane (**a**) (95%) (Kim *et al.* 2012). Here, TLC analysis showed that the reaction remained unchanged even after prolonged heating. However, a crude NMR analysis showed that the product was attained successfully. Variety of solvent couples were explored, however, compound **3** and compound **4** always co-eluted together which hindered purification efforts. To circumvent this issue, the reaction was continued for 5 days with concurrent addition of catalyst to push the reaction to completion. The approach worked successfully, and target coupled product **4** was attained in satisfying yield (76%) (Dyes *et al.,* 2014). Compound **4** can be effectively iodinated in the presence of NIS to get compound **5** in high yield (83%) (Fu *et al.* 2011).

2.3. Synthesis of Target Photosensitizers and Fluorescent Control

Scheme 2.2 represents the synthetic pathways for the target photosensitizers and fluorescent control:

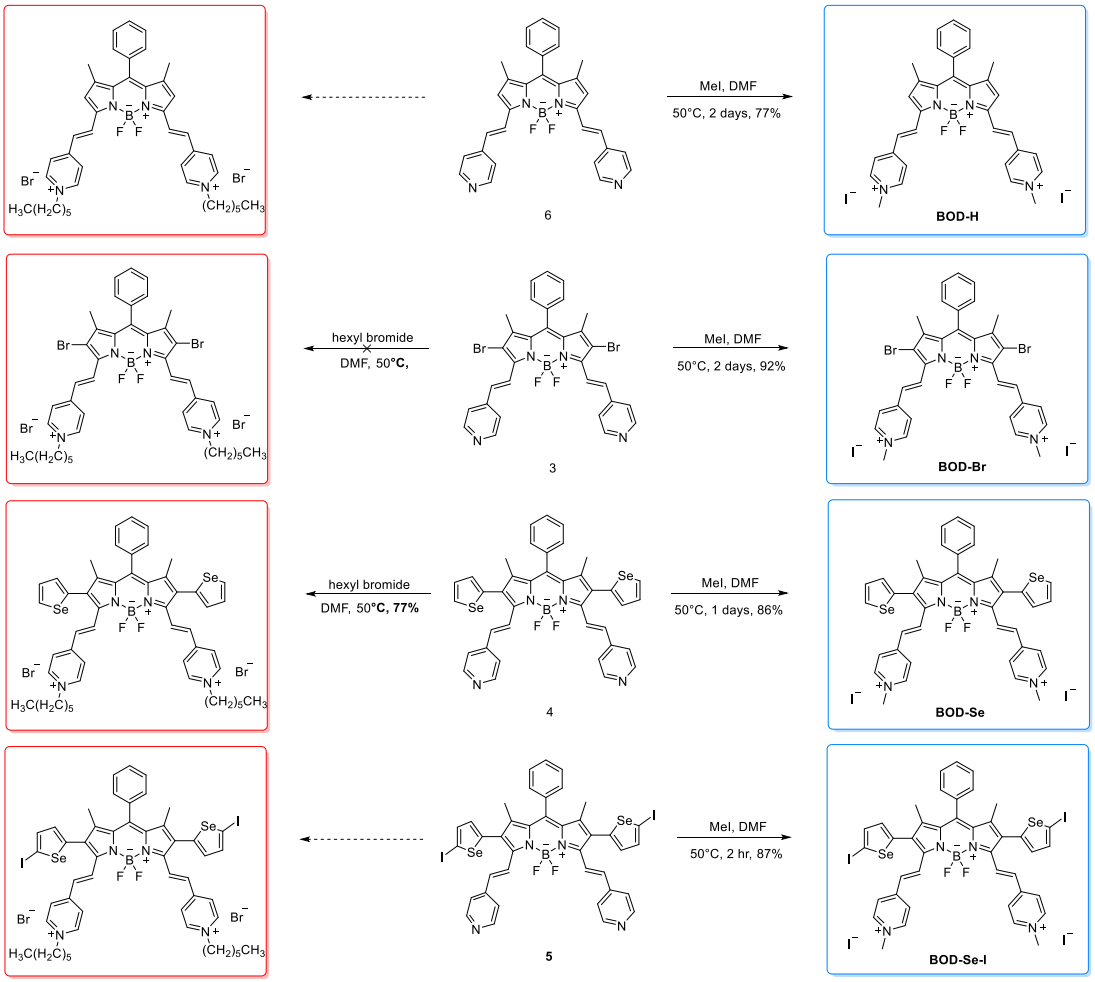

Scheme 2. 2. The synthetic pathway of the target photosensitizers and fluorescent control.

In order to synthesize methyl pyridinium derivatives same methodology was applied. Excess methyl iodide was used in DMF solvent with moderate heating and pure products were gathered by the precipitating the product from reaction mixture by diethyl ether. The target molecules **BOD-H**, **BOD-Br**, **BOD-Se**, and **BOD-Se-I** were synthesized successfully with a yields of 77%, 92%, 86% and 87% respectively (Odeh *et al.*, 2014). In this reaction, an impurity at 3.1 ppm at ^{1}H NMR spectrum was observed which could not be monitored on TLC. Then it was acknowledged that it

belonged to tetramethyl ammonium salt formed by the reaction between DMF decomposition product, dimethylamine and excess methyl iodide. Tetramethyl ammonium salt was then removed by washing with few milliliters of distilled water, exploiting its high water solubility (Neumeyer & Cannon, 1961).

In order to enhance hydrophobicity and mitochondria targeting hexyl pyridinium derivative was also tried to be synthesized by using hexyl bromide reagent under same conditions and as a result, selenophene containing derivative was synthesized successfully. The same procedure was applied in the synthesis of bromo analogue. However, we could not obtain any product. Hexyl bromide was used a lot in excess and the reaction temperature was increased gradually to force the reaction to shift to the product side, but it resulted in the decomposition of the starting material.

Due to failing in synthesis of bromo analogue, other derivatives were not synthesized and further studies focused on methyl pyridinium derivatives.

All in all, water soluble selenophene containing PDT agents **BOD-Se** and **BOD-Se-I** were synthesized from compound **4** and **5** respectively. Compound **3** was also converted to **BOD-Br** to compare its performance with selenium-containing derivatives (**BOD-Se, BOD-Se-I**). Additionally, due to low fluorescence quantum efficiencies of **BOD-Br**, **BOD-Se**, **BOD-Se-I**, no heavy atom containing derivative **BOD-H** was also prepared for fluorescence microscopy imaging studies starting from compound **1**.

2.4. ^{1}H and ^{13}C NMR Spectra of BOD-Se and BOD-Se-I

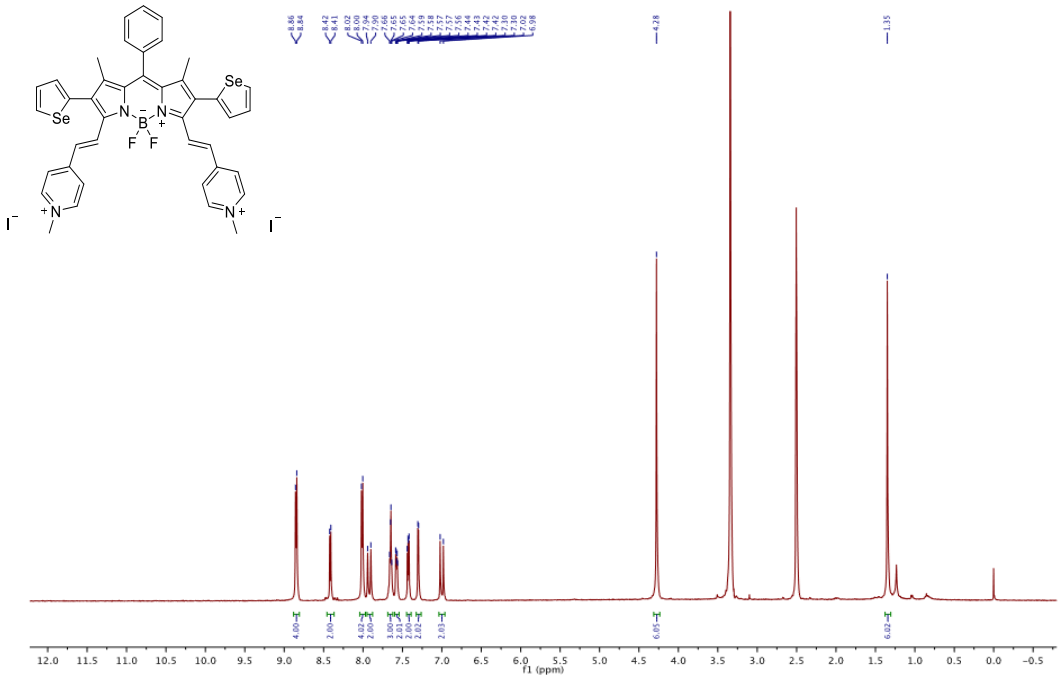

Figure 2.6. ^{1}H NMR Spectrum of compound BOD-Se in DMSO.

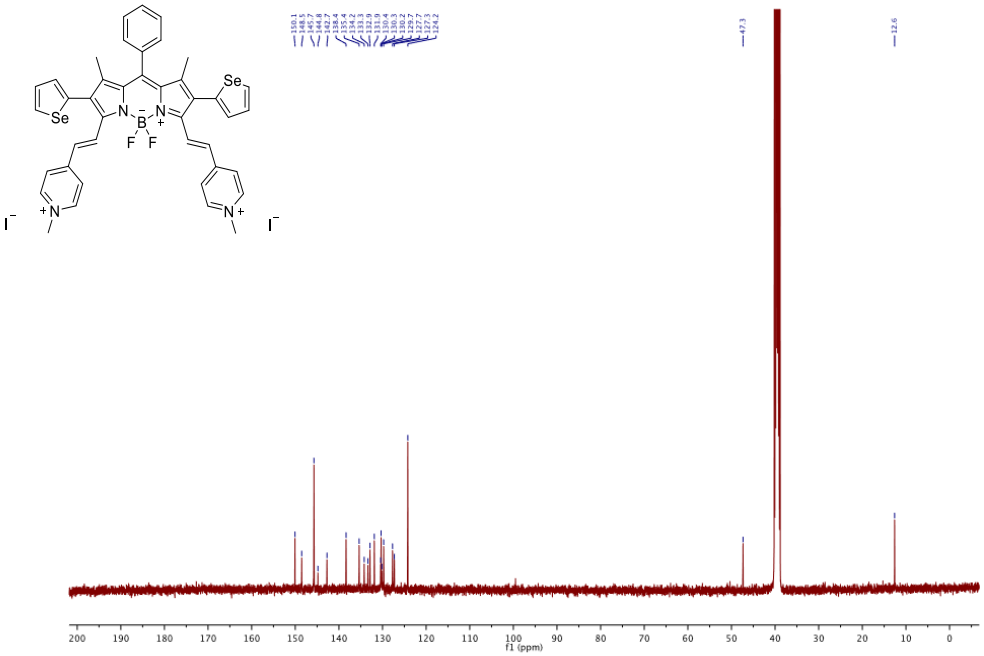

Figure 2.7. ^{13}C NMR spectrum of compound BOD-Se in DMSO.

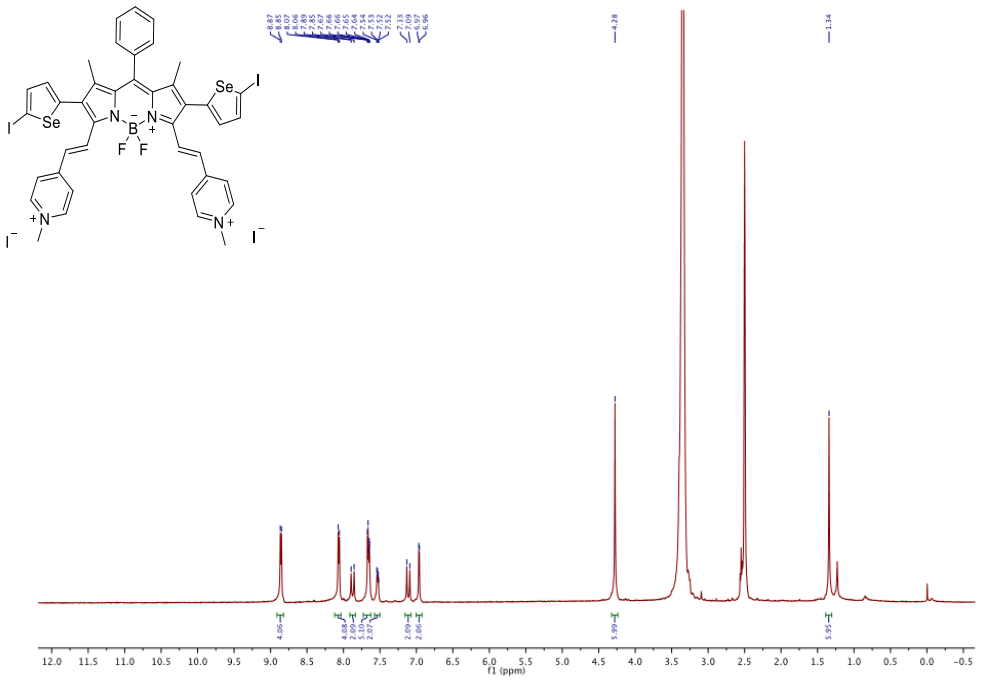

Figure 2.8. ^{1}H NMR spectrum of compound BOD-Se-I in DMSO.

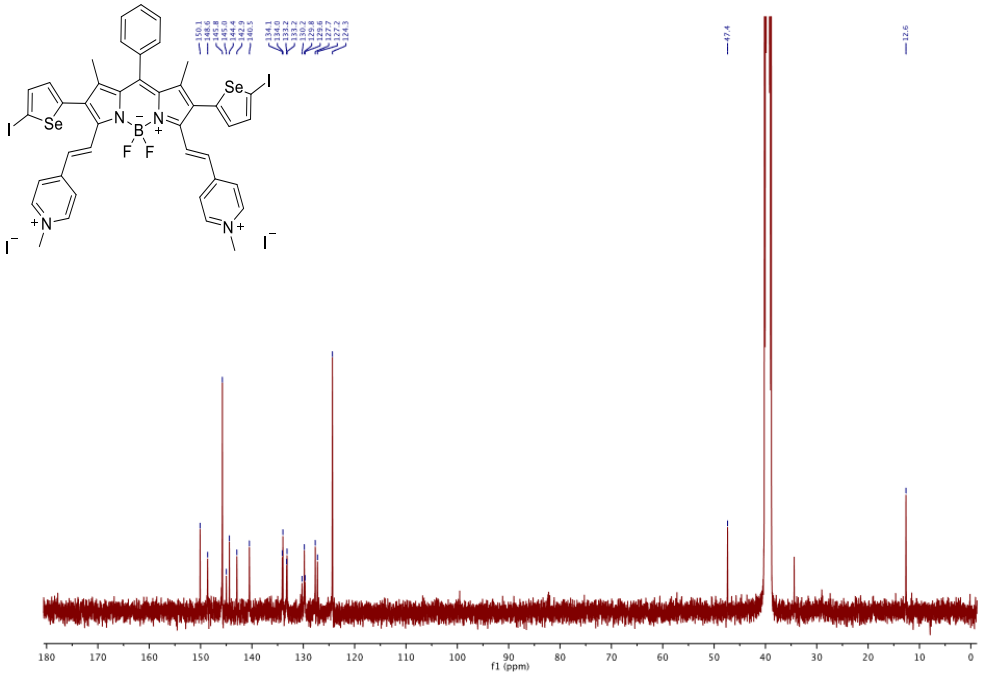

Figure 2.9. ^{13}C NMR spectrum of compound BOD-Se-I in DMSO.

2.5. Optical Properties of Target Photosensitizers

In the design of **BOD-Se** and **BOD-Se-I**, hydrophobic 2,6-Diseleneophenyl BODIPY cores were converted to water-soluble agents by modifying them with methyl pyridinium (MP) moieties through Knoevenagel condensation reaction. Introducing two styryl groups at 3,5-positions extended the π-conjugation on BODIPYs and placed the absorption maxima of the photosensitizers into the therapeutic window as a result of remarkable bathochromic shift. Singlet oxygen generation capacities of both **BOD-Se** and **BOD-Se-I** in aqueous solution were evaluated and compared with the conventional **BOD-Br**. **BOD-Se-I** showed the highest $^1O_2$ quantum yield. The studies were conducted at Koç University under supervision of Assist Prof. Dr. Safacan Kölemen.

The optical properties of the photosensitizers were investigated in aqueous solution (PBS pH 7.4, 1% DMSO) and both **BOD-Se** and **BOD-Se-I** exhibited strong absorption signals above 650 nm as a result of extended π-conjugation (Figure 2.10, Table 2.1). Absorption maxima were slightly red-shifted (5-10 nm) compared to conventional halogenated BODIPYs bearing MP moieties (**BOD-Br**, Figure 2.12, Table 2.1) showing the minor contribution of selenophene ring to the BODIPY π-system. As expected, both photosensitizers are almost non-fluorescent predominately due to the heavy atom effect. However, exceptionally low fluorescence quantum yields of **BOD-Se** and **BOD-Se-I** can be further attributed to the presence of intramolecular charge transfer (ICT) character originating from the cationic MP groups and other thermal relaxation pathways.

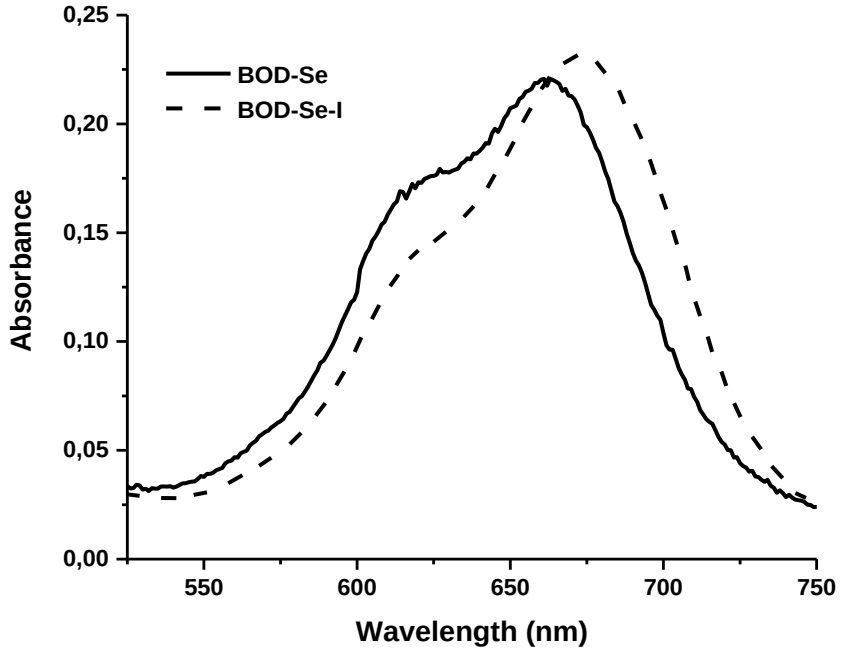

Figure 2.10. Absorption spectra of BOD-Se (5 μM) and BOD-Se-I (5 μM) in PBS buffer (pH 7.4, 1% DMSO).

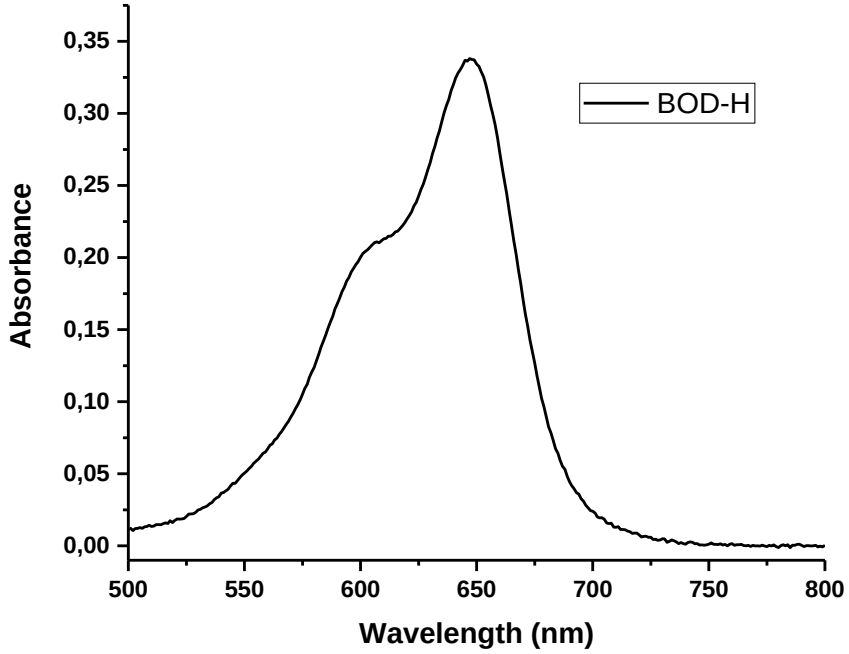

Figure 2.11. Absorption spectra of BOD-H (5 μM) in PBS buffer (pH 7.4, 1% DMSO).

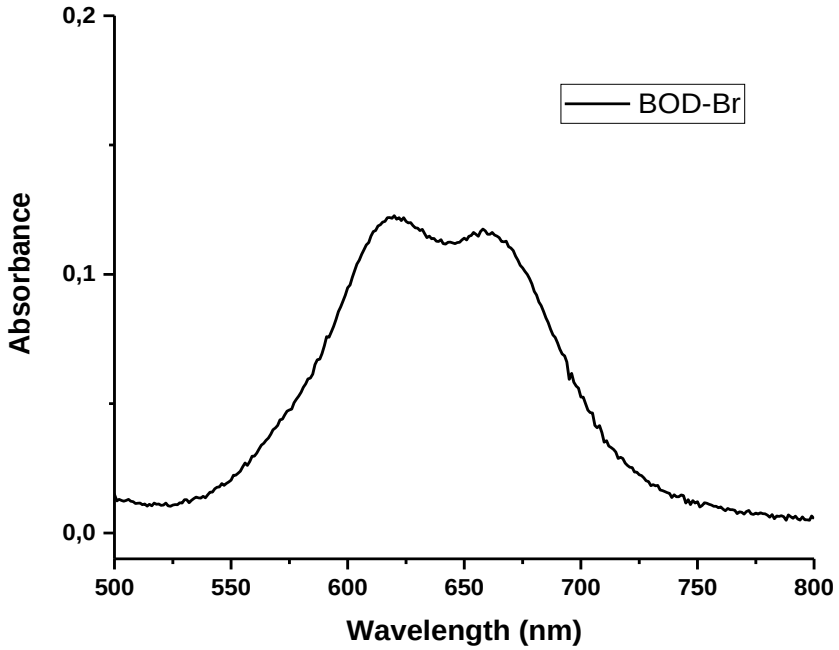

Figure 2.12. Absorption spectra of BOD-Br (5 μM) in PBS buffer (pH 7.4, 1% DMSO).

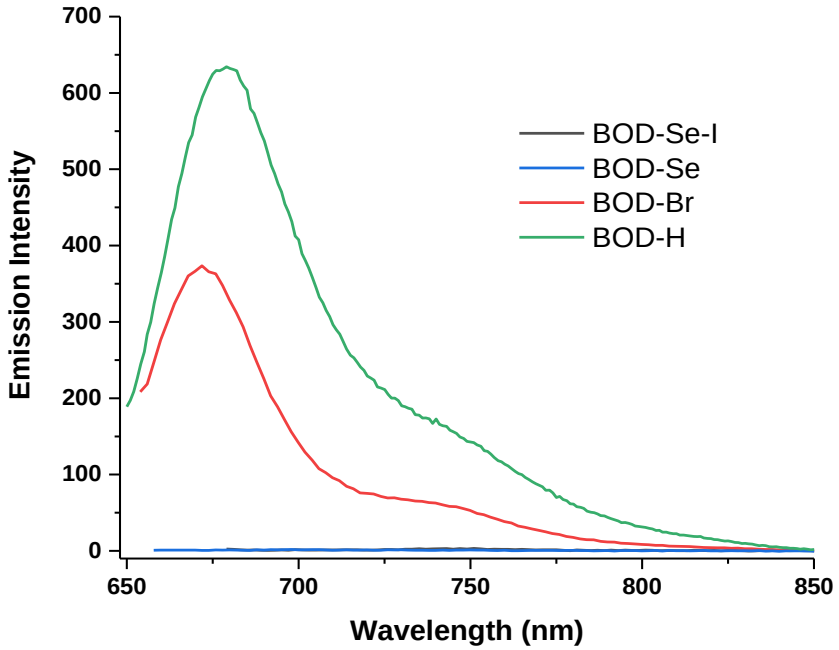

Figure 2.13. Fluorescence spectra of BODIPYs in PBS buffer (pH 7.4, 1% DMSO).

Table 2.1. *Photophysical properties and singlet oxygen quantum yields of the BODIPY derivatives.*

PDT Agents	λ_{abs} / nm[(a)]	ε / M^{-1} cm^{-1} [(a)]	λ_{ems} / nm[(a)]	φ_F (%)[(a,b)]	φ_Δ (%)[(a,c)]
BOD-Br	658	24000	671	8.0	10
BOD-Se	663	44000	n.d. [(d)]	n.d.[(d)]	17
BOD-Se-I	671	46000	n.d. [(d)]	n.d. [(d)]	32
BOD-H	647	68000	679	10.0	n.d. [(d)]

(a) measured in PBS buffer (pH 7.4, 1% DMSO) (b) calculated via spectrophotometer with integrated sphere detector (c) methylene blue was used as a reference in PBS buffer (φ_Δ = 0.52) (d) not determined.

Singlet oxygen generation capacities of the photosensitizers were evaluated by using a water-soluble trap molecule 2,2'-(anthracene-9,10-diyl)bis(methylene)dimalonic acid (ADMDA) in aqueous solutions (PBS pH 7.4, 1% DMSO). Upon irradiation of **BOD-Se-I** and **BOD-Se** with a 630 nm light-emitting diode (LED) light (4.0 mW cm^{-2}), a gradual decrease in the absorbance of ADMDA at 380 nm was detected in each case, clearly indicating the photosensitized singlet oxygen generation (Figure 2.14). The $^1O_2$ quantum yields were calculated by using methylene blue (φ_Δ = 0.52 in PBS buffer) as a reference and were found to be 0.32, 0.17 and 0.10 for **BOD-Se-I** and **BOD-Se** and **BOD-Br** respectively (Table 2.1.). **BOD-Se-I** showed a higher yield compared to both **BOD-Se** and the previously reported halogenated BODIPY that have MP groups on their structures (**BOD-Br**), as it exhibits stronger heavy atom effect, which is in good agreement with our design principles.

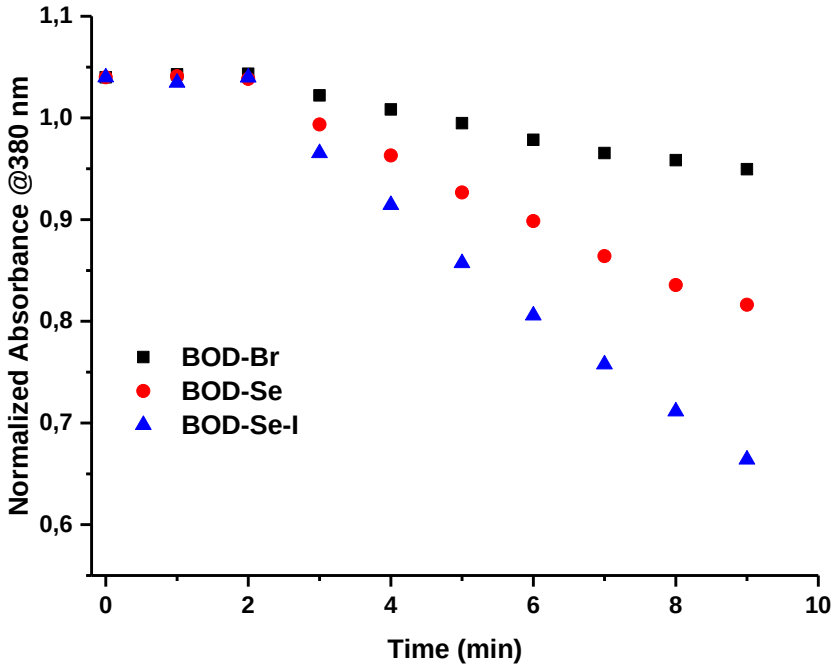

Figure 2.14. Relative $^1O_2$ generation efficiency of the photosensitizers (5 μM) (BOD-Br), (BOD-Se) and (BOD-Se-I) in PBS buffer (pH 7.4, 1% DMSO) as evidenced by the decrease in the absorbance of ADMDA at 380 nm. During first 2 minutes, the samples were kept in the dark.

2.6. In Vitro Cell Studies

2.6.1. Mitochondrial Co-localization Studies

Subcellular accumulation of MP containing BODIPYs was examined by staining the HeLa and NIH 3T3 with commercially available MitoTracker Green and **BOD-H** under fluorescence microscope. **BOD-H** is a heavy atom free and emissive analogue of **BOD-Se-I**, which carries the same mitochondria targeting MP moieties (Figure 2.16, Table 2.1). Figure 2.16. clearly demonstrates the selective mitochondria localization of MP containing **BOD-H** in HeLa cells with a Pearson's correlation coefficient of 0.82. In the case of NIH 3T3, the overlap is weaker (0.62) as expected due to the lower membrane potential of healthy cells (Shin *et al.*, 2016).

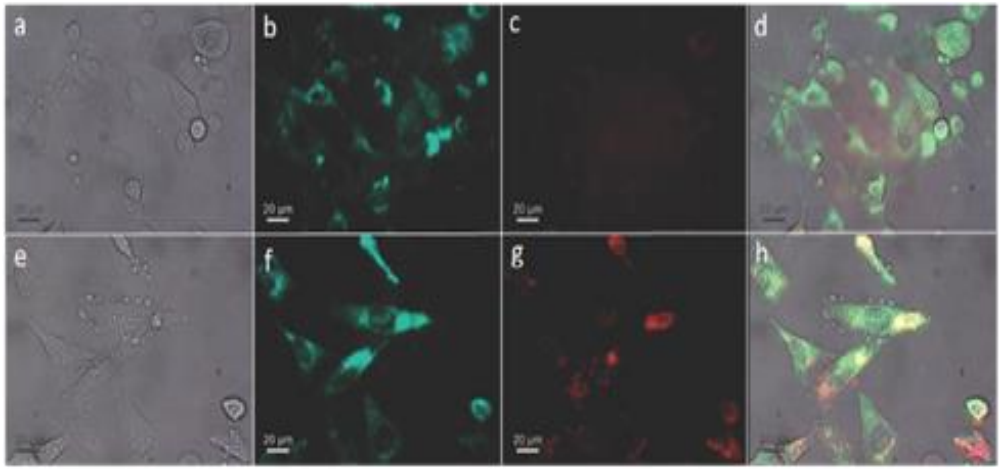

Figure 2.15. Fluorescence microscopy images of BOD-H and MitoTracker Green in NIH 3T3 (top): (a) DIC, (b) MitoTracker Green, (c) BOD-H, (d) merged and HeLa cells (bottom): (e) DIC, (f) MitoTracker Green, (g) BOD-H, (h) merged

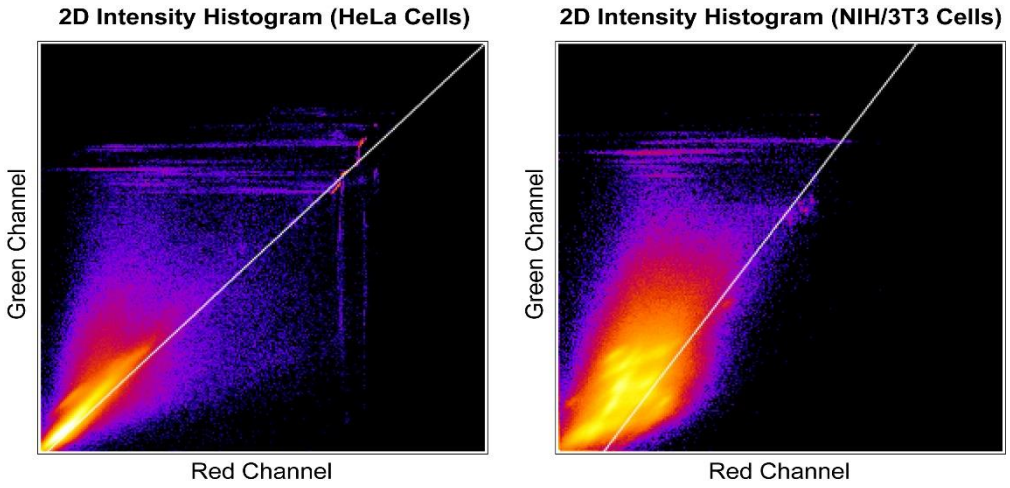

Figure 2.16. Fluorescence intensity correlation plot of BOD-H (red channel) with Mitotracker Green (green channel) in HeLa (left) and NIH 3T3 (right) cells.

2.6.2. Cytotoxicity Analysis of BOD-Se-I

In vitro PDT effect of **BOD-Se-I** was further tested in different cell cultures. Varying concentrations of the drug was incubated with HeLa and normal NIH 3T3 cells. Cells were irradiated with a LED light (660 nm) for 4 hours and then kept at dark for 20 hours in order to provide sufficient time for apoptosis. Cytotoxicity of the drug was examined by a regular MTT (3-(4,5-dimethylthiazol)-2,5-diphenyltetrazolium bromide) assay. Cell viability decreased gradually in HeLa cancer cells as the

concentration of the drug increases (Figure 2.17). IC_{50} value was calculated as 0.29 μM, showing the high efficacy of the drug in HeLa cells. Apoptotic cell death was also confirmed under fluorescence microscopy by staining the HeLa cells with an apoptotic cell marker Annexin V-FTIC. In contrast, **BOD-Se-I** exhibited lower cytotoxicity in non-cancerous NIH-3T3 cells with a higher IC_{50} value (2.37 μM) (Figure 2.18). The NIH 3T3 cells incubated with 625 nM **BOD-Se-I** maintained 70% cell viability, while HeLa cells showed only 25% viability at the same concentration (Figure 2.20). Cancer cell selectivity can be attributed to the different mitochondrial membrane potential of cancerous and healthy cells, which leads to preferential localization of the drug in cancer cell mitochondria and enhances the cytotoxicity by triggering the mitochondria induced apoptosis in cancer cells (Shin *et al.*, 2016). **BOD-Se-I** showed negligible dark toxicity in both cell types as evidenced by the high survival rate of the cells when there is no light illumination (Figure 2.19, Figure 2.20). In good correlation with the singlet oxygen trap experiments, **BOD-Se-I** gave better results in HeLa cells compared to **BOD-Br** (Figure 2.17). In NIH-3T3 fibroblast cells, **BOD-Br** performed similarly to the **BOD-Se-I** and showed low cytotoxicity (Figure 2.18).

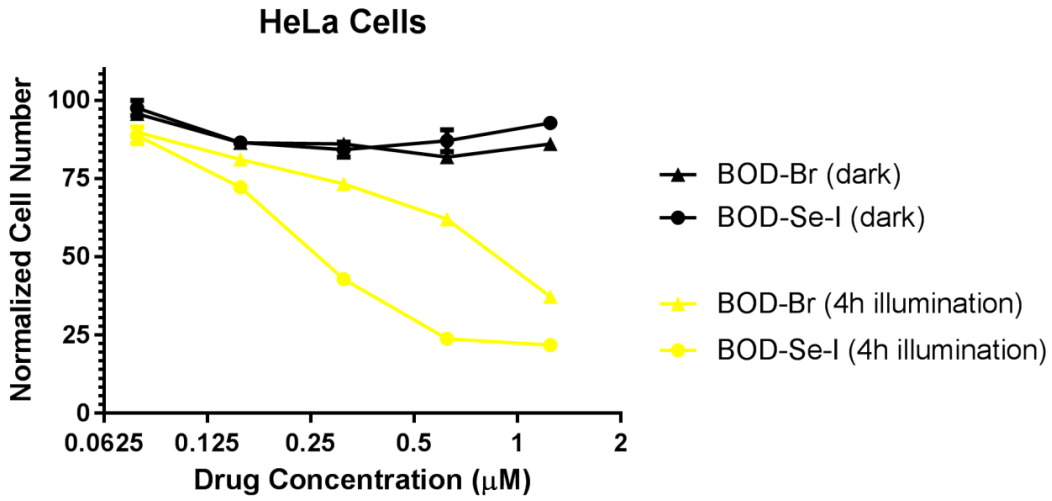

Figure 2.17. In vitro cell viability graph of BOD-Br and BOD-Se-I in HeLa cells under dark and 4h light illumination.

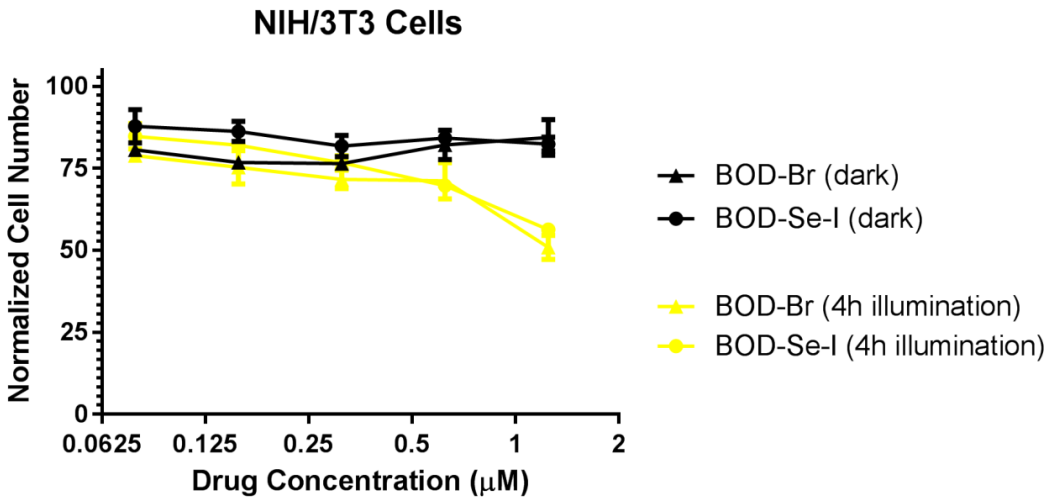

Figure 2.18. In vitro cell viability graph of BOD-Br and BOD-Se-I in NIH 3T3 cells under dark and 4h light illumination.

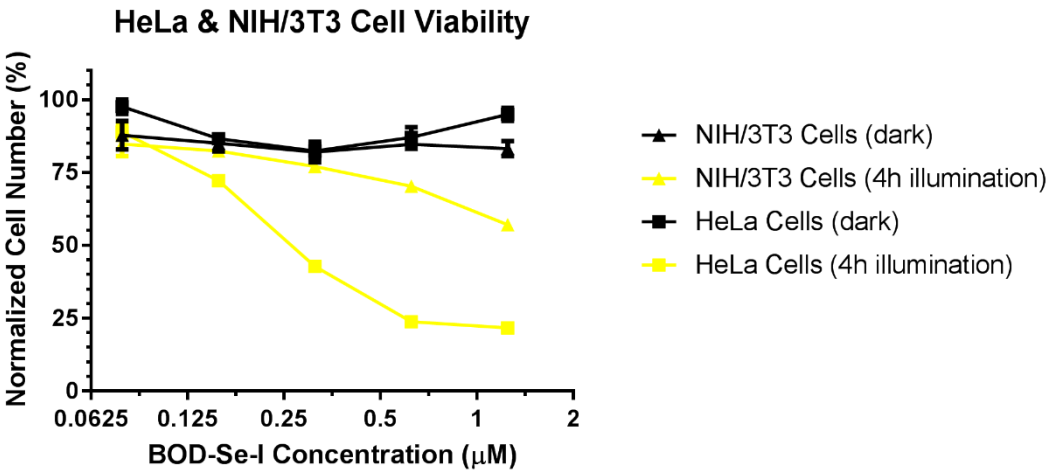

Figure 2.19. In vitro cell viability of HeLa and NIH 3T3 cells as evidenced by the MTT assay. The cells were incubated with varying concentrations of BOD-Se-I and either kept at dark or irradiated for 4 hours with a 660 nm LED.

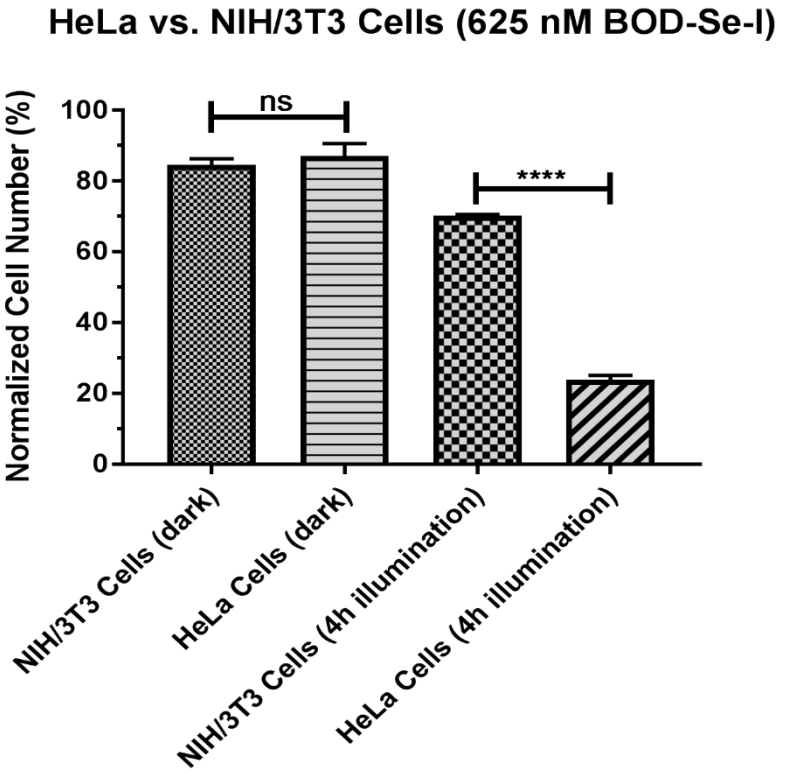

Figure 2.20. Demonstration of Cell viability difference between cancerous HeLa and healthy NIH 3T3 cells when they were incubated with 625 nM BOD-Se-I (ns: not significant, ****,p <0,0001)

Finally, phototoxicity of the **BOD-Se-I** in HeLa cells was tested under hypoxic conditions (5% O_2). To do so, cells were incubated with the drug and then placed into the hypoxia chamber. Oxygen level in the chamber was adjusted to 5% by purging N_2/O_2 gas mixture continuously. Before MTT assay, cells were irradiated with 660 nm LED for 4 hours and then kept at dark for 20 hours. Cell viability results showed that under hypoxic conditions IC_{50} value (0.90 μM) of **BOD-Se-I** is higher compared to normoxia (0.29 μM) as a result of reduced oxygen level, however it is important to note that at slightly high concentrations (1.25 μM) cell viability ratio is close to the one at normoxic conditions, suggesting high PDT efficiency of **BOD-Se-I** even under hypoxia (Figure 2.21). The efficacy of **BOD-Se-I** under hypoxic conditions was also compared with the micelle embedded **compound 5** (ctrl-BOD), which lacks the mitochondria targeting moiety. IC_{50} value (4.60 μM) was found to be higher compared to mitochondria localized **BOD-Se-I**, clearly indicating the role of high mitochondrial

oxygen content in PDT action under hypoxia. Comparison of IC_{50} values are given in figure 2.22.

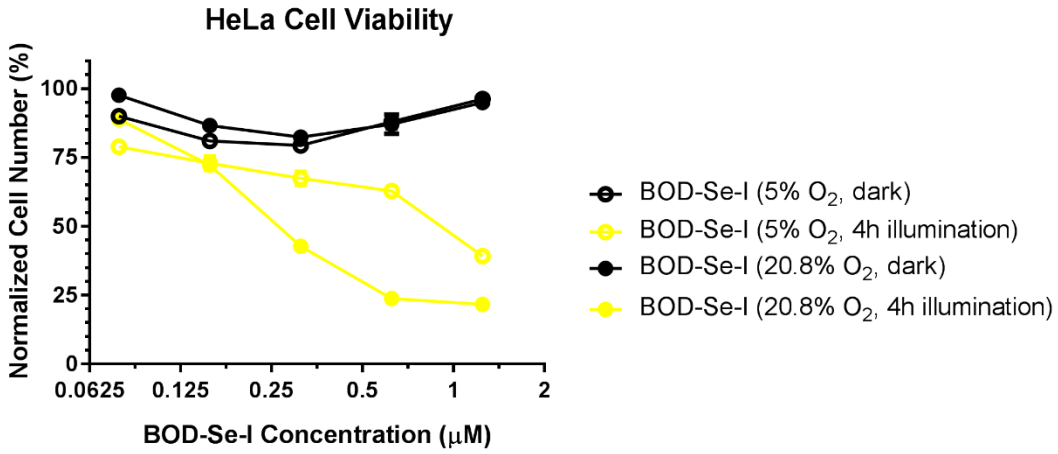

Figure 2.21. Cell viability graph of BOD-Se-I in HeLa cells under hypoxia and normoxia conditions.

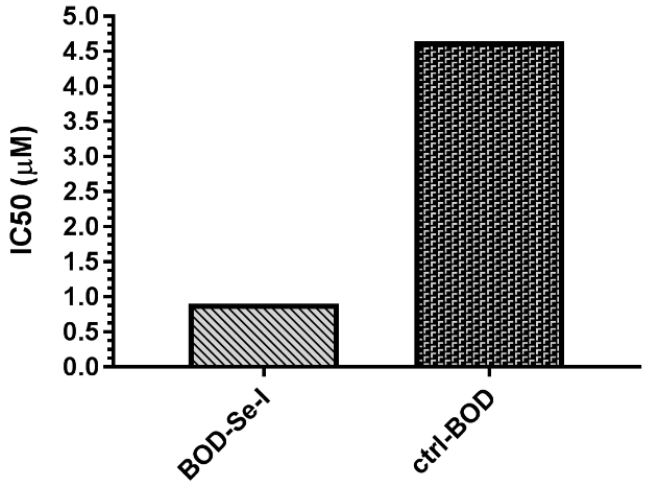

Figure 2.22. Demonstration of IC_{50} value difference of BOD-Se-I and compound 5 (ctrl-BOD)

2.7. Enhancement of Target Photosensitizers

2.7.1. Necessity of Advanced Target Photosensitizers

Although target photosensitizers showed good performance in vitro cell studies and in singlet oxygen generation, they could not come up to absorbance maxima expectations. Introducing selenophene did not make remarkable difference due to steric congestion, which resulted in low level of planarization with the BODIPY core. As a consequence of lower than expected absorption maxima of target photosensitizers, enhancements on target molecules has emerged. It is well known that in the literature, introducing acetylene to the BODIPY core has great impact on absorption maxima (Jiao *et al.*, 2010). So, considering this knowledge, advanced version of former target photosensitizers were designed and one of them was synthesized in this thesis study.

2.7.2. Synthesis of Advanced Target Photosensitizers

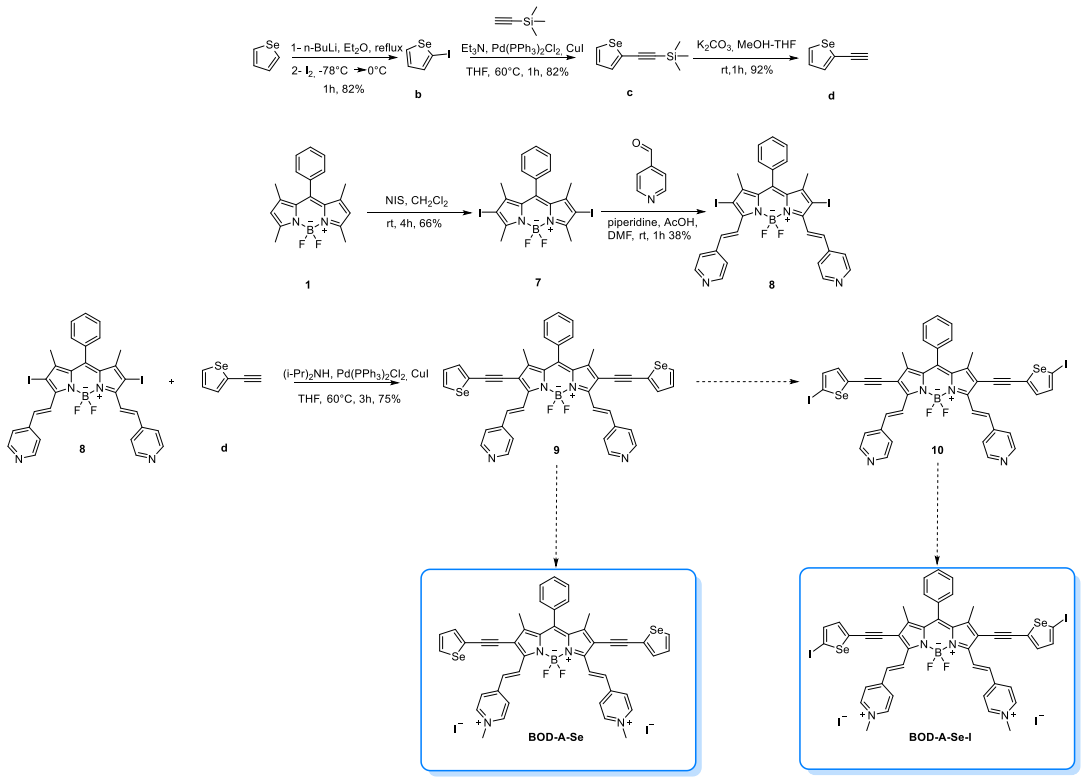

Scheme 2. 3. Synthetic pathway of advanced photosensitizers.

Synthesis of advanced target photosensitizers covers synthesis of compound **8** and compound **d** and combination of them to yield compound **9**. Compound **9** can either be converted to compound **10** which is the precursor of the target photosensitizer **BOD-A-Se-I** or can be directly converted to target photosensitizer **BOD-A-Se**. Synthesis of compound **d** started with iodination of selenophene. Rate of dropwise addition is the key parameter of reaching high yield (82%) (Takahashi & Tarutani, 1996). In the second step first Sonogashira coupling reaction was done. We did Sonogashira coupling reaction in the presence of the $Pd(PPh_3)_2Cl_2$, CuI and PPh_3 in catalytic amounts in THF media at room temperature. However, product was not obtained. Conditions were revised according to literature (Shigeta *et al.* 2013). Treatment of starting materials with Et_3N and heating reaction up to 60 °C was proved to be effective for convertion of the starting material to target compound **c** in a good yield (82%). Finally, deprotection of TMS was done with K_2CO_3 in MeOH-THF mixture. First reaction was performed in small scale however; product obtained in a very low yield even TLC shows all starting material converted to product. Reason of the low yield should be low boiling point of compound d. So reaction repeated with quite larger scale with and the product was concentrated with extra care. Overall, reaction yielded to compound **d** in a high yield (92%) (Boydston *et al.* 2002). In the first step of the synthesis of compound **8**, compound **1**, which was formerly synthesized, iodinated with NIS in DCM. Yield of the reaction was quite low compared to bromination of compound **1**. An appreciable amount of mono-iodinated product was obtained. 66% of the starting material was converted to di-iodinated form of compound **1** which is labeled as compound **7**. Then compound **8** was obtained by Knoevenagel type reaction under the knowledge gained from the synthesis of compound **3**. Reaction conditions should be optimized to reach higher yield. Compound **8** was obtained in a quite low but acceptable yield (38%) considering the difficulty of control in this reaction. Combination of compound **8** and compound **d** done with the Sonogashira coupling reaction. First starting materials treated with $(i\text{-}Pr)_2NH$ then $Pd(PPh_3)_2Cl_2$ and CuI was added in a catalytic amount. Reaction mixture heated up to 60 °C. Reaction finished after 3 hours of stirring at that temperature

according to TLC. Crude product was purified by flash column chromatography and compound **9** isolated in a good yield. (75%) (Lobo *et al.* 2017). In future studies, compound **9** will converted to compound **10** with NIS and both compound **9** and compound **10** will converted to desired, advanced target photosensitizers **BOD-A-Se** and **BOD-A-Se-I** respectively.

2.7.3. Optical Properties of Advanced Target Photosensitizers

The optical properties of the photosensitizers were investigated in an organic media (DCM) and compound **9** exhibited strong absorption signal at 666 nm as a result of acetylene groups (Figure 2.23). Absorption maxima were red-shifted (40 nm) compared to compound **4.**

Singlet oxygen generation ability of compounf **9** was proved by trap experiment in organic media (DCM) by using trap molecule 1,3-diphenlyisobenzofuran (DPBF). Upon irradiation of compound **9** with a 633 nm light-emitting diode (LED) light (4.0 mW cm^{-2}), a gradual decrease in the absorbance of DPBF at 410 nm was detected in each case, clearly indicating the photosensitized singlet oxygen generation (Figure 2.23). Singlet oxygen generation efficacy and emission maxima of compound **9** have not been determined yet.

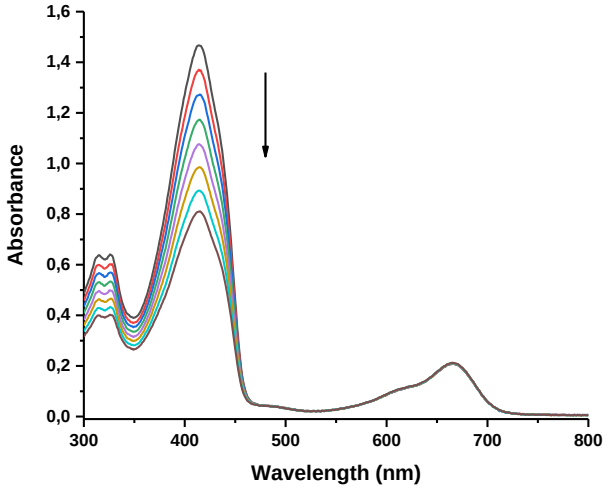

Figure 2.23. Decrease in the absorbance of DPBF in DCM upon irradiation of compound 9 (5 μM).

CHAPTER 3

CONCLUSION

In this thesis study, two novel, red absorbing, water soluble and mitochondria-targeted photosensitizers bearing either selenophene (**BOD-Se**) or 2-iodoselenophene (**BOD-Se-I**) units on 2,6-positions of BODIPY core were designed and synthesized. Additionally, to extend absorption maxima of target photosensitizers acetylene substituted derivatives **BOD-A-Se** and **BOD-A-Se-I** were designed and compound **9** which is the precursor of these advanced target photosensitizers were successfully synthesized.

This thesis study marks the first cell studies utilizing a selenophene containing BODIPY derivative. Study also highlights the first example of a mitochondria targeted selenophene containing BODIPY dye, which performs effectively under hypoxic conditions.

The optical properties of the target photosensitizers were investigated with the collaboration of Assist. Prof. Dr. Safacan Kölemen and his research group. **BOD-Se** and **BOD-Se-I** exhibited strong absorption signals above 650 nm. Absorption maxima were slightly red-shifted compared to **BOD-Br**, which was synthesized for comparing its performance to selenium containing derivatives. **BOD-Se-I** showed higher singlet oxygen generation yield compared to both **BOD-Se** and **BOD-Br,** which is in good agreement with our design principles. Accordingly, **BOD-Se-I** was chosen as a model photosensitizer for in vitro cell culture studies.

BOD-H, which is the heavy atom free and emissive analogue of **BOD-Se-I** was used to show subcellular accumulation of the target photosensitizers. Results reveal selective mitochondria localization of **BOD-H** in HeLa cells and weaker overlap in NIH 3T3 cells.

In vitro PDT effect of **BOD-Se-I** was tested in HeLa and NIH 3T3 cells under normoxic and hypoxic conditions with presence and lack of light illumination. Results showed that, in normoxic conditions (20.8% O_2), cell viability decreased gradually in HeLa cancer cells as the concentration of the drug increases. Low IC_{50} value indicates the high efficacy of the drug. **BOD-Se-I** exhibited lower cytotoxicity in non-cancerous NIH-3T3 cells with a higher IC_{50} value. **BOD-Se-I** showed negligible dark toxicity in both cell types as evidenced by the high survival rate of the cells when there is no light illumination. In good correlation with the singlet oxygen trap experiments, **BOD-Se-I** gave better results in HeLa cells and NIH 3T3 cells compared to **BOD-Br**. Photocytotoxicity of **BOD-Se-I** in HeLa cells and NIH 3T3 was further tested under hypoxic conditions (5% O_2). Cell viability results showed that under hypoxic conditions **BOD-Se-I** has higher IC_{50} value compared to normoxia. The efficacy of **BOD-Se-I** under hypoxic conditions was also compared with the compound **5**, which lacks the mitochondria localizing moieties, in order to evaluate the effect of mitochondria targeting. IC_{50} value of micelle-embedded compound **5** was found to be much higher compared to mitochondria localized **BOD-Se-I**, clearly indicating the role of high mitochondrial oxygen content in PDT action under hypoxic conditions.

As a consequence of lower than expected absorption maxima of target photosensitizers, enhancements on target molecules were designed. Acetylene introduced target photosensitizers **BOD-A-Se** and **BOD-A-Se-I** were designed and their precursor compound **9** was synthesized. Optical properties of compound **9** indicates advanced target photosensitizers show longer absorption maxima compared to compound **4**. As a future work, advanced target photosensitizers **BOD-A-Se** and **BOD-A-Se-I** will be synthesized and their optical properties and in vitro studies will be performed.

CHAPTER 4

EXPERIMENTAL

4.1. Materials and Methods

The ^{1}H and ^{13}C-NMR spectra were recorded on a Bruker Avance III Ultrashield (400 MHz) spectrometer. The chemical shifts are reported in parts per million (ppm) downfield from an internal TMS (trimethylsilane) reference. Coupling constants (J) are reported in hertz (Hz), and the spin multiplicities were specified by the following symbols: s (singlet), d (doublet), t (triplet), and m (multiplet). NMR spectrums were processed with MestReNova program. Column chromatography was performed by using thick walled glass columns and silica Gel 60 (Merck 230-400 mesh). Thin layer chromatography (TLC Merck Silica Gel 60 F254) was performed by using commercially prepared 0.25 mm silica gel plates and visualization was provided by UV lamp. The relative proportions of solvents in chromatography solvent mixtures refer to the volume: volume ratio. All reagents were commercial available and used without further purification unless otherwise noted. All dry solvents used in reactions were directly obtained from the Mbraun MBSPS5 solvent drying system. The inert atmosphere was obtained by Argon.

4.2. Equipments

$CDCl_3$ and d6-DMSO was used as the solvents for the ^{1}H and ^{13}C-NMR analyses on Bruker Spectrospin Avance DPX-400 Spectrometer and tetramethylsilane was used as the internal reference. High resolution mass spectroscopy was performed in order to determine the exact masses of the novel synthesized compounds using Waters Synapt MS System.

4.3. Synthesis of Compound 1

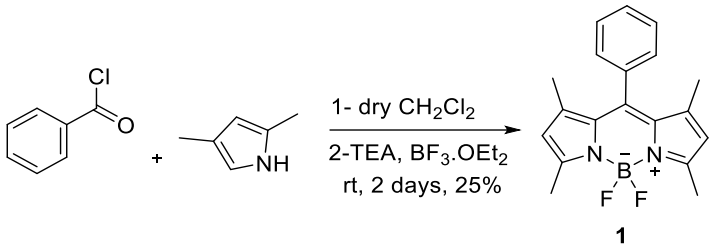

Figure 4.1. Synthetic route of compound 1.

To a 250 mL two neck flask dry CH_2Cl_2 (95 mL) was added and the solvent was purged with argon for 1 hour. Then, 2,4-dimethylpyrrole (1.20 g, 12.6 mmol) and benzoyl chloride (0.975 g, 6.94 mmol) was added and the mixture was stirred under Argon (Ar) atmosphere at room temperature (rt) overnight. Triethylamine (6.5 mL, 47 mmol) and $BF_3.OEt_2$ (6.5 mL, 54 mmol) were added dropwise at 0 °C respectively, and the mixture was stirred overnight at rt. Then the mixture was washed with water (100 mL) and saturated Na_2CO_3 (100 mL). The organic layer was dried over anhydrous Na_2SO_4 and the solvent was evaporated under reduced pressure. The crude product was purified by column chromatography (silica gel, ethyl acetate:hexane – 7:1) to yield the target product as an orange solid (0.511 g, 25%) ^{1}H NMR (400 MHz, $CDCl_3$) δ: 7.51 – 7.44 (m, 3H), 7.32 – 7.23 (m, 2H), 5.98 (s, 2H), 2.56 (s, 6H), 1.37 (s, 6H); ^{13}C NMR (100 MHz, $CDCl_3$) δ: 155.4, 143.2, 141.7, 135.0, 131.4, 129.1, 128.9, 127.9, 121.2, 14.6, 14.3.

4.4. Synthesis of Compound 2

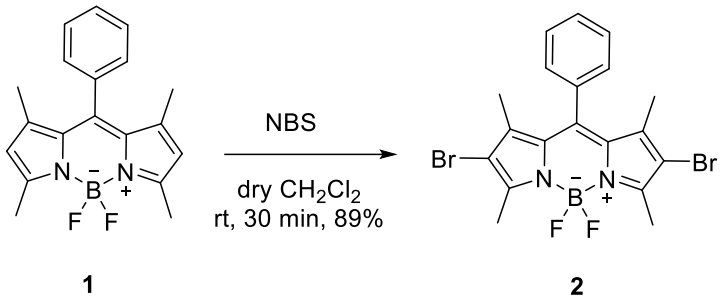

Figure 4.2. Synthetic route of compound 2.

To a solution of compound **1** (0.200 g, 0.616 mmol) in dry CH_2Cl_2 (30 mL), solution of *N*-bromosuccinimide (NBS) (0.275 g, 1.54 mmol) in dry CH_2Cl_2 (20 mL) was added slowly. After 30 min stirring at rt, thin layer chromatography (TLC) showed that the reaction was completed. The crude product was washed with water (50 mL) and then brine (50 mL). The organic layer was dried over anhydrous Na_2SO_4 and the solvent was evaporated under reduced pressure. The crude product was purified by column chromatography (silica gel, hexane: CH_2Cl_2 – 1:1) to yield target the product as a dark red solid (0.265 g, 89%) ^{1}H NMR (400 MHz, $CDCl_3$) δ: 7.56 – 7.49 (m, 3H), 7.29 – 7.23 (m, 2H), 2.61 (s, 6H), 1.37 (s, 6H); ^{13}C NMR (100 MHz, $CDCl_3$) δ: 154.1, 142.3, 140.8, 134.5, 130.6, 129.7, 129.6, 127.9, 111.9, 13.8.

4.5. Synthesis of Compound 3

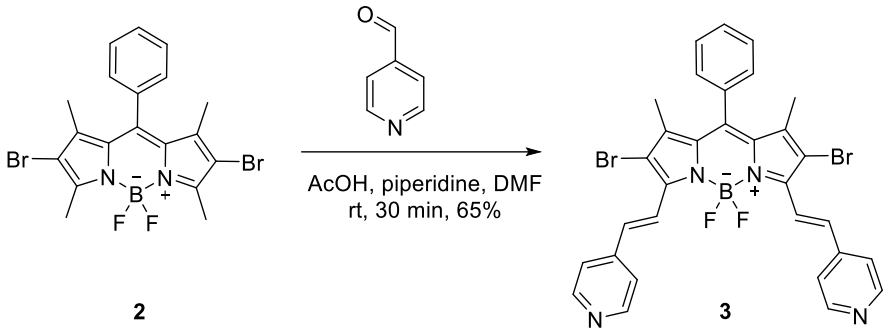

Figure 4.3. Synthetic route of compound 3.

In a 10 mL schlenck tube, compound **2** (50.0 mg, 0.104 mmol) and 4-pyridinecarboxyaldehyde (44.0 mg, 0.411 mmol) was dissolved with dry DMF (3.3 mL). To this solution, piperidine (0.2 mL) and acetic acid (0.2 mL) was added dropwise respectively. After 30 min, the TLC showed that the reaction was completed. The reaction solvent was evaporated under reduced pressure immediately. Then, the crude product was purified by column chromatography (silica gel, $CHCl_3$: MeOH – 98:2) to yield target the product as a blue solid (33 mg, 65%) ^{1}H NMR (400 MHz, $CDCl_3$) δ: 8.68 (d, 4H, *J* = 6.0 Hz), 8.05 (d, 2H, *J* = 16.7), 7.88 (d, 2H, *J* = 16.7), 7.61 – 7.57 (m, 3H), 7.55 (d, 4H, *J* = 6.0 Hz), 7.32 – 7.29 (m, 2H), 1.45 (s, 6H). ^{13}C NMR (100 MHz, $CDCl_3$) δ: 150.2, 147.9, 144.0, 142.4, 142.0, 136.4, 134.2, 132.8, 130.0, 129.7, 127.9, 122.1 121.5, 111.3, 13.8. HRMS calculated for $C_{31}H_{23}BBr_2F_2N_4$: 661.0408. Found: 661.0439.

4.6. Synthesis of Compound 4

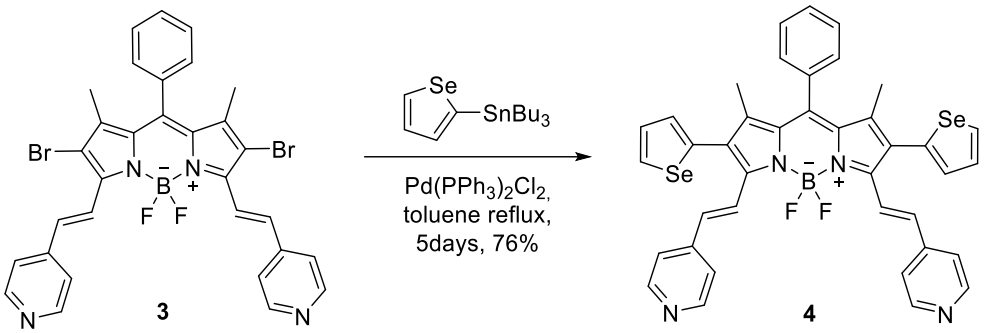

Figure 4.4. Synthetic route of compound 4.

In a 25 mL schlenck tube, compound **3** (0.050 g, 0.076 mmol) was dissolved in toluene (5 mL). To this solution, tributyl(selenophen-2-yl)stannane (0.060 g, 0.142 mmol) and $Pd(PPh_3)_2Cl_2$ (7.00 mg, 0.010 mmol) was added and the mixture was heated to reflux (115 °C). After the reaction was stirred for 24 hours and an additional amount of $Pd(PPh_3)_2Cl_2$ (3.50 mg, 0.005 mmol) was added. The reaction was stirred for 48 hours then $Pd(PPh_3)_2Cl_2$ (3.50 mg, 0.005 mmol) was added. The mixture stirred for additional 24 hours and cooled to rt. Toluene was evaporated and the residue was diluted with saturated KF solution (500 mL) and CH_2Cl_2. The organic layer was separated and dried over anhydrous Na_2SO_4. The solvent was evaporated under reduced pressure and the crude product was purified by column chromatography (silica gel, EtOAc : Hexane – 7:1) to yield target the product as a dark blue solid (0.044 g, 76%). ^{1}H NMR (400 MHz, $CDCl_3$) δ: 8.58 (d, 4H, *J* = 5.9 Hz), 8.17 (d, 2H, *J* = 5.9 Hz), 7.85 (d, 2H, *J* = 16.6 Hz), 7.56 – 7.50 (m, 3H), 7.39 – 7.33 (m, 4H), 7.23 (d, 2H, *J* = 5.9 Hz), 7.12 (d, 2H, *J* = 2.8 Hz), 6.78 (d, 2H, *J* = 16.6 Hz), 1.33 (s, 6H); ^{13}C NMR (100 MHz, $CDCl_3$) δ: 149.0, 143.1, 141.6, 141.0, 139.8, 135.2, 133.7, 132.6, 132.2, 130.0, 129.1, 128.6, 128.5, 128.1, 127.0, 121.5, 120.3, 11.7 HRMS calculated for $C_{39}H_{29}BF_2N_4Se_2$: 763.0872. Found: 763.0878.

4.7. Synthesis of Compound 5

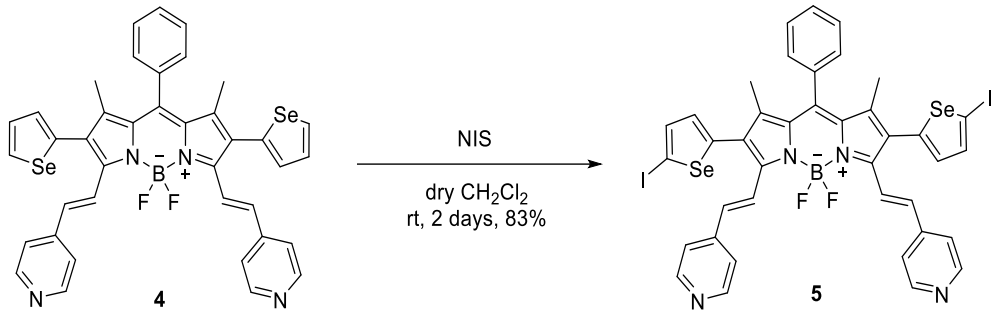

Figure 4.5. Synthetic route of compound 5.

To a solution of compound **4** in dry CH_2Cl_2 (4 mL), a solution of *N*-iodosuccinimide (26.0 mg, 0.116 mmol) in dry CH_2Cl_2 (3 mL) was added slowly and the mixture was stirred 2 days at rt until TLC showed reaction was finished. The crude product was diluted with CH_2Cl_2 (50 mL) and washed with water (50 mL) and then sat. $NaHCO_3$ solution (50 mL). The organic layer was dried over anhydrous Na_2SO_4 and the solvent was evaporated under reduced pressure. The crude product was purified by column chromatography (silica gel, CH_2Cl_2 : MeOH – 98:2) to yield target the product as blue solid (0.038 g, 83%) ^{1}H NMR (400 MHz, $CDCl_3$) δ: 8.60 (d, 4H, *J* = 6.0 Hz), 7.83 (d, 2H, *J* = 16.6 Hz), 7.57 – 7.51 (m, 5H), 7.36 – 7.31 (m, 2H), 7.29 – 7.27 (m, 2H), 6.92 (d, 2H, *J* = 16.6 Hz), 6.74 (d, 2H, *J* = 4.0 Hz), 1.32 (s, 6H); ^{13}C NMR (100 MHz, $CDCl_3$) δ: 150.4, 150.0, 147.5, 143.8, 142.9, 142.5, 140.6, 136.8, 134.6, 133.7, 132.7, 129.9, 129.7, 128.3, 128.0, 124.0, 122.3, 121.5, 12.8 HRMS calculated for $C_{39}H_{27}BF_2I_2N_4Se_2$: 1014.8795 Found: 1014.8820.

4.8. Synthesis of Compound 6

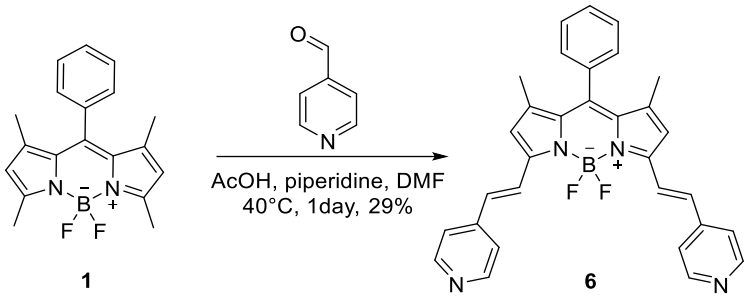

Figure 4.6. Synthetic route of compound 6.

In a 25 mL schlenck tube, compound **1** (0.100 g, 0.309 mmol) and 4-pyridinecarboxyaldehyde (0.193 g, 0.411 mmol) was dissolved in dry DMF (7.0 mL). To this solution, piperidine (0.3 mL) and acetic acid (0.3 mL) was added dropwise. Reaction mixture heated to 40 °C and was stirred overnight until thin TLC showed that the reaction was completed. The reaction solvent was evaporated under reduced pressure and the crude product was purified by column chromatography (silica gel, $CHCl_3$: MeOH – 98:2) to get the target product as a blue solid (0.045 g, 29%) ^{1}H NMR (400 MHz, CD_3OD) δ: 8.63 (d, 4H, *J* = 5.3 Hz), 7.89 (d, 2H, *J* = 16.3 Hz), 7.54 – 7.51 (m, 3H), 7.46 (d, 4H, *J* = 5.9 Hz), 7.34 – 7.29 (m, 2H), 7.31 (d, 1H, *J* = 2.0 Hz), 7.14 (d, 2H, *J* = 16.3 Hz), 6.67 (s, 2H), 1.45 (s, 6H). ^{13}C NMR (100 MHz, $CDCl_3$) δ: 151.8, 150.2, 143.6, 143.3, 141.1, 134.5, 134.1, 133.3, 129.4, 129.3, 128.0, 123.3, 121.4, 118.6, 14.7. HRMS calculated for $C_{31}H_{25}BF_2N_4$: 503.2219. Found: 503.2201

4.9. Synthesis of Compound BOD-H

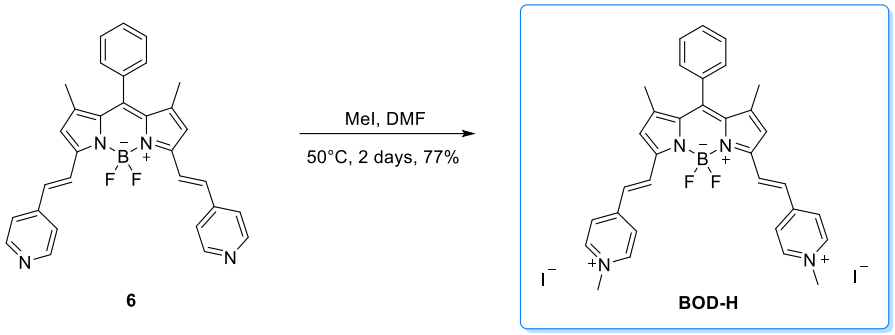

Figure 4.7. Synthetic route of compound BOD-H.

In a 25 mL schlenck tube, compound **6** (0.030 g, 0.059 mmol) and iodomethane (2.0 mL, 32 mmol) were dissolved in dry DMF (5 mL) and the mixture was stirred for 2 days at 50 °C until TLC showed reaction was completed. Reaction mixture was precipitated and washed with diethyl ether (100 mL) and then washed with water (10mL) to yield the target product as a green solid (0.035 g, 77%). ^{1}H NMR (400MHz, DMSO – d_6) δ: 8.92 (d, 4H, *J* = 6.6 Hz), 8.21 (d, 4H, *J* = 6.6 Hz), 7.95 (d, 2H, *J* = 16.3), 7.86 (d, 2H, *J* = 16.3), 7.68 – 7.62 (m, 3H), 7.53 – 7.48 (m, 2H), 7.20 (s, 2H), 4.33 (s, 6H), 1.48 (s, 6H). ^{13}C NMR (100 MHz DMSO – d_6) δ: 150.9, 150.3, 145.6, 144.0, 143.0, 134.8, 133.1, 131.7, 129.9, 129.5, 127.7, 127.2, 124.3, 120.8, 47.3, 14.3. HRMS calculated for $C_{33}H_{31}BF_2N_4$: 532.2610 Found: 532.2586

4.10. Synthesis of Compound BOD-Br

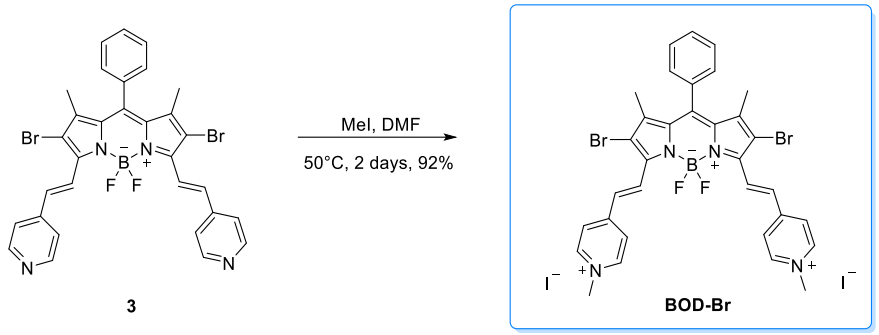

Figure 4.8. Synthetic route of compound BOD-Br.

To a 25 mL schlenck tube compound **3** (0.030 g, 0.045 mmol) and iodomethane (2.0 mL, 32 mmol) were added and dissolved in dry DMF (5 mL) and stirred 2 days at 50 °C until TLC showed reaction was completed. Reaction mixture was precipitated and washed with diethyl ether (100 mL) and then washed with water (10 mL) and $CHCl_3$ (10 mL) to yield the target product as a green solid (0.039 g, 92%). ^{1}H NMR (400MHz, DMSO – d_6) 8.95 (d, 4H, *J* = 6.4 Hz), 8.35 (d, 4H, *J* = 6.4 Hz), 8.15 (d, *J* = 16.7) 7.92 (d, *J* = 16.7) , 7.76 – 7.61 (m, 3H), 7.62 – 7.48 (m, 2H), 4.33 (s, 6H), 1.46 (s, 6H) HRMS calculated for $C_{33}H_{29}BF_2Br_2N_4$: 690.0800. Found: 690.0820

4.11. Synthesis of Compound BOD-Se

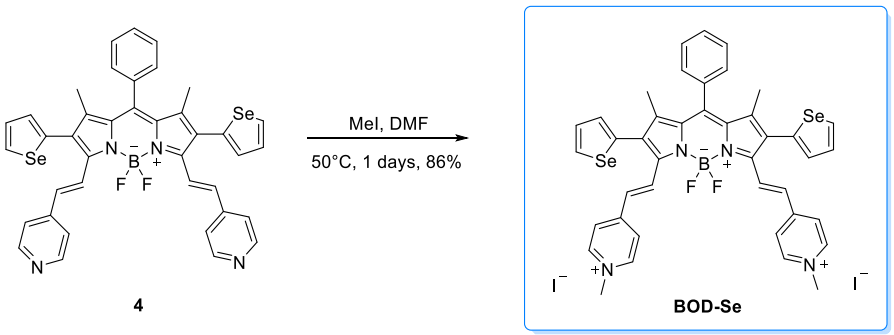

Figure 4.9. Synthetic route of compound BOD-Se.

To a 25 mL schlenck tube compound **4** (0.030 g, 0.039 mmol) and iodomethane (2.0 mL, 32 mmol) were added and dissolved in dry DMF (5 mL) and stirred 1 day at 50 °C TLC showed reaction was completed. Reaction mixture was precipitated and

washed with diethyl ether (100 mL) and then washed with water (10 mL) to yield the target product as a green solid (0.036 g, 86%). ^{1}H NMR (400 MHz, DMSO – d_6) δ: 8.85 (d, 4H, *J* = 6.7 Hz), 8.42 (d, 2H, *J* = 5.6 Hz), 8.02 (d, 4H, *J* = 6.7 Hz), 7.92 (d, 2H, *J* = 16.4 Hz), 7.69 – 7.62 (m, 3H), 7.60 – 7.54 (m, 2H), 7.45 – 7.39 (m, 2H), 7.30 (d, 2H, *J* = 3.5 Hz), 7.00 (d, 2H, *J* = 16.4 Hz), 4.28 (s, 6H), 1.35 (s, 6H); ^{13}C NMR (100 MHz, DMSO – d_6) δ: 150.1, 148.5, 145.7, 144.8, 142.7, 138.4 135.4, 134.2, 133.3, 132.9, 131.9, 130.4, 130.3, 130.2, 129.7, 127.7, 127.3, 124.2, 47.3, 12.6 HRMS calculated for $C_{41}H_{35}BF_2N_4Se_2$: 792.1263 Found: 792.1299.

4.12. Synthesis of Compound BOD-Se-I

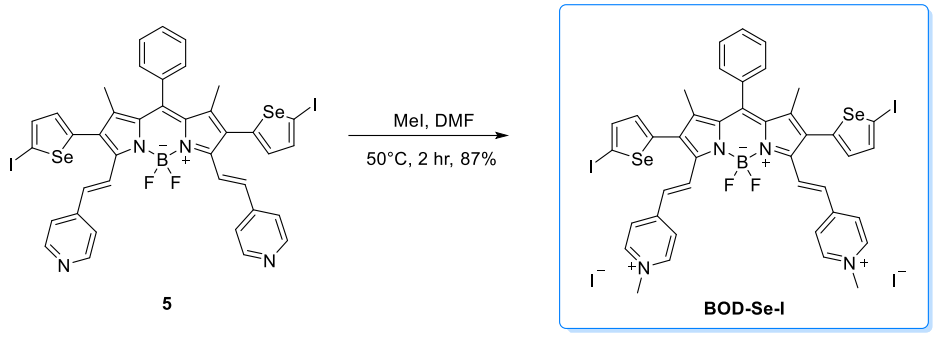

Figure 4.10. Synthetic route of compound BOD-Se-I.

To a 25 mL schlenck tube compound **5** (0.038 g, 0.038mmol) and iodomethane (2.0 mL, 32 mmol) were added and dissolved in dry DMF (5 mL) and stirred 2 hours at 50 °C TLC showed reaction was completed. Reaction mixture was precipitated and washed with diethyl ether (100 mL) and then washed with water (10 mL) to yield target the product as a green solid (0.043 g, 87%). ^{1}H NMR (400MHz, DMSO – d_6) δ: 8.87 (d, 4H, *J* = 6.8 Hz), 8.07 (d, 4H, *J* = 6.8 Hz), 7.89 (d, 2H, *J* = 16.4 Hz), 7.73 – 7.63 (m, 5H), 7.57 – 7.50 (m, 2H), 7.11 (d, 2H, *J* = 16.6 Hz), 6.97 (d, 2H, *J* = 4.0 Hz), 4.28 (s, 6H), 1.34 (s, 6H); ^{13}C NMR (100MHz, DMSO – d_6) δ: 150.1, 148.6, 145.8, 145.0, 144.4, 142.9, 140.5, 134.1, 134.0, 133.2, 133.2, 130.2, 129.8, 129.6, 127.7, 127.2, 124.3, 47.4, 12.6. HRMS calculated for $C_{41}H_{33}BF_2I_2N_4Se_2$: 1043.9175 Found: 1043.9202.

4.13. Synthesis of Compound a

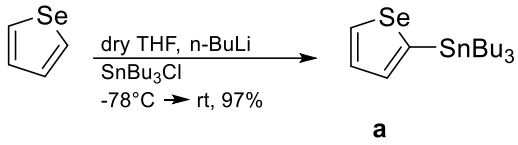

Figure 4.11. Synthetic route of compound a.

To a 50 mL two neck reaction flask, selenophene (1.00 g, 7.63 mmol) was added and dissolved in dry THF (25 mL) under argon atmosphere. Then, solution cooled to -78 °C and n-BuLi (3.40 mL, 8.50 mmol, 2.5 M in hexane) was added dropwise over 40 minutes. Reaction mixture was stirred for 1.5 h at -78 °C. Tributyltin chloride (2.50 mL, 9.20 mmol) was added dropwise over 20 minutes at -78 °C. Then, reaction mixture warm to the room temperature and stirred overnight. Then, mixture quenched with distilled water and aqueous phase was extracted with DCM (100 mL). The organic layer was dried over anhydrous Na_2SO_4 and the solvent was evaporated under reduced pressure. The crude product was obtained as brown oil (3.04 g, 95%) and used without making any further purification. ^{1}H NMR (400 MHz, $CDCl_3$) δ: 8.40 – 8.32 (m, 1H), 7.57 – 7.45 (m, 2H), 1.63 – 1.52 (m, 6H), 1.42 – 1.29 (m, 6H), 1.14 – 1.08 (m, 6H), 0.95 – 0.86 (m, 9H) ^{13}C NMR (100 MHz, $CDCl_3$) δ: 143.5, 137.9, 135.3, 130.6, 29.0, 27.3, 13.7, 11.1.

4.14. Synthesis of Compound b

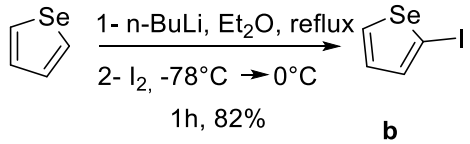

Figure 4.12. Synthetic route of compound b.

To a solution of Selenophene (1.00 g, 7.63 mmol) in dry Et_2O (25 mL), n-BuLi (3.00 mL, 7.63 mmol, 2.5 M in hexane) was added dropwise in rt, over 25 min. Then solution heated to reflux (34.6 °C) for 10 min. After being cooled to -78 °C, to this solution, solution of iodine (1.94 g, 7.63 mmol) in dry Et_2O (40 mL) was added dropwise over 50 min. The solution was allowed to warm 0 °C stirred 1 hour at that

temperature. After being warmed to rt, reaction mixture poured into ice-cold water and extract with Et_2O. The organic layer was separated and wash with saturated $NaHSO_3$ (50 mL) and brine (50 mL). The organic layer dried over $MgSO_4$ and the solvent was evaporated under reduced pressure. The crude product purified by flash column chromatography (silica, petroleum ether) to yield target the product as light yellow oil (1.60 g, 82%). ^{1}H NMR (400 MHz, $CDCl_3$) δ: 8.09 (d, 1H, J=7.0 Hz), 7.53 (d, 1H, J=3.7 Hz), 6.97 (dd, 1H, J= 5.9, 3.8 Hz), ^{13}C NMR (100 MHz, $CDCl_3$) δ: 140.1, 137.2, 131.4.

4.15. Synthesis of Compound c

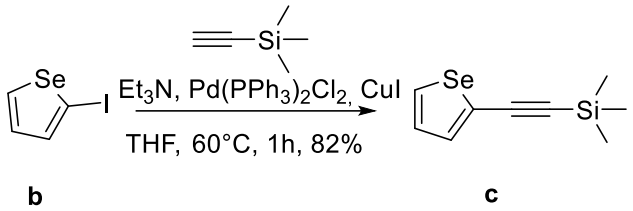

Figure 4.13. Synthetic route of compound c.

Solution of compound **b** (0.100, 0.389 mmol), trimethylsilylacetylene (0.053, 0.537 mmol), $PdCl_2(PPh_3)_2$ (2.50 mg, 0.004 mmol), CuI (1 mg, 0.005 mmol) and NEt_3 (0.5 mL) in dry THF (2 mL) heated to 80 °C. After 30 min stirring, the TLC showed that the reaction was completed. Then reaction mixture was allowed to cool rt and 1N HCl (0.5 mL) was added and extracted with ethyl acetate. The organic layer was separated and washed with brine (25 mL) and saturated $NaHCO_3$ (25 mL). The organic layer dried over Na_2SO_4 and solvent was evaporated under reduced pressure. The crude product purified by flash column chromatography (silica, petroleum ether) to yield target the product as yellow oil (73 mg, 82%). ^{1}H NMR (400 MHz, $CDCl_3$) δ: 7.96 (d, 1H, J=5.6 Hz), 7.43 (d, 1H, J=3.7 Hz), 6.97 (dd, 1H, J=5.6, 3.8 Hz), 0.25 (s, 9H) ^{13}C NMR (100 MHz, $CDCl_3$) δ: 135.1, 133.3, 129.5, 127.6, 100.7, 99.8, 0.0

4.16. Synthesis of Compound d

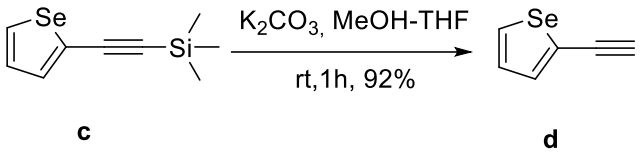

Figure 4.14. Synthetic route of compound d.

Compound **c** (0.870 g, 3.829 mmol) was dissolved in MeOH-THF mixture (50 mL, 1:1) and K_2CO_3 was added to solution and was stirred at rt. Reaction monitorized by TLC and upon completion after 1 hour, the reaction mixture diluted with Et_2O and washed with saturated NH_4Cl and brine respectively. The organic layer dried over $MgSO_4$ and concentrated under reduced pressure. The crude product purified by flash column chromatography (silica, hexane) to yield target the product as yellow oil (0.547 g, 92%). ^{1}H NMR (400 MHz, $CDCl_3$) δ: 7.99 (d, 1H, J=6.6 Hz), 7.48 (d, 1H, J=3.7 Hz), 7.21 (dd, 1H, J= 5.6, 3.8 Hz), ^{13}C NMR (100 MHz, $CDCl_3$) δ: 135.6, 133.5, 129.4, 126.4, 83.0, 79.1.

4.17. Synthesis of Compound 7

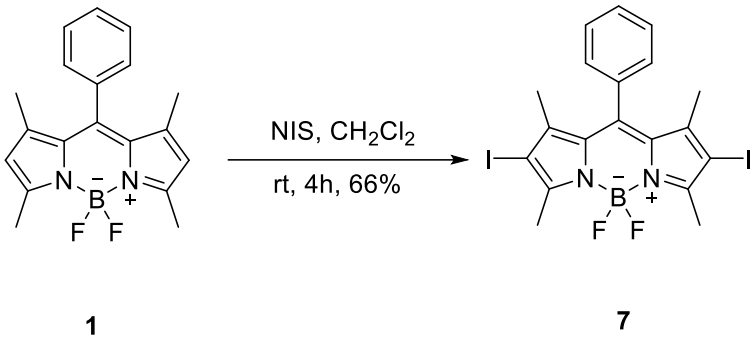

Figure 4.15. Synthetic route of compound 7.

To a solution of compound **1** (0.190 g, 0.586 mmol) in dry CH_2Cl_2 (30 mL), solution of *N*-iodosuccinimide (NIS) (0.330 g, 1.47 mmol) in dry CH_2Cl_2 (20 mL) was added slowly. After 3 hours stirring at rt, TLC showed that the reaction was completed. The crude product was washed with water (50 mL) and then brine (50 mL). The organic layer was dried over anhydrous Na_2SO_4 and the solvent was evaporated under reduced pressure. The crude product was purified by column chromatography (silica gel,

hexane: CH_2Cl_2 – 1:1) to yield target the product as a dark red solid (0.223 g, 66%) ^{1}H NMR (400 MHz, $CDCl_3$) δ: 7.57 – 7.49 (m, 3H), 7.30 – 7.22 (m, 2H), 2.65 (s, 6H), 1.39 (s, 6H). ^{13}C NMR (100 MHz, $CDCl_3$) δ: 156.7, 145.3, 141.3, 134.7, 131.3, 129.5, 129.4, 127.7, 85.7, 16.9, 16.0.

4.18. Synthesis of Compound 8

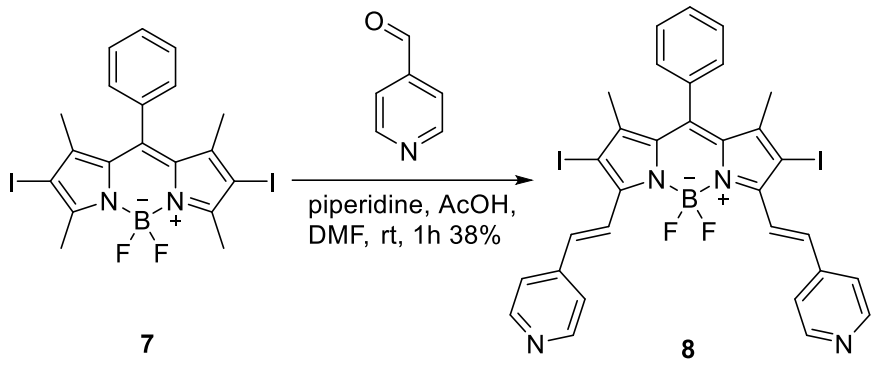

7 8

Figure 4.16. Synthetic route of compound 8.

In a 10 mL schlenck tube, compound **7** (50.0 mg, 0.087 mmol) and 4-pyridinecarboxyaldehyde (37.0 mg, 0.347 mmol) was dissolved with dry DMF (3.3 mL). To this solution, piperidine (0.2 mL) and acetic acid (0.2 mL) was added dropwise respectively. After 1 hour, the TLC showed that the reaction was completed. The reaction solvent was evaporated under reduced pressure immediately. Then, the crude product was purified by column chromatography (silica gel, CH_2Cl_2 : MeOH – 98:2) to yield target the product as a blue solid (25 mg, 38%) ^{1}H NMR (400 MHz, $CDCl_3$) δ: 8.68 (d, 4H, J=5.8 Hz), 8.07 (d, 2H,J=16.8 Hz), 7.85 (d, 2H, J=16.7 Hz), 7.61 – 7.56 (m, 3H), 7.56 – 7.52 (m, 4H), 7.33 – 7.28 (m, 2H), 1.48 (s, 6H). ^{13}C NMR (100 MHz, $CDCl_3$) δ: 148.5, 148.3, 145.5, 142.2, 139.9, 135.0, 133.0, 131.9, 128.3, 128.1, 126.2, 121.2, 119.9, 119.5, 15.9

4.19. Synthesis of Compound 9

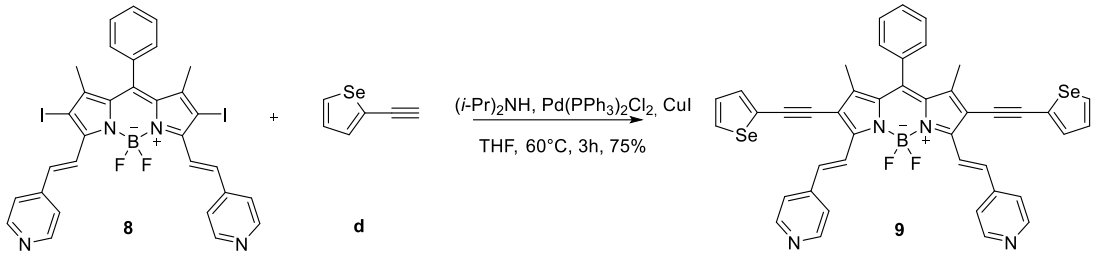

Figure 4.17. Synthetic route of compound 9.

Solution of compound **8** (50 mg, 0.066 mmol) and compound **d** (31 mg , 0.199 mmol) in dry THF (7 mL) was treated with (*i*-Pr)$_2$NH (0.7 mL) for 5 min then CuI (3.00 mg, 0.016 mmol) and $PdCl_2(PPh_3)_2$ (7.00 mg, 0.010 mmol) was added and mixture was heated to 60 °C and stirred 3 hours at that temperature. Upon completion, solvent was evaporated under reduced pressure and the crude product was purified by flash column chromatography (silica, CH_2Cl_2 : MeOH - 97:3) to yield the target the product as green solid (40 mg, 75%) ^{1}H NMR (400 MHz, $CDCl_3$) δ: 8.75 – 8.60 (m, 4H), 8.24 (d, 2H, J=16.4 Hz), 8.07 (d, 2H, J=5.5 Hz), 7.96 (d, 2H, J=16.4 Hz), 7.60 – 7.54 (m, 3H), 7.54 – 7.50 (m, 4H), 7.47 – 7.41 (m, 2H),7.37 – 7.31 (m, 2H), 7.29 – 7.26 (m, 2H), 1.57 (s, 6H) ^{13}C NMR (100 MHz, $CDCl_3$) δ: 151.5, 150.3, 145.7, 143.9, 142.1, 136.3, 134.0, 134.0, 133.8, 133.8, 133.8, 129.9, 129.6, 127.9, 126.9, 121.6, 114.9, 94.2, 88.4, 13.4.

4.20. Fluorescence Quantum Yield

Fluorescence quantum yields of the samples were investigated by using a fluorescence spectrometer (FLS 1000, Edinburgh Instruments) with an integrating sphere accessory. A continuous-wave xenon lamp was used as the excitation source and the emitted fluorescence was detected with a standard photomultiplier (PMT-900) covering a wavelength range of 200-800 nm. During the measurements, the PMT was cooled down to -20 °C by using a built-in housing to reduce the undesired dark current noise.

For quantum yield measurement, an integrating sphere (Edinburgh Instruments) was placed inside the sample compartment of the spectrometer. Internal cavity of the sphere was coated with a PTFE-like material to enable a reflectance of approximately >99% (>95%) over the wavelength range between 400 and 1500 nm (250 and 2500 nm). The sphere had two ports which were 90° apart. The excitation beam was sent to the sample through the excitation port and the fluorescence was collected from the emission port. The excitation port of the sphere consisted of a lens to effectively focus the beam on the sample. The emission port was open aperture.

Prior to the experiments performed with the BODIPYs, the blank spectra were measured by using the reference solvents (PBS (pH 7.4, 1% DMSO)). For both of the measurements (blank and sample), two identical quartz cuvettes with equal volumes were used. First, the reference sample was placed inside the sphere and the emission/excitation slits were adjusted at the excitation wavelength so that the response of the PMT remained linear during the measurements. In order to cover a scattering range, the emission scans were started from 20 nm below the actual excitation wavelengths and finished at 750 nm. Furthermore, the step size and the integration time of the measurements were set to 1 nm and 0.2 seconds, respectively. The emission scans of the samples were performed by using the same parameters as their references (BOD-Br sample; Ex. = 10 nm, Em. = 0.23 nm, λ_{start} = 638 nm and Bod-H sample; Ex. = 1 nm, Em. = 1 nm, λ_{start} = 627 nm).

After the all the emission measurements of the samples and references were complete, the quantum yields of the samples were determined by using the Fluoracle® software. The built-in analysis tool calculates the quantum yield (QY) as

$$QY = \frac{E_s - E_B}{S_B - S_s} \quad ,$$

where E_s (E_B) and S_s (S_B) are the selected areas for the emitted and scattered signals of the sample (blank).

4.21. Singlet Oxygen Trap Experiment

Singlet oxygen quantum yields were calculated using following equation and a reference fluorophore as methylene blue. singlet oxygen trap experiment of the methylene blue is performed at pH = 7.4 (in phosphate saline buffer) and is found as 0.52 from the literature1. The relative quantum yields were calculated with reference to methylene blue in phosphate saline buffer. Oxygen saturated PBS was obtained by bubbling molecular oxygen for 10 minutes. Then cuvette was filled with 5 μM photosensitizer which corresponds to the absorbance around 0.2-0.3. 9,10-antracenediyl-bis(methyelene)dimalonic acid (ADMDA) is added then as a trap and its absorbance was adjusted in between 0.6-1.9.

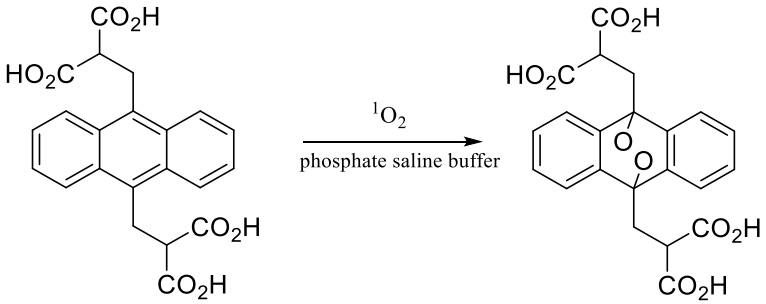

Figure 4.18. Reaction between photosensitized $^1O_2$ and ADMDA.

Taking several measurements in dark to stabilize the trap solubility, cuvette was exposed to the red light with absorption maxima of 650 nm. Each irradiation took 1 min from 10 cm of distance. The decrease in trap's absorbance at 380 nm was recorded and is repeated for several times. The graphics recorded are shown below. Then, slope for each photosensitizer were calculated plotting the trap's absorbance at 380 nm versus time graph. Singlet oxygen quantum yield were calculated according to the equation:

$$\Phi_{\Delta}(\text{bod}) = \Phi_{\Delta}(\text{ref}) \times \frac{\text{m(bod)}}{\text{m(ref)}} \times \frac{\text{F(ref)}}{\text{F(bod)}} \times \frac{\text{PF(ref)}}{\text{PF(bod)}}$$

Where bod and ref represent BODIPY derivatives, and methylene blue, respectively. m is the slope for BODIPY derivatives, where trap's absorbance at 380 nm vary with irradiation time, F is the correction factor, which is given by $F = 1 - 10^{-OD}$ (OD at absorption maxima of irradiation wavelength, which is 650 nm), and PF is absorbed photonic flux in μEinstein $dm^{-3}s^{-1}$.

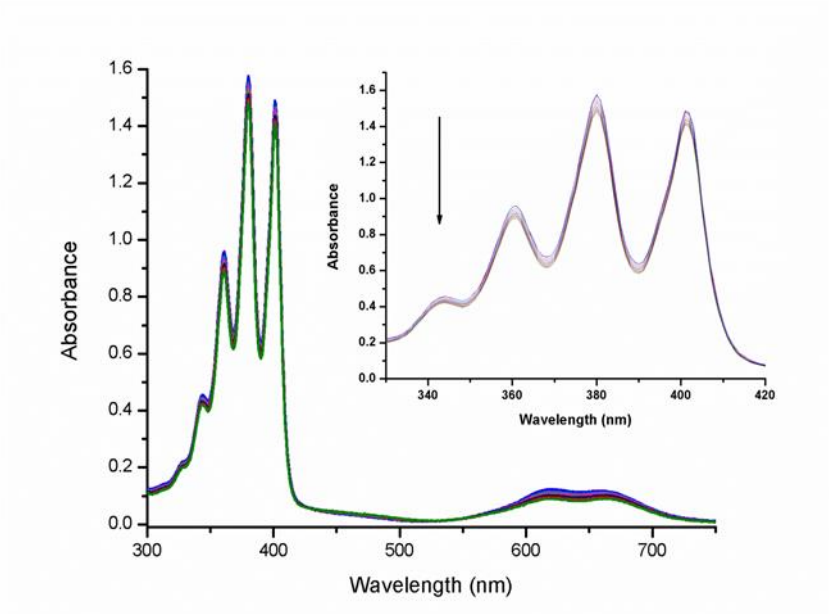

Figure 4.19. Decrease in the absorbance of ADMDA in PBS (pH 7.4, 1% DMSO) upon irradiation of BOD-Br (5 μM).

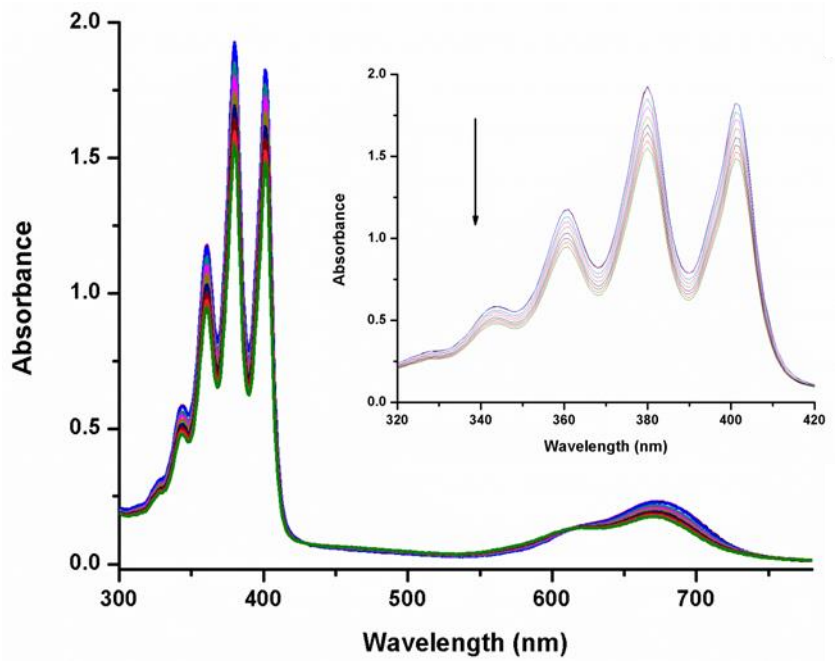

Figure 4.20. Decrease in the absorbance of ADMDA in PBS (pH 7.4, 1% DMSO) upon irradiation of BOD-Se (5 μM).

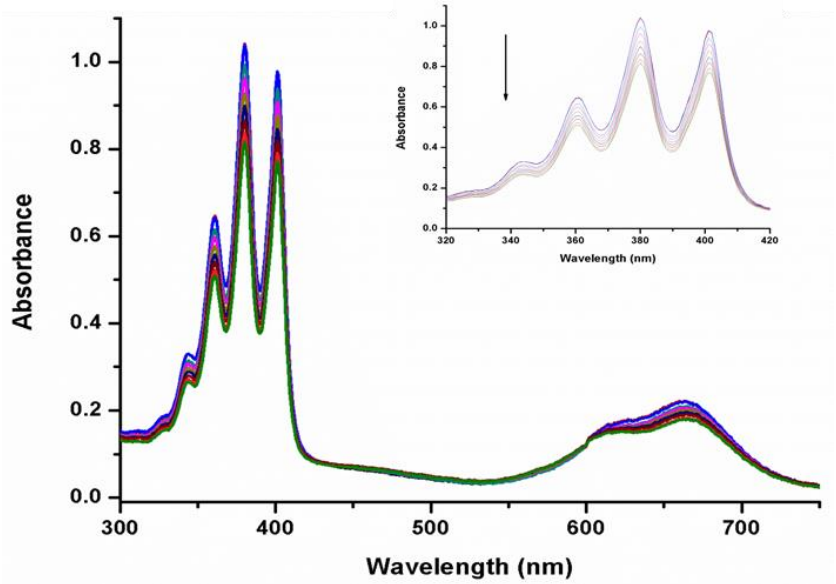

Figure 4.21. Decrease in the absorbance of ADMDA in PBS (pH 7.4, 1% DMSO) upon irradiation of BOD-Se-I (5 μM).

4.22. Micelle Preparation of Compound 5 (ctrl-BOD)

Compound **5** (ctrl-BOD) (12 mg, $1.19x10^{-5}$mol) was dissolved in 2.0 mL dry THF. To this solution, mixture of CrEL / 1,2-propanediol (10:3 v/v) (0.2 mL) was added. Resulting mixture placed in sonic bath for 1 hour. Then the THF was removed under reduced pressure and the remaining mixture was dissolved in phosphate buffered saline (PBS) solution (15 mL). Then, this solution was passed through a Minisart syringe filter (with 0.2 μm pore size). Remaining solution was diluted up to total 25 mL with PBS. Zetasizer Nano-ZS (Malvern Instruments Ltd., U.K.) was used to detect hydrodynamic size of micelle. Average size was found as 52.65 nm with standard deviation 6.74 nm by number and 244.2 with standard deviation 7.4 by intensity.

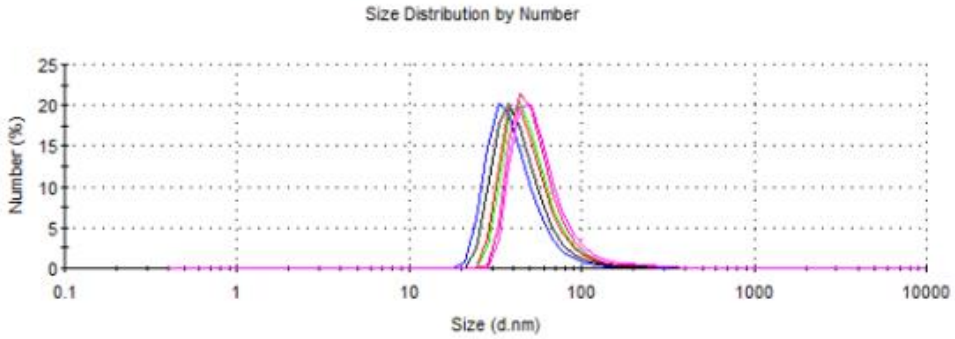

Figure 4.22. Size distribution by number graph of compound 5 (ctrl-BOD), which was embedded in micelle.

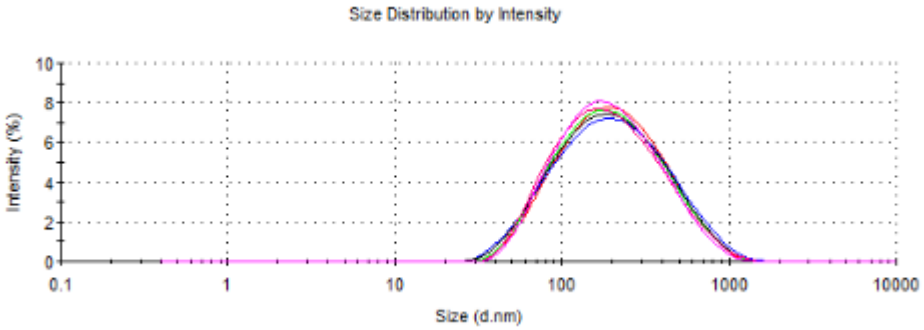

Figure 4.23. Size distribution by intensity graph of compound 5 (ctrl-BOD), which was embedded in micelle.

4.23. Cell Culture and MTT Assay

HeLa human cervix cancer cells were cultured in 25 cm^2 culture flasks containing Dulbecco's Modified Eagle Medium (DMEM) supplemented with 2 mM L-glutamine, 10% fetal bovine serum, 100 units/ml penicillin and 100 µg/ml streptomycin in a cell culture incubator at 37 °C, 5% CO_2 and 60% humidity. Photosensitizers **BOD-Br** and **BOD-Se-I** were diluted in complete medium and assay concentrations were freshly prepared. Cell viability / death was evaluated by MTT (3-(4, 5- dimethylthiazolyl-2)-2,5-diphenyltetrazolium bromide) assay. Briefly, 50 µL cell suspensions in complete DMEM containing 3 x 10^3 HeLa cells were plated in 96-well flat-bottom culture plates (Corning, MA, USA) and incubated for 12 hours to recover from handling. Varying concentrations of the chemical compounds in complete DMEM were added into each well (the final concentrations were 9 nM – 2.5 µM) in triplicate. The experimental group of the cells were illuminated with a red light source (655 nm, 324µmol.m^{-2} .s^{-1}, distance between light source and cells: 10 cm) for 4 hours illumination in a culture incubator (37 °C, 5% CO_2, 60% humidity) and kept 20 hours in dark. The control group of the cells were incubated in the dark, for the duration of 24 hours under identical environmental conditions except illumination. According to the assay protocol, 25 µl of the MTT reagent (Sigma-Aldrich, MO, USA) was added to each well in order to assess cell viability (final concentration: 1 mg/ml) at the end of the 24 hours incubation period. Following a 4 hours incubation of the cells with the MTT reagent, the generated formazan precipitates were solubilized by the addition of the lysing buffer (80 µL, pH: 4.7), which is composed of 23% SDS (Sodium dodecyl sulfate) dissolved in a solution of 45% DMF (N,N-Dimethylformamide). After an overnight incubation at 37 °C, the absorbance values (of each well) were measured at 570 nm in a microtiter plate reader (Spectramax Plus, Molecular Devices, CA, USA) at 25 °C. Cells incubated in culture medium only (without any chemical compounds) served as the control for cell viability both for the illuminated plates and for the ones kept in the dark; whereas DMSO (50%, v/v) was used to observe maximum cell death. Cell viability (%) was assessed with the normalization of the values calculated by the

formula “optical density (OD) of control cells – OD of treated cells”. The IC50 values of the compounds both in the dark and illuminated conditions were estimated by fitting a model with non-linear regression. Also, same procedure was followed for NIH – 3T3 cells.

4.24. Normoxia - Hypoxia Chamber Experiments

HeLa cells were cultured in 25 cm^2 culture flasks containing DMEM supplemented with 2 mM L-glutamine, 10 % fetal bovine serum, 100 units/ml penicillin and 100 µg/ml streptomycin in a cell culture incubator at 37 °C, 5% CO_2 and 60% humidity. Photosensitizers **BOD-Se-I** and **ctrl-BOD** were diluted in complete medium and assay concentrations were freshly prepared. Briefly, 50 µL cell suspensions in complete DMEM containing 6 x 10^3 HeLa cells were plated in 96-well flat-bottom culture plates (Corning, MA, USA) and incubated for 12 hours to recover from handling. Varying concentrations of the chemical compounds in complete DMEM were added into each well in triplicate. These plates were placed in a Modular Incubator Chamber (Billups-Rothenberg, Inc.). The chamber was purged with 5% O_2, 5% CO_2, 90% N_2 for 5 minutes (20 L/min). Cell viability was evaluated by MTT assay, which was described above.

4.25. Mitotracker Green FM Staining

Mitotracker Green FM staining was performed according to the manufacturer’s (Invitrogen) instructions. Both HeLa and NIH/3T3 cells were incubated under relevant conditions for 24 hours in glass-bottom dishes before staining the cells with MitoTracker Green FM. The working concentration of the Mitotracker Green FM was 200 nM and the incubation time was 45 minutes. Colocalization was analyzed using Pearson’s correlation coefficient (R) after a background subtraction in all channels.

4.26. Annexin V Staining

Annexin V staining was performed according to the manufacturer’s (Biolegend) instructions. The cells were washed twice with cold cell staining buffer and then, Annexin V binding buffer was added. 5 µl of PE Annexin V was added for each 100

µl of Annexin V binding buffer. The cells were gently shaken and then incubated for 15 minutes at room temperature in the dark. 400 µl of Annexin V binding buffer was added onto each initial 100 µl of Annexin V binding buffer. The cells were then analyzed with a fluorescence microscope.

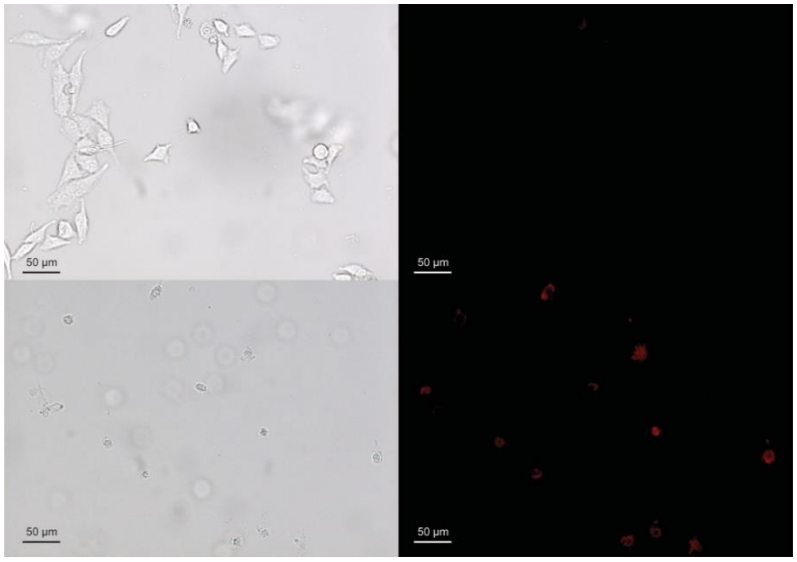

Figure 4.24. Fluorescence microscope images of PE Annexin V stained and BOD-Se-I (5µM) incubated HeLa cells. Top: cells were kept under dark, bottom: cells were irradiated with 660 nm LED for 4 hours.

REFERENCES

Ackroyd, R., Kelty, C., Brown, N., & Reed, M. (2001). 30 Ejemplos de Antioxidantes, *74*(5), 656–669.

Agostinis, P., Berg, K., Cengel, K. A., Foster, T. H., Girotti, A. W., Gollnick, S. O., … Golab, J. (2011). Photodynamic therapy of cancer: An update. *CA: A Cancer Journal for Clinicians*, *61*(4), 250–281.

Atilgan, S., Ekmekci, Z., Dogan, A. L., Guc, D., & Akkaya, E. U. (2006). Water soluble distyryl-boradiazaindacenes as efficient photosensitizers for photodynamic therapy. *Chemical Communications*, (42), 4398–4400.

Atkins, P. W., & Paula, J. de. (2008). *Kurzlehrbuch Physikalische Chemie*. Germany: Wiley-VCH, Weinheim.

Auler, H., & Banzer, G. (1942). Untersuchungen ueber die rolle der porphyrine bei geschwulstkranken menschen und tieren. *Z Krebsforsch*, *53*, 65–68.

Awuah, S. G., Polreis, J., Biradar, V., & You, Y. (2011). Singlet oxygen generation by novel NIR BODIPY dyes. *Organic Letters*, *13*(15), 3884–3887.

Awuah, S. G., & You, Y. (2012). Boron dipyrromethene (BODIPY)-based photosensitizers for photodynamic therapy. *RSC Advances*, *2*(30), 11169–11183.

Balchum, O. J., Doiron, D. R., & Huth, G. C. (1984). Photoradiation therapy of endobronchial lung cancers employing the photodynamic action of hematoporphvrin derivative. *Lasers in Surgery and Medicine*, *4*(1), 13–30.

Bartelmess, J., Francis, A. J., Roz, K. A. El, Castellano, F. N., Weare, W. W., & Sommer, R. D. (2014). Light-Driven Hydrogen Evolution by BODIPY-Sensitized Cobaloxime Catalysts. *Inorganic Chemistry*, *53*(9), 4527–4534.

Biel, M. A. (1998). Photodynamic therapy and the treatment of head and neck neoplasia. *Laryngoscope*, *108*(9), 1259–1268.

Bonnett, R. (1995). Photosensitizers of the porphyrin and phthalocyanine series for photodynamic therapy. *Chemical Society Reviews*, *24*(1), 19.

Bown, S. G., Rogowska, a Z., Whitelaw, D. E., Lees, W. R., Lovat, L. B., Ripley, P., … Hatfield, a W. R. (2002). Photodynamic therapy for cancer of the pancreas.

Gut, *50*(4), 549–557.

Boydston, A. J., Haley, M. M., Williams, R. V., & Armantrout, J. R. (2002). Diatropicity of 3,4,7,8,9,10,13,14-Octadehydro[14]annulenes: A Combined Experimental and Theoretical Investigation. *Journal of Organic Chemistry*, *67*, 8812–8819.

Brancaleon, L., & Moseley, H. (2002). Laser and Non-laser Light Sources for. *Lasers in Medical Science*, *17*(3), 173–186.

Cairnduff, F., Stringer, M. R., Hudson, E. J., Ash, D. V., & Brown, S. B. (1994). Superficial photodynamic therapy with topical 5-aminolaevulinic acid for superficial primary and secondary skin cancer. *British Journal of Cancer*, *69*(3), 605–608.

Castano, A. P., Mroz, P., & Hamblin, M. R. (2006). Photodynamic therapy and anti-tumor immunity. *Lasers in Surgery and Medicine*, *38(5)*, 509–515.

Chen, Y., Zhao, J., Guo, H., & Xie, L. (2012). Geometry Relaxation-Induced Large Stokes Shift in Red-Emitting Borondipyrromethenes (BODIPY) and Applications in Fluorescent Thiol Probes. *Journal of Organic Chemistry*, *77*, 2192–2206.

Cihaner, A., & Algi, F. (2009). Synthesis and properties of 4,4-difluoro-4-bora-3a,4a-diaza-s-indacene (BODIPY)-based conducting copolymers. *Reactive and Functional Polymers*, *69*(1), 62–67.

D.E.J.G.J. Dolmans, Fukumura, D., & K.Jain, R. (2003). Photodynamic therapy for cancer. *Nature Reviews Cancer*, *3*, 380–387.

Danial, N. N., & Korsmeyer, S. J. (2004). Cell Death: Critical Control Points. *Cell*, *116*(2), 205–219.

Deniz, E., Isbasar, G. C., Bozdemir, Ö. A., Yildirim, L. T., Siemiarczuk, A., & Akkaya, E. U. (2008). Bidirectional switching of near IR emitting boradiazaindacene fluorophores. *Organic Letters*, *10*(16), 3401–3403.

Diamond, I.; Granelli, S.G.; McDonagh, A.F.; Nielsen, S.; Wilson, C.B.; Jaenicke, R. (1972). Photodynamic therapy of malignant tumours. *Lancet*, *300*(7788), 1175–1177.

Dimofte, A., Zhu, T. C., Hahn, S. M., & Lustig, R. A. (2002). In vivo light dosimetry for motexafin lutetium-mediated PDT of recurrent breast cancer. *Lasers in Surgery and Medicine*, *31*(5), 305–312.

Dost, Z., Atilgan, S., & Akkaya, E. U. (2006). Distyryl-boradiazaindacenes: facile synthesis of novel near IR emitting fluorophores. *Tetrahedron*, *62*(36), 8484–8488.

Dougherty, T. J., Grindey, G. B., Fiel, R., Weishaupt, K. R., & Boyle, D. G. (1975). Photoradiation Therapy. II. Cure of Animal Tumors With Hematoporphyrin and Light. *JNCI: Journal of the National Cancer Institute*, *55*(1), 115–121.

Dougherty, T. J., Kaufman, K. E., Goldfarb, A., Weishaupt, K. R., Boyle, D., & Mittleman, A. (1978). Photodynamic therapy for the treatment of malignant tumors. *Can. Res.*, *38*(August), 2628–2635.

Dyes, B., Wang, H., Fronczek, F. R., Grac, M., Vicente, H., & Smith, K. M. (2014). Functionalization of 3,5,8-Trichlorinated BODIPY Dyes. *Journal of Organic Chemistry*, *79*, 10342−10352.

Finsen, N. (1901). *Phototherapy*. (E. Arnold, Ed.). London.

Foote, C. S. (1991). Definition of Type I and Type I1. *Photochemistry and Photobiology*, *54*(5), 659.

Fu, G.-L., Pan, H., Zhao, Y.-H., & Zhao, C.-H. (2011). Solid-state emissive triarylborane-based BODIPY dyes: Photophysical properties and fluorescent sensing for fluoride and cyanide ions. *Organic & Biomolecular Chemistry*, *9*(23), 8141–8146.

Galluzzi, L., N., B. V. T. V., Buettner, Eisenberg, S., & Vandenabeele, T. P. (2011). Programmed necrosis from molecules to health and disease. In *International Review of Cell and Molecular Biology* (pp. 1–35). Elsevier Inc.

Gilchrest, B. . (2010). Photodynamic Therapy and Selected Off-label Uses. In Proceedings of the Winter Clinical Dermatology Conference. In S. Tuleya (Ed.) (pp. 10–12). Kohala Coast, HI, USA: HMP Communications.

Gold, M. H., & Goldman, M. P. (2004). 5-Aminolevulinic acid photodynamic therapy: Where we have been and where we are going. *Dermatologic Surgery*, *30*(8),

1077–1083.

Hage, R., Ferreira, J., Bagnato, V. S., Vollet-Filho, J. D., & Plapler, H. (2012). Pharmacokinetics of photogem using fluorescence spectroscopy in dimethylhydrazine-induced murine colorectal carcinoma. *International Journal of Photoenergy*, *2012*, 8.

Hammerer, F., Poyer, F., Fourmois, L., Chen, S., Garcia, G., Maillard, P., & Mahuteau-betzer, F. (2017). Mitochondria-targeted cationic porphyrin-triphenylamine hybrids for enhanced two-photon photodynamic therapy. *Bioorganic & Medicinal Chemistry*, *26*, 107.

Hausmann, W. (1911). Die sensiblisierende Wirkung des Hematoporphyrins. *Biochem. Zeitung*, *30*, 276–316.

Hayashi, Y., Yamaguchi, S., Cha, W. Y., Kim, D., & Shinokubo, H. (2011). Synthesis of directly connected BODIPY oligomers through Suzuki-Miyaura coupling. *Organic Letters*, *13*(12), 2992–2995.

Hayata, Y., Kato, H., Konaka, C., Ono, J., & Takizawa, N. (1982). Hematoporphyrin derivative and laser photoradiation in the treatment of lung cancer. *Chest*, *81*(3), 269–277.

Hayata, Y., Kato, H., Okitsu, H., Kawaguchi, M., & Konaka, C. (1985). Photodynamic therapy with hematoporphyrin derivative in cancer of the upper gastrointestinal tract. *Seminars in Surgical Oncology*, *1*(1), 1–11.

He, H., Lo, P. C., Yeung, S. L., Fong, W. P., & Ng, D. K. P. (2011a). Preparation of unsymmetrical distyryl BODIPY derivatives and effects of the styryl substituents on their in vitro photodynamic properties. *Chemical Communications*, *47*(16), 4748–4750.

He, H., Lo, P. C., Yeung, S. L., Fong, W. P., & Ng, D. K. P. (2011b). Synthesis and in vitro photodynamic activities of pegylated distyryl boron dipyrromethene derivatives. *Journal of Medicinal Chemistry*, *54*(8), 3097–3102.

Hill, M. D. Daniell, J. S. (1991). a History of Photodynamic Therapy. *Australian and New Zealand Journal of Surgery*, *61*(5), 340–348.

Hinkeldey, B., Schmitt, A., & Jung, G. (2008). Comparative photostability studies of

BODIPY and fluorescein dyes by using fluorescence correlation spectroscopy. *ChemPhysChem*, *9*(14), 2019–2027.

Huang, H., Yu, B., Zhang, P., Huang, J., Chen, Y., Gasser, G., … Chao, H. (2015). Highly Charged Ruthenium(II) Polypyridyl Complexes as Lysosome-Localized Photosensitizers for Two-Photon Photodynamic Therapy. *Angewandte Chemie - International Edition*, *54*, 14049 –14052.

Jiao, L., Yu, C., Uppal, T., Liu, M., Li, Y., Zhou, Y., … Vicente, M. G. H. (2010). Long wavelength red fluorescent dyes from 3,5-diiodo-BODIPYs. *Organic and Biomolecular Chemistry*, *8*(11), 2517–2519.

K. Umezawa, Y. Nakamura, H. Makino, D. Citterio, K. S. (2008). Bright, Color-Tunable Fluorescent Dyes in the Vis-NIR region. *Chemistry - A European Journal European Journal*, *15*(5), 1096–1106.

Kamkaew, A., Lim, S. H., Lee, H. B., Kiew, L. V., Chung, L. Y., & Burgess, K. (2013). BODIPY dyes in photodynamic therapy. *Chemical Society Reviews*, *42*(1), 77–88.

Kelly, J. F., Snell, E., & Berenbauai, M. C. (1975). PHOTODYNAMIC DESTRUCTION OF HUMAN BLADDER CARCINOMA. *British Journal of Cancer*, *31*, 237–244.

Kelly, J. F., & Snell, M. E. (1976). Hematoporphyrin derivative: a possible aid in the diagnosis and therapy of carcinoma of the bladder. *Journal of Urology*, *115*(2), 150–151.

Kennedy, J. C., Pottier, R. H., & Pross, D. C. (1990). Photodynamic therapy with endogenous protoporphyrin. IX: Basic principles and present clinical experience. *Journal of Photochemistry and Photobiology, B: Biology*, *6*(1–2), 143–148.

Kessel, D., Vicente, M. G. H., & Reiners, J. J. (2006). Initiation of apoptosis and autophagy by photodynamic therapy. *Autophagy*, *2*(4), 289–290.

Kim, B., Yeom, H. R., Yun, M. H., Kim, J. Y., & Yang, C. (2012). to Lower of the Bandgap for Efficient Polymer Solar Cells. *Macromolecules*, *45*, 8658−8664.

Kroemer, G., & Jäättelä, M. (2005). Lysosomes and autophagy in cell death control. *Nature Reviews Cancer*, *5*(11), 886–897.

Landau, I. M. E., Steen, B., & Seregard, S. Photodynamic therapy for circumscribed choroidal haemangioma (2002).

Leach, A. G., & Houk, K. N. (2002). Diels-Alder and ene reactions of singlet oxygen, nitroso compounds and triazolinediones: Transition states and mechanisms from contemporary theory. *Chemical Communications*, *2*(12), 1243–1255.

Lipson, R. L., & Baldes, E. J. (1960). The photodynamic properties of a particular hematoporphyrin derivative. *Arch. Dermatol.*, *82*, 508–516.

Lobo, F., Lo, J. C., Oliden, A., & Ban, J. (2017). One-Pot Synthesis of Rotationally Restricted, Conjugatable, BODIPY Derivatives from Phthalides. *Journal of Organic Chemistry*, *82*, 1240−1247.

Luby, M., D., C. W., & Zheng, G. (2018). Advanced Photosensitizer Activation Strategies for Smarter Photodynamic Therapy Beacons. *Angewandte Chemie - International Edition*.

Martin, W. C. (1971). Table of Spin-Orbit Energies for p-Electrons in Neutral Atomic {core)np Configurations. *JOURNAL OF RESEARCH of Toe Notional Bureau of Standards - A. Physics and Chemistry*, *75A*(2), 109–111.

McCaughan, J. S., Hicks, W., Laufman, L., May, E., & Roach, R. (1984). Palliation of esophageal malignancy with photoradiation therapy. *Cancer*, *54*(12), 2905–2910.

Meyer–Betz, F. (1913). Untersuchungen uber die biologische photodynamische Wirkung des Hematoporphyrins und anderer Derivative des Blut und Galenafarbstoffs. *Dtsch. Arch. Klin.*, *112*, 476–503.

Moan, J., & Berg, K. (1991). the Photodegradation of Porphyrins in Cells Can Be Used To Estimate the Lifetime of Singlet Oxygen. *Photochemistry and Photobiology*, *53*(4), 549–553.

Morton, C. A., Brown, S. B., Collins, S., Ibbotson, S., Jenkinson, H., Kurwa, H., … Rhodes, L. E. (2002). Guidelines for topical photodynamic therapy: Report of a workshop of the British Photodermatology Group. *British Journal of Dermatology*, *146*, 552–567.

Neumeyer, J. L., & Cannon, J. G. (1961). Reaction of Methyl Bromide with

Dimethylformamide. *Journal of Organic Chemistry*, *26*(11), 4681–4682.

Odeh, A. M., Craik, J. D., Ezzeddine, R., Tovmasyan, A., Batinic-haberle, I., & Benov, L. T. (2014). Targeting Mitochondria by Zn (II) N-Alkylpyridylporphyrins : The Impact of Compound Sub- Mitochondrial Partition on Cell Respiration and Overall Photodynamic Efficacy. *Plos One*, *9*(9).

Ormond, A. B., & Freeman, H. S. (2013). Dye sensitizers for photodynamic therapy. *Materials*, *6*(3), 817–840.

Ortiz, M. J., Agarrabeitia, A. R., Duran-Sampedro, G., Bañuelos Prieto, J., Lopez, T. A., Massad, W. A., … Lopez Arbeloa, I. (2012). Synthesis and functionalization of new polyhalogenated BODIPY dyes. Study of their photophysical properties and singlet oxygen generation. *Tetrahedron*, *68*(4), 1153–1162.

Pavani, C., Uchoa, A. F., Oliveira, C. S., Iamamoto, Y., & Baptista, M. S. (2009). Effect of zinc insertion and hydrophobicity on the membrane interactions and PDT activity of porphyrin photosensitizers. *Photochemical and Photobiological Sciences*, *8*, 233–240.

Prime, J. (1900). *Les accidents toxiques par l'eosinate de sodium.* (J. and Boyer, Ed.). Paris.

Pushpan, S. K., Venkatraman, S., Anand, V. G., Sankar, J., Parmeswaran, D., Ganesan, S., & Chandrashekar, T. K. (2002). Porphyrins in photodynamic therapy - a search for ideal photosensitizers. *Curr Med Chem Anticancer Agents*, *2*, 187–207.

Raab, O. (1900). Uber die Wirkung fluoreszierender Stoffe auf Infusorien. *Zeitung Biol.*, *39*, 524–526.

Rio, M., Lobo, F., Lopez, J. C., Oliden, A., Lopez-arbeloa, I., García-moreno, I., & Gomez, A. M. (2016). One-Pot Synthesis of Rotationally Restricted , Conjugatable , BODIPY Derivatives from Phthalides . *Journal of Organic Chemistry*.

Rohand, T., Qin, W., Boens, N., & Dehaen, W. (2006). Palladium-catalyzed coupling reactions for the functionalization of BODIPY dyes with fluorescence spanning the visible spectrum. *European Journal of Organic Chemistry*, (20), 4658–4663.

Rosenthal, M. A., Kavar, B., Hill, J. S., Morgan, D. J., Nation, R. L., Stylli, S. S., … Kaye, A. H. (2001). Phase I and pharmacokinetic study of photodynamic therapy for high-grade gliomas using a novel boronated porphyrin. *Journal of Clinical Oncology*, *19*(2), 519–524.

Rubio, N., Fleury, S. P., & Redmond, R. W. (2009). Spatial and temporal dynamics of in vitro photodynamic cell killing: Extracellular hydrogen peroxide mediates neighbouring cell death. *Photochemical and Photobiological Sciences*, *8*(4), 457–464.

Sakamoto, K., Kato, T., Kawaguchi, T., Ohno-Okumura, E., Urano, T., Yamaoka, T., … Cook, M. J. (2002). Photosensitizer efficacy of non-peripheral substituted alkylbenzopyridoporphyrazines for photodynamic therapy of cancer. *Journal of Photochemistry and Photobiology A: Chemistry*, *153*, 245–253.

Santoro, O., Bandieramonte, G., Lepera, P., Palo, G. De, Melloni, E., Marchesini, R., & Zunino, F. (1990). Photodynamic Therapy by Topical meso-Tetraphenylporphinesulfonate Tetrasodium Salt Administration in Superficial Basal Cell Carcinomas. *Cancer Research*, *50(15)*, 4501–4503.

Schwartz, S. K., Abolon, K., & Vermund, H. (1955). Some relationships of porphyrins, X-rays and tumors. *Univ. Minn. Med. Bull*, *27*, 7–8.

Sessler, J. L., Murai, T., Lynch, V., & Cyr, M. (1988). An "Expanded Porphyrin": The Synthesis and Structure of a New Aromatic Pentadentate Ligand. *Journal of the American Chemical Society*, *110*(16), 5586–5588.

Shigeta, M., Watanabe, J., Konishi, G., & Materials, P. (2013). Phenoxide-mediated Sonogashira Coupling of Trimethylsilylalkynes and Aryliodides : Practical Synthesis of Phenolic-Hydroxy-Substituted Diarylethynes and 1 , 4-Diarylbutadiynes. *Tetrahedron Letters*, *54*(13), 1761–1764.

Shin, W. S., Lee, M. G., Verwilst, P., Lee, J. H., Chi, S. G., & Seung, J. K. (2016). Mitochondria-Targeted Aggregation Induced Emission Theranostics: Crucial Importance of In Situ Activation. *Royal Society of Chemistry*, *7*(9), 6050–6059.

Sorbellini, E., Rucco, M., & Rinaldi, F. (2018). Photodynamic and photobiological effects of light-emitting diode (LED) therapy in dermatological disease : an

update. *Lasers in Medical Science*, *33*, 1431–1439.

Star, W. M., Hans, A., P.Marijnissen, Anneke, E., Versteeg, van den B.-B. J. A. C., Franken, K. A. P., & Reinhold, H. S. (1986). Destruction of Rat Mammary Tumor and Normal Tissue Microcirculation by Hematoporphyrin Derivative Photoradiation Observed in Vivo in Sandwich Observation Chambers. *Cancer Research*, *46*(5), 2532–2540.

Taguchi, D., Nakamura, T., Horiuchi, H., Saikawa, M., & Nabeshima, T. (2018). Synthesis and Unique Optical Properties of Selenophenyl BODIPYs and Their Linear Oligomers. *Journal of Organic Chemistry*, *83*(9), 5331–5337.

Takahashi, K., & Tarutani, S. (1996). EFFICIENT SYNTHESIS OF 2-IODO AND 2-DICYANOMETHYL DERIVATIVES OF THIOPHENE, SELENOPHENE, TELLUROPHENE, AND THIEN0[3,2-b1THIOPHENE. *Heterocycles*, *43*(9), 1927–1935.

Tappeiner, H. von, & Jodlbauer, A. (1907). *Die sensiblilisierende Wirkung fluoreszierender Substanzer Gesammte Untersuchungen uber die photodynamische Erscheinerung*. *Voger, F. C.: Leipzig*.

Tayyaba Hasan, Ortel, B., Moor, A. C. E., & Pogue, B. W. (2003). Photodynamic Therapy of Cancer. In K. DW, P. RE, & W. RR (Eds.), *Holland-Frei Cancer Medicine* (6th ed.). BC Decker Inc.

Tian, Y., Wang, L., & Wang, W. (2008). Progress in Photodynamic Therapy on Tumors. *Laser Phys.*, *18*(10), 1119–1123.

Umezawa, K., Matsui, A., Nakamura, Y., Citterio, D., & Suzuki, K. (2009). Bright, color-tunable fluorescent dyes in the Vis/NIR region: Establishment of new “tailor-made” multicolor fluorophores based on borondipyrromethene. *Chemistry - A European Journal*, *15*(5), 1096–1106.

Valko, M., Morris, H., & Cronin, M. (2005). Metals, Toxicity and Oxidative Stress. *Current Medicinal Chemistry*, *12*(10), 1161–1208.

Wallace, D. C. (2012). Mitochondria and cancer. *Nature Reviews Cancer*, *12*, 685–698.

Wang, X., Peralta, S., & Moraes, C. T. (2013). *Mitochondrial Alterations During*

Carcinogenesis : A Review of Metabolic Transformation and Targets for Anticancer Treatments. *Advances in Cancer Research* (1st ed., Vol. 119). Elsevier Inc.

Weyergang, A., Berg, K., Kaalhus, O., Peng, Q., & Selbo, P. K. (2009). Photodynamic therapy targets the mTOR signaling network in Vitro and in Vivo. *Molecular Pharmaceutics*, *6*, 255–264.

Wilson, W. R., & Hay, M. P. (2011). Targeting hypoxia in cancer therapy. *Nature Reviews Cancer*, *11*(6), 393–410.

Yogo, T., Urano, Y., Ishitsuka, Y., Maniwa, F., & Nagano, T. (2005). Highly efficient and photostable photosensitizer based on BODIPY chromophore. *Journal of the American Chemical Society*, *127*(35), 12162–12163.

Yoo, J. O., & Ha, K. S. (2012). *New Insights into the Mechanisms for Photodynamic Therapy-Induced Cancer Cell Death*. *International Review of Cell and Molecular Biology* (1st ed., Vol. 295). Elsevier Inc. Retrieved from

Yoon, I., Li, J. Z., & Shim, Y. K. (2013). Advance in photosensitizers and light delivery for photodynamic therapy. *Clinical Endoscopy*, *46*, 7–23.

Zhu, T. C., & Finlay, J. C. (2008). The role of photodynamic therapy (PDT) physics. *Medical Physics*, *35*(7), 3127–3136.

APPENDICES

A. NMR Spectra

Each compound analyzed by Bruker Spectrospin Avance DPX-400 Spectrometer with $CDCl_3$ or DMSO as the solvent and TMS as the internal reference.

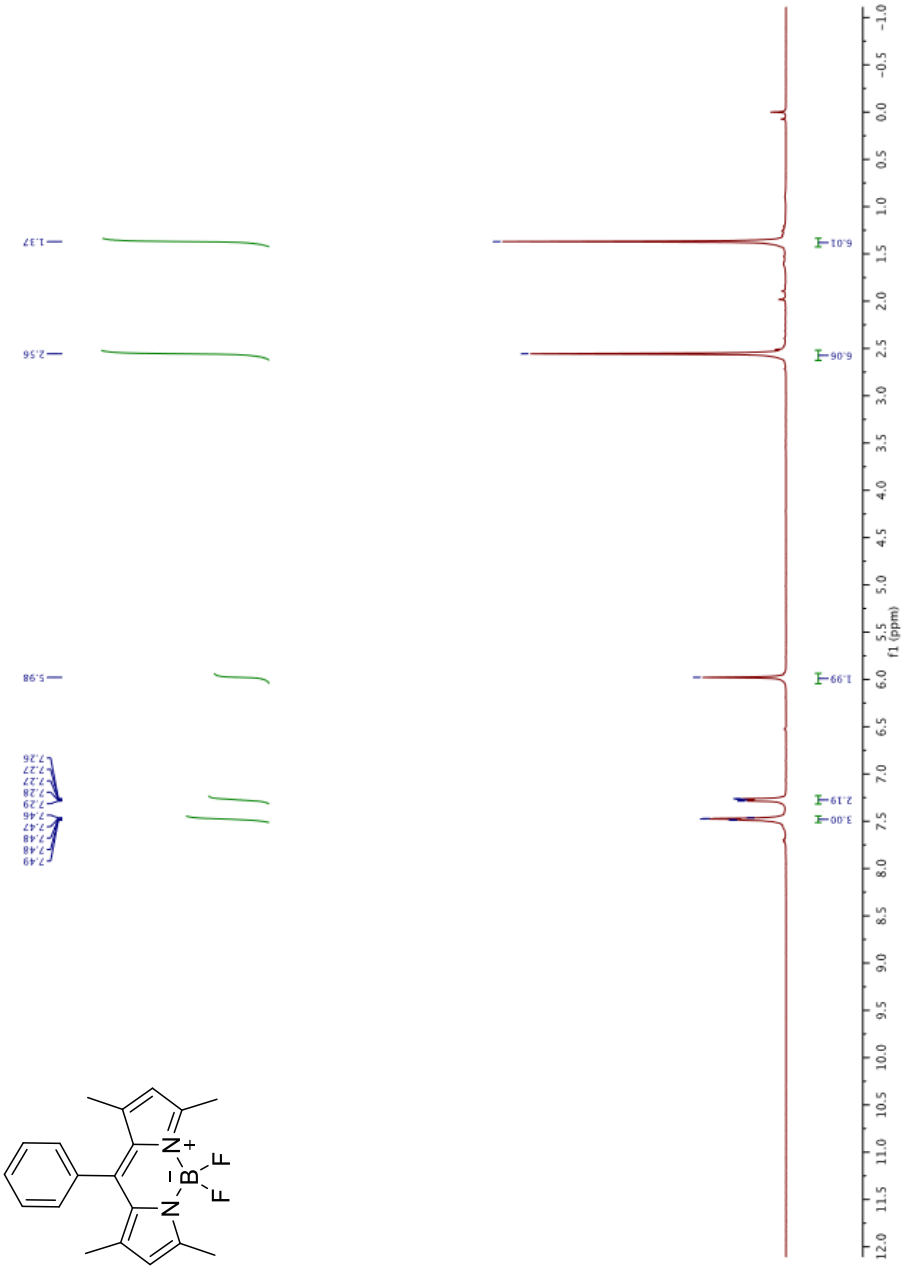

Figure A. 1. ^{1}H NMR spectrum of compound 1 in $CDCl_3$.

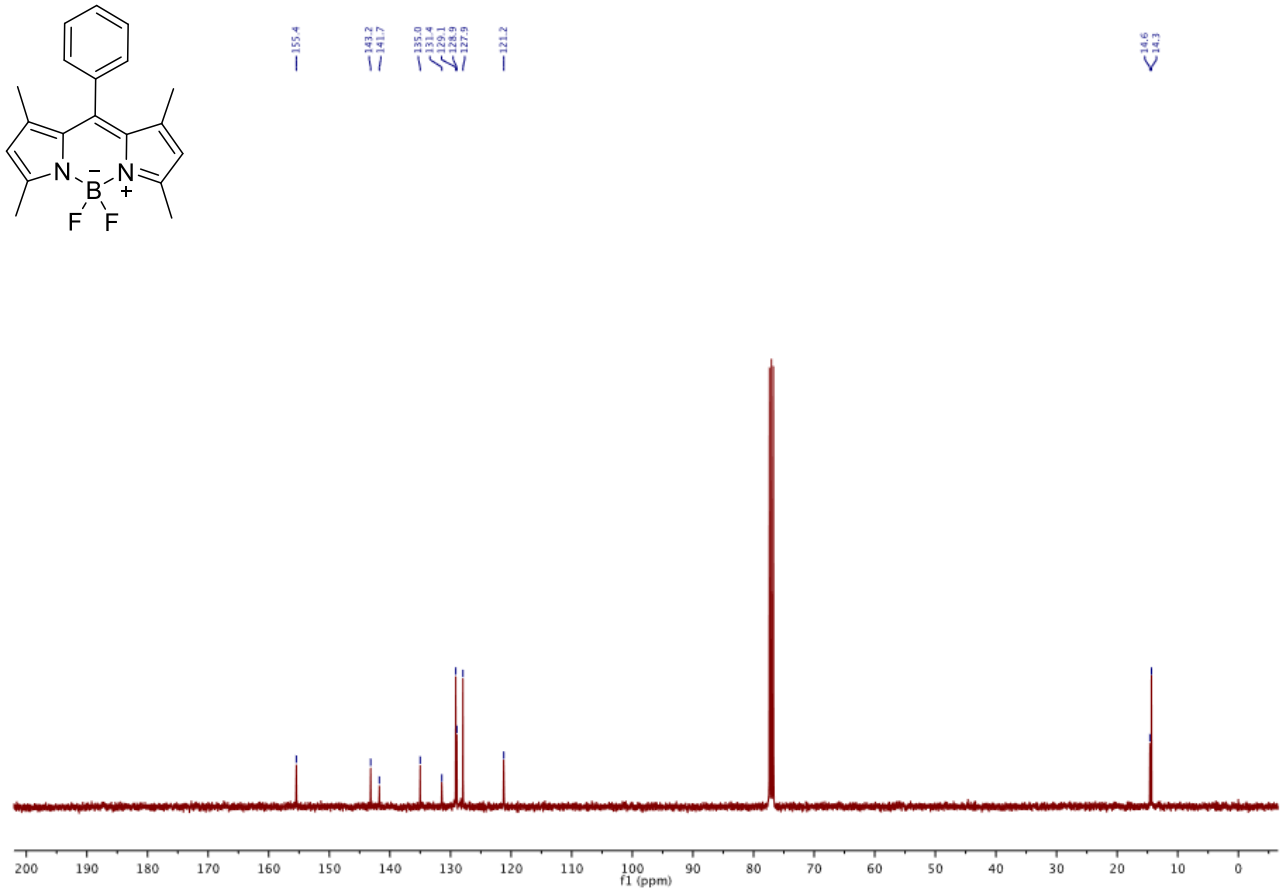

Figure A. 2. ^{13}C NMR spectrum of compound 1 in $CDCl_3$.

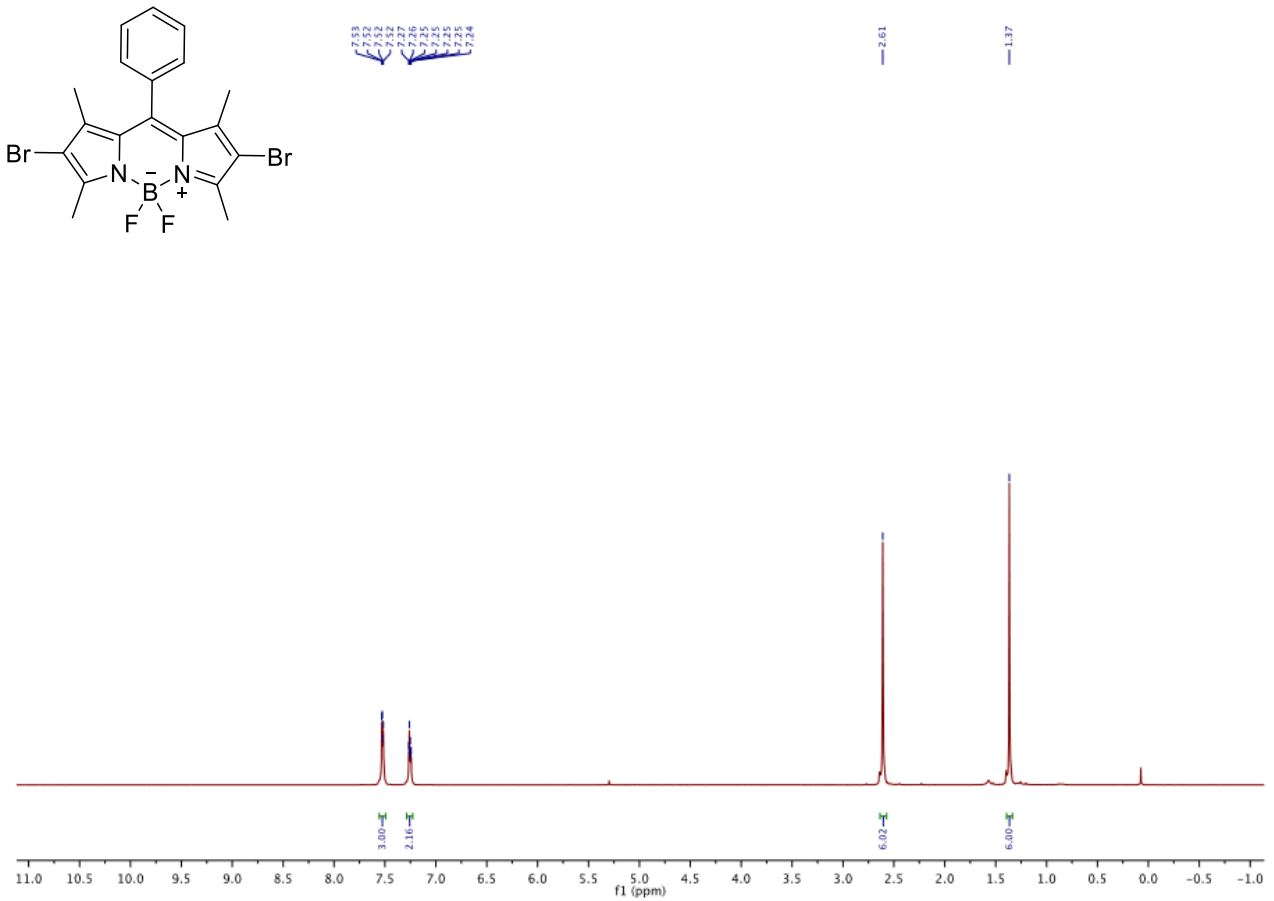

Figure A. 3. ^{1}H NMR spectrum of compound 2 in $CDCl_3$.

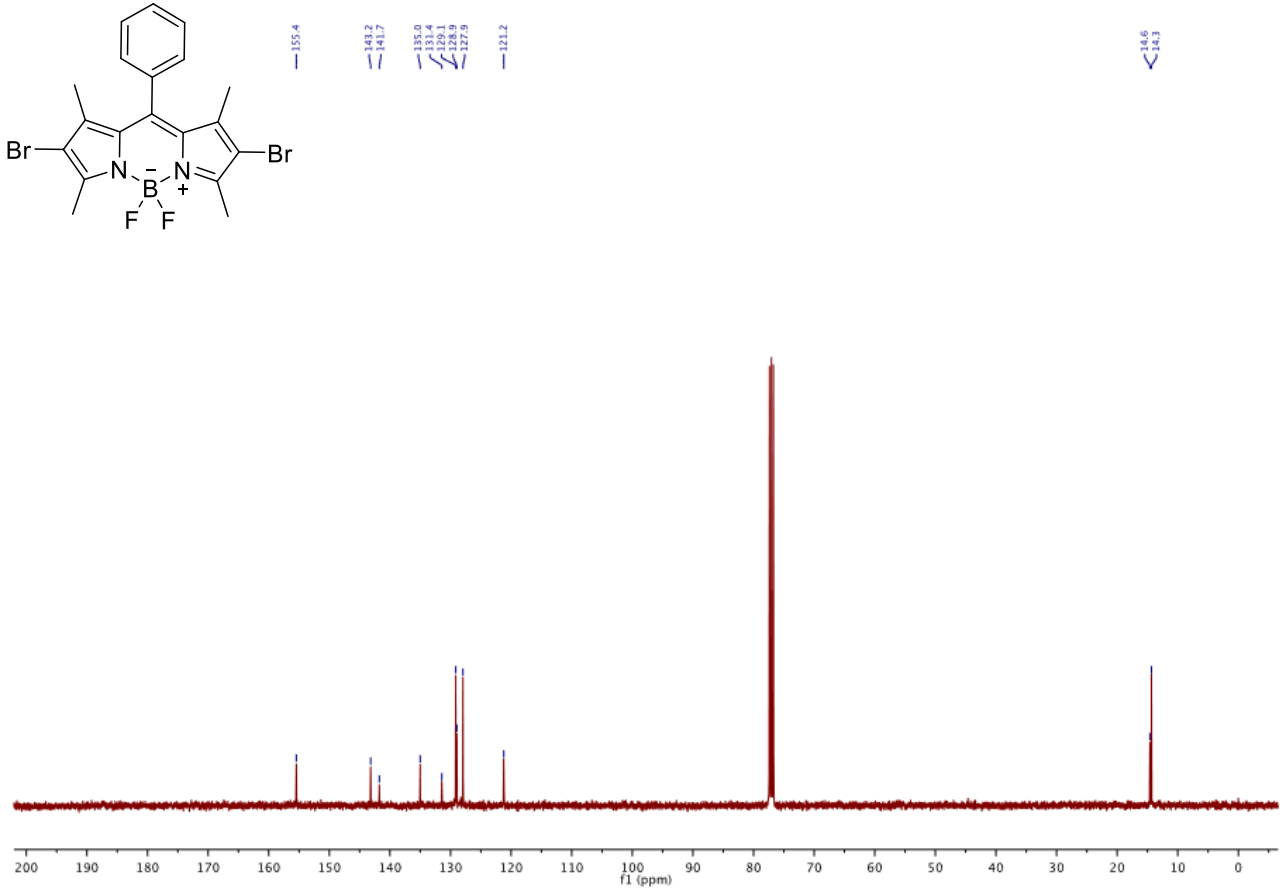

Figure A. 4. ^{13}C NMR spectrum of compound 2 in $CDCl_3$.

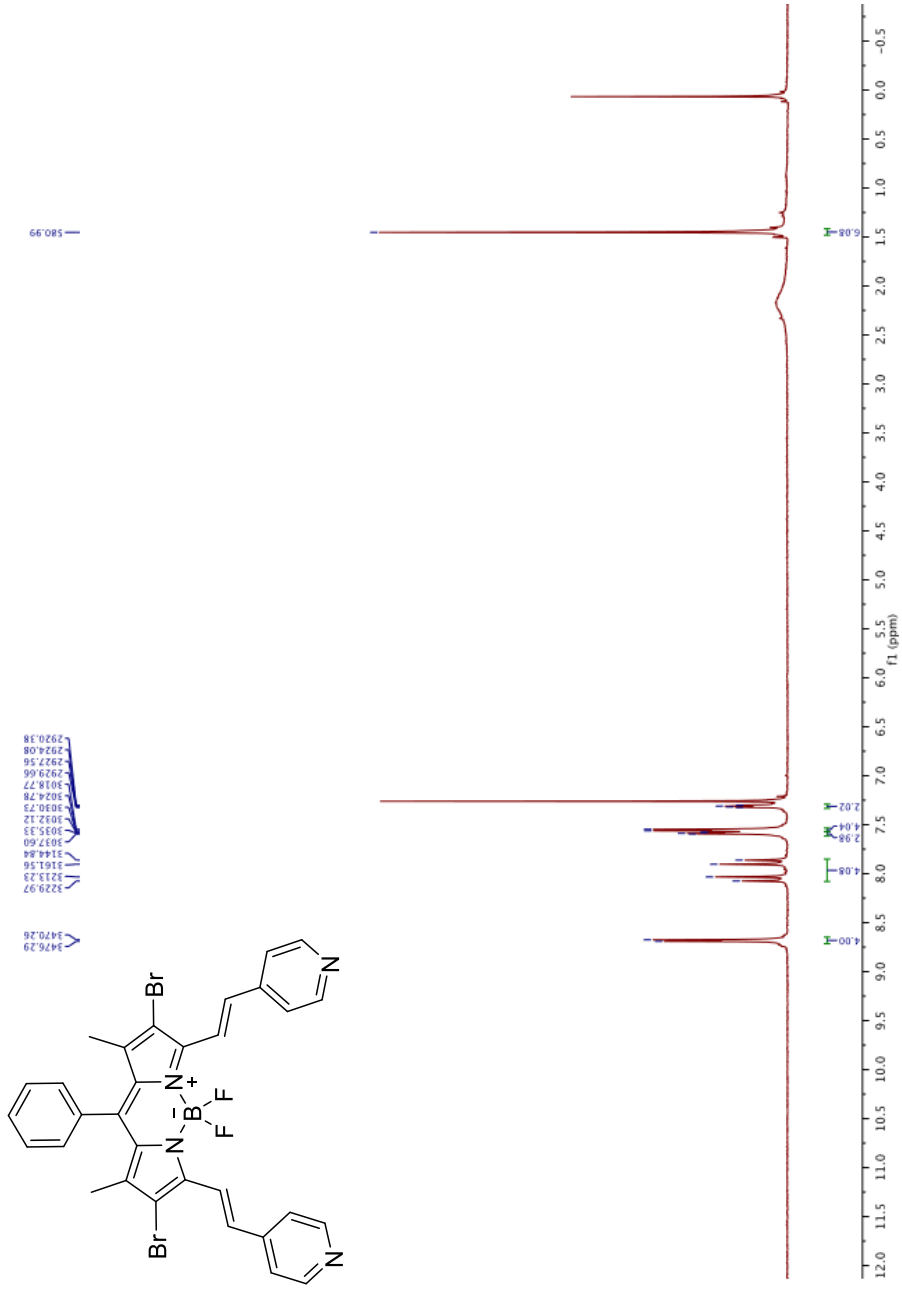

Figure A. 5. ^{1}H NMR spectrum of compound 3 in $CDCl_3$.

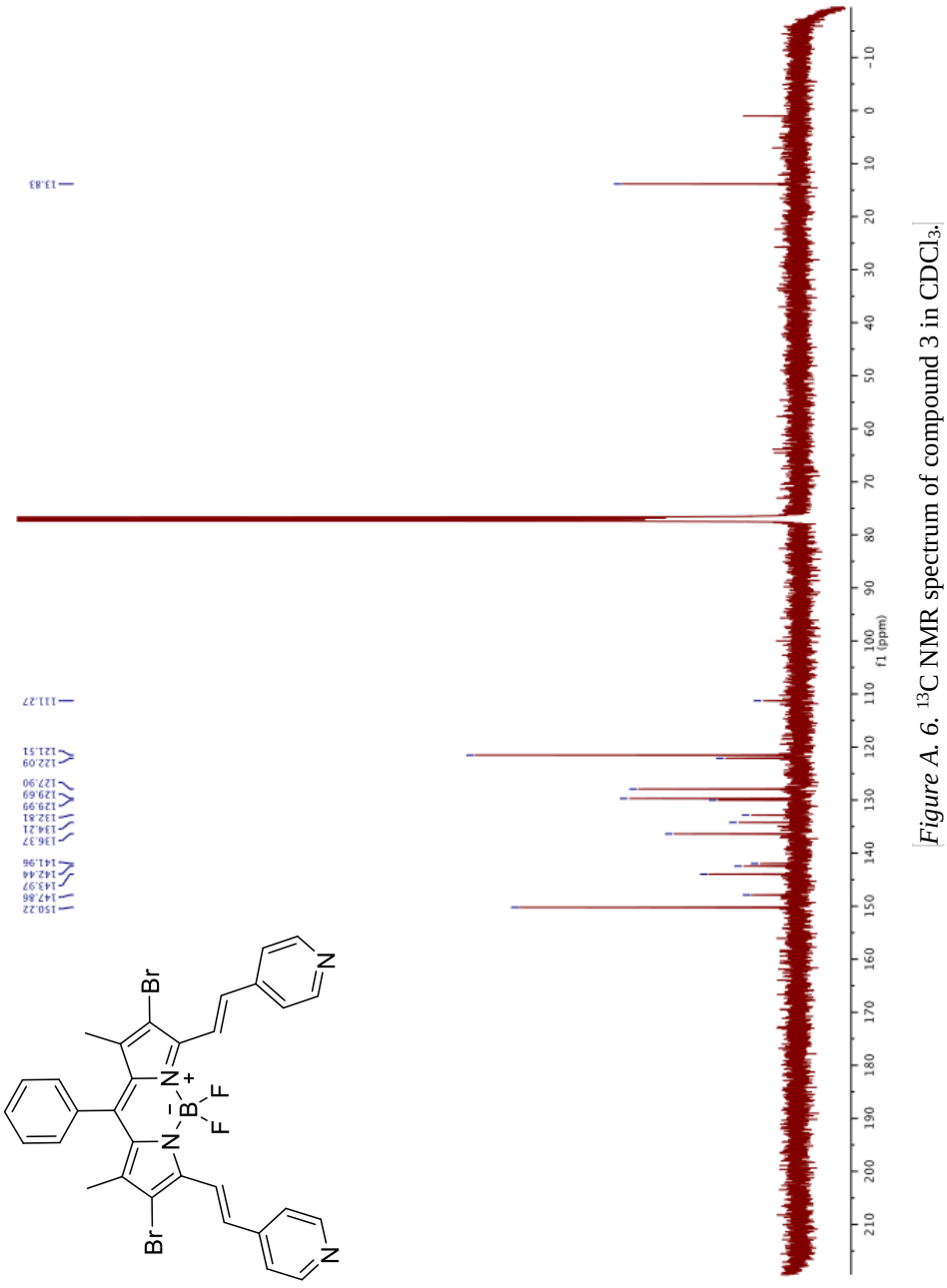

Figure A. 6. ^{13}C NMR spectrum of compound 3 in $CDCl_3$.

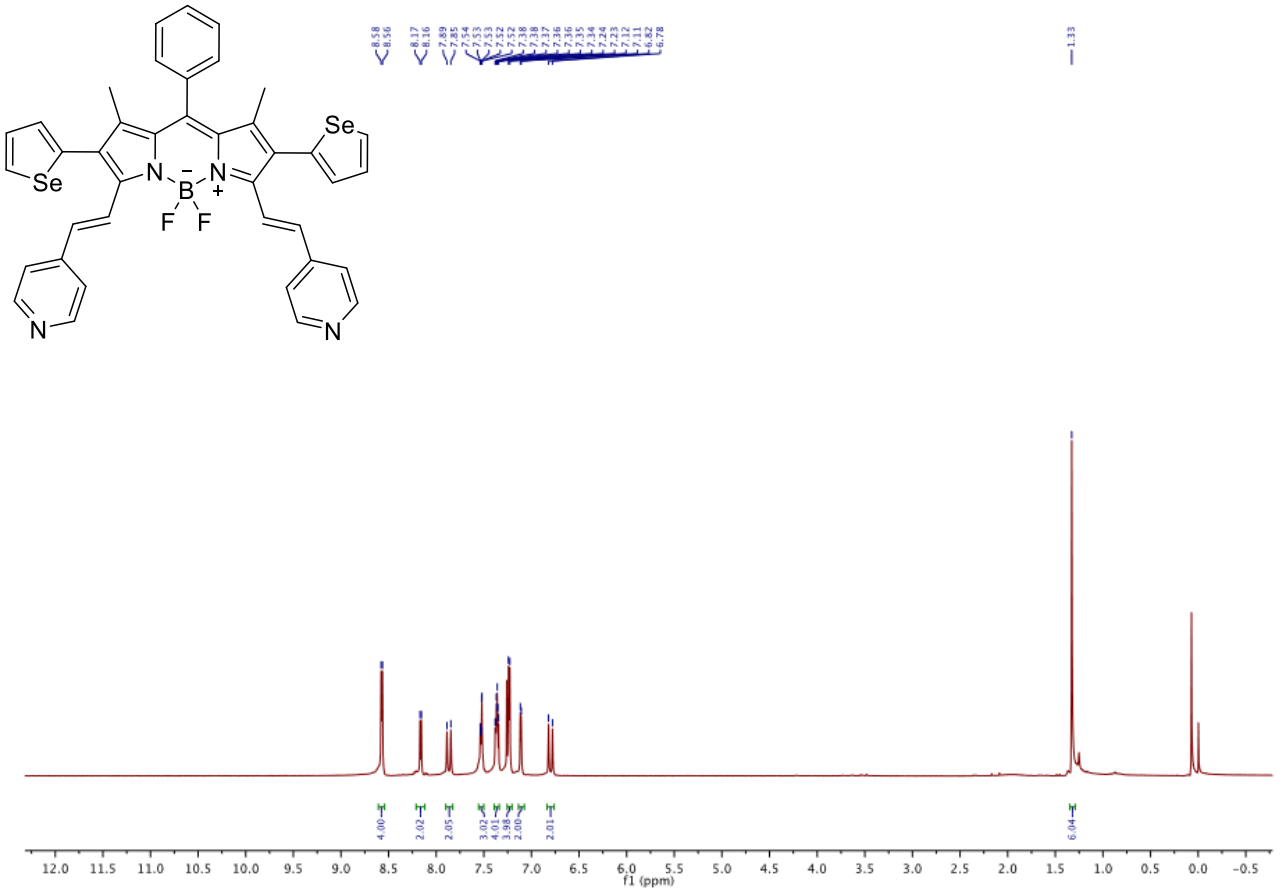

Figure A. 7. ^{1}H NMR spectrum of compound 4 in $CDCl_3$.

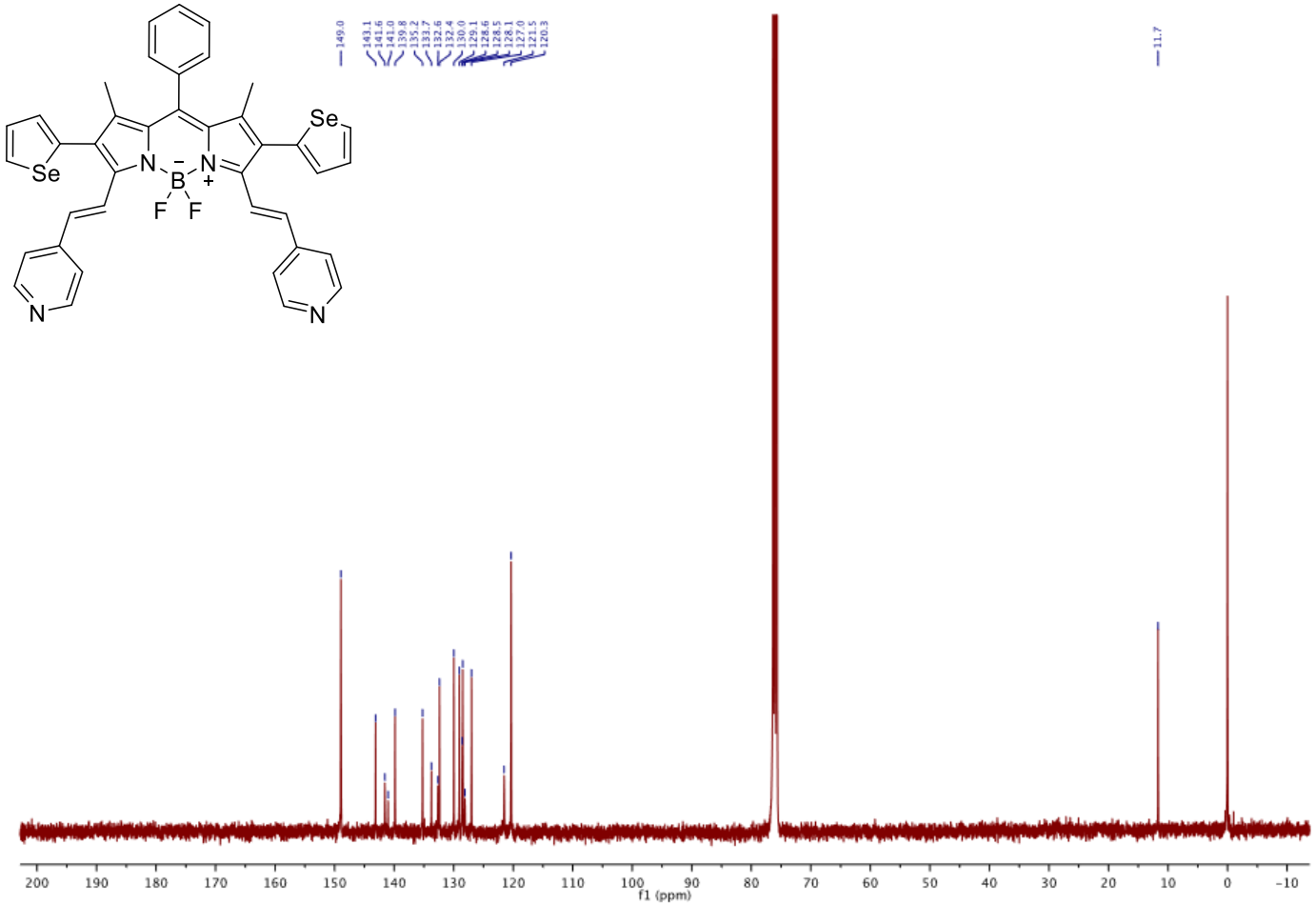

Figure A. 8. ^{13}C NMR spectrum of compound 4 in $CDCl_3$.

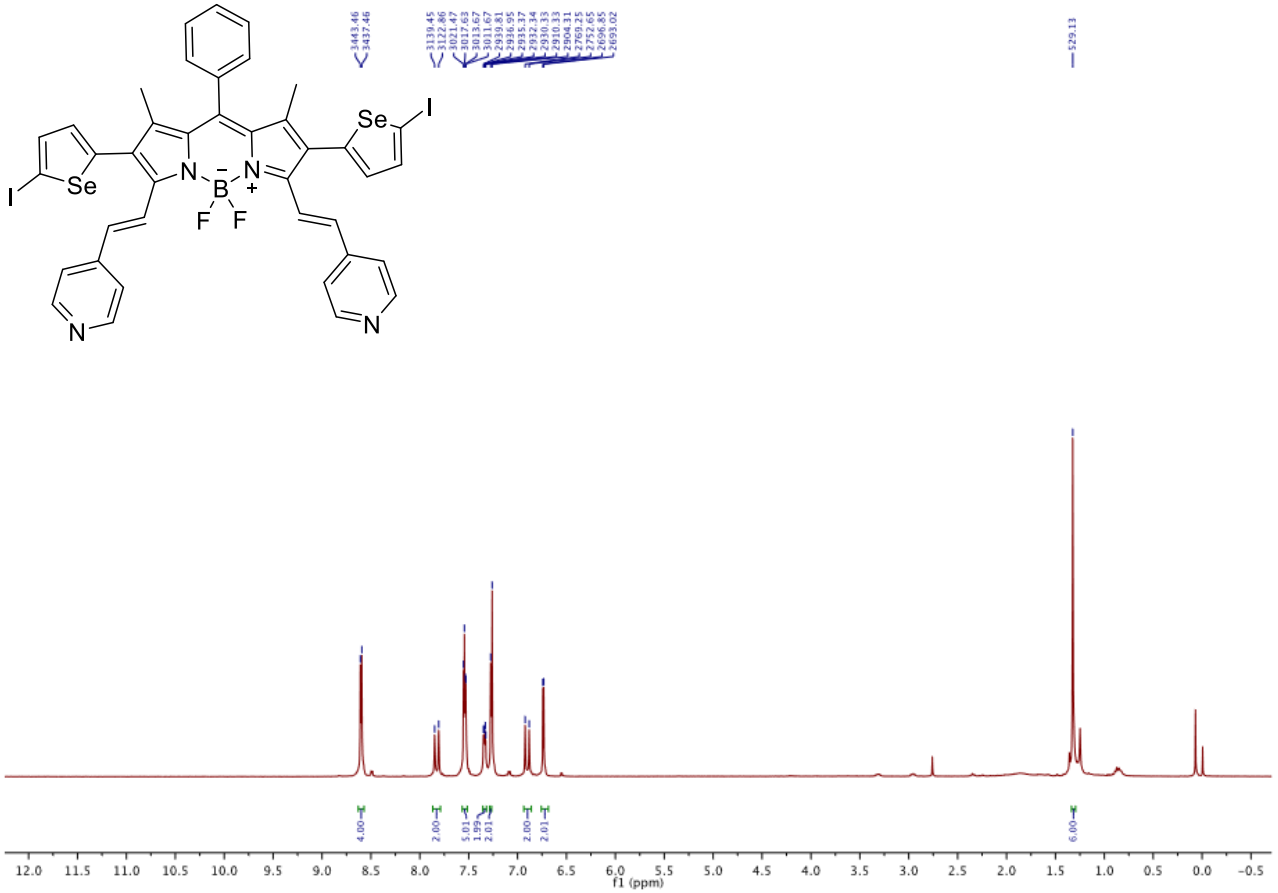

Figure A. 9. ^{1}H NMR spectrum of compound 5 in $CDCl_3$.

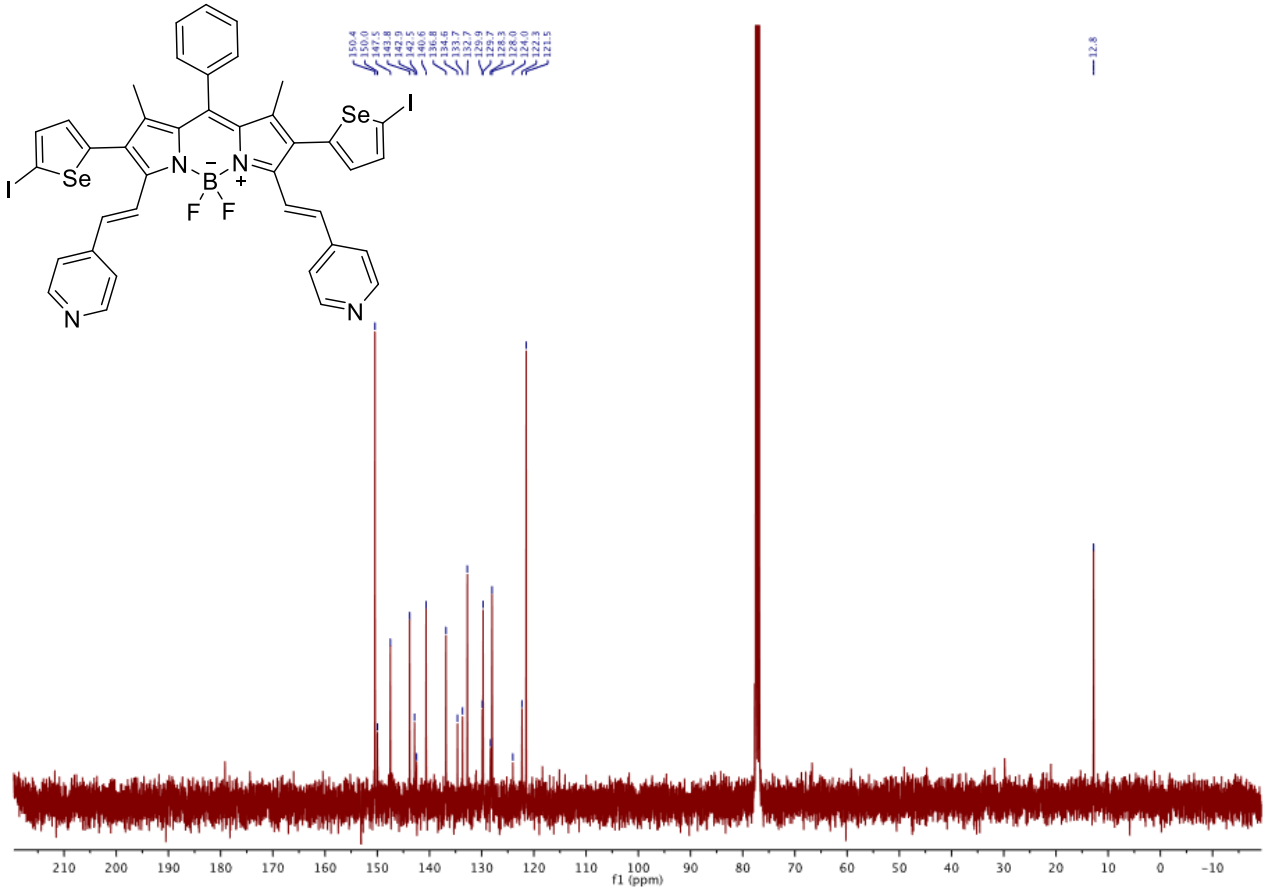

Figure A. 10. ^{13}C NMR spectrum of compound 5 in $CDCl_3$.

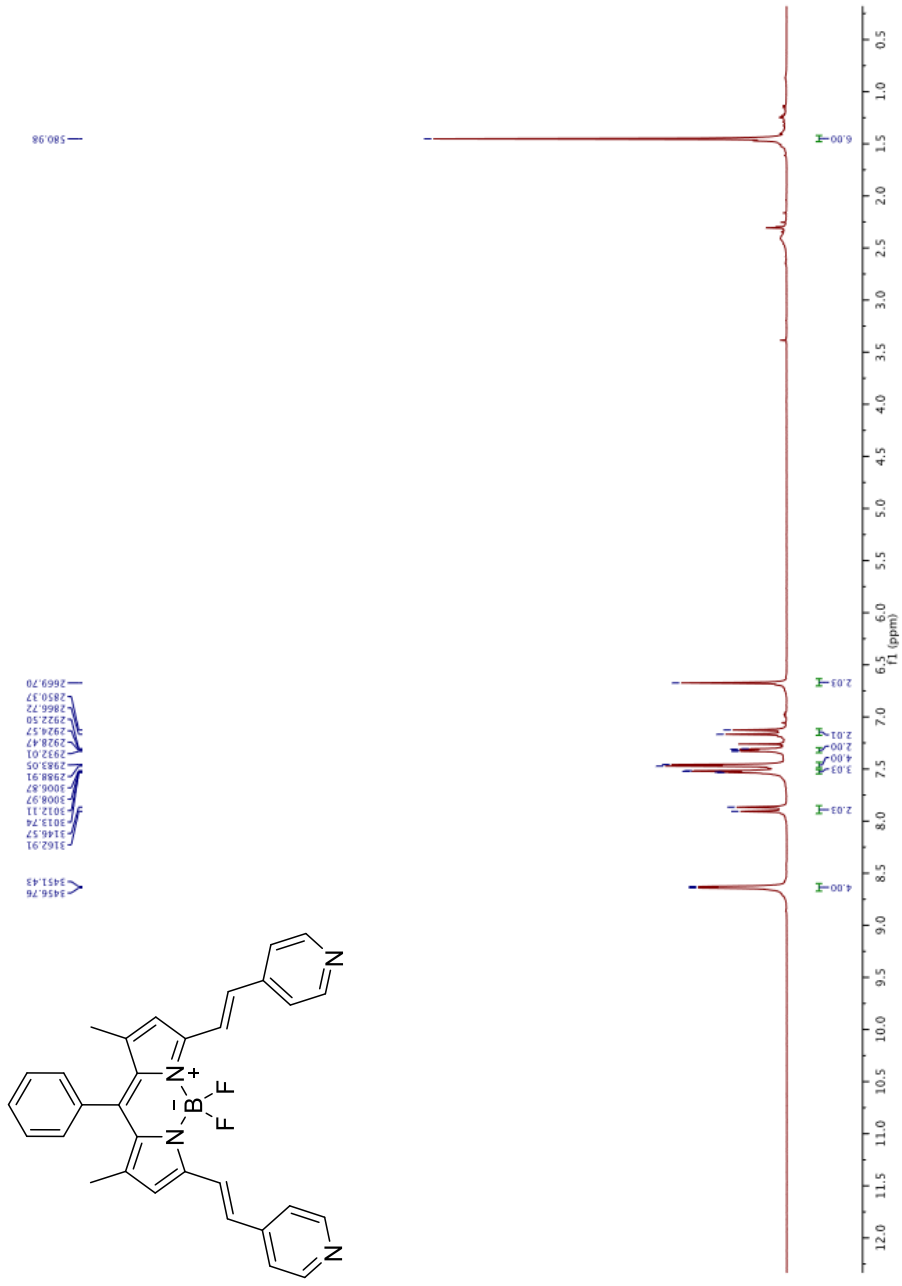

Figure A. 11. ^{1}H NMR spectrum of compound 6 in $CDCl_3$.

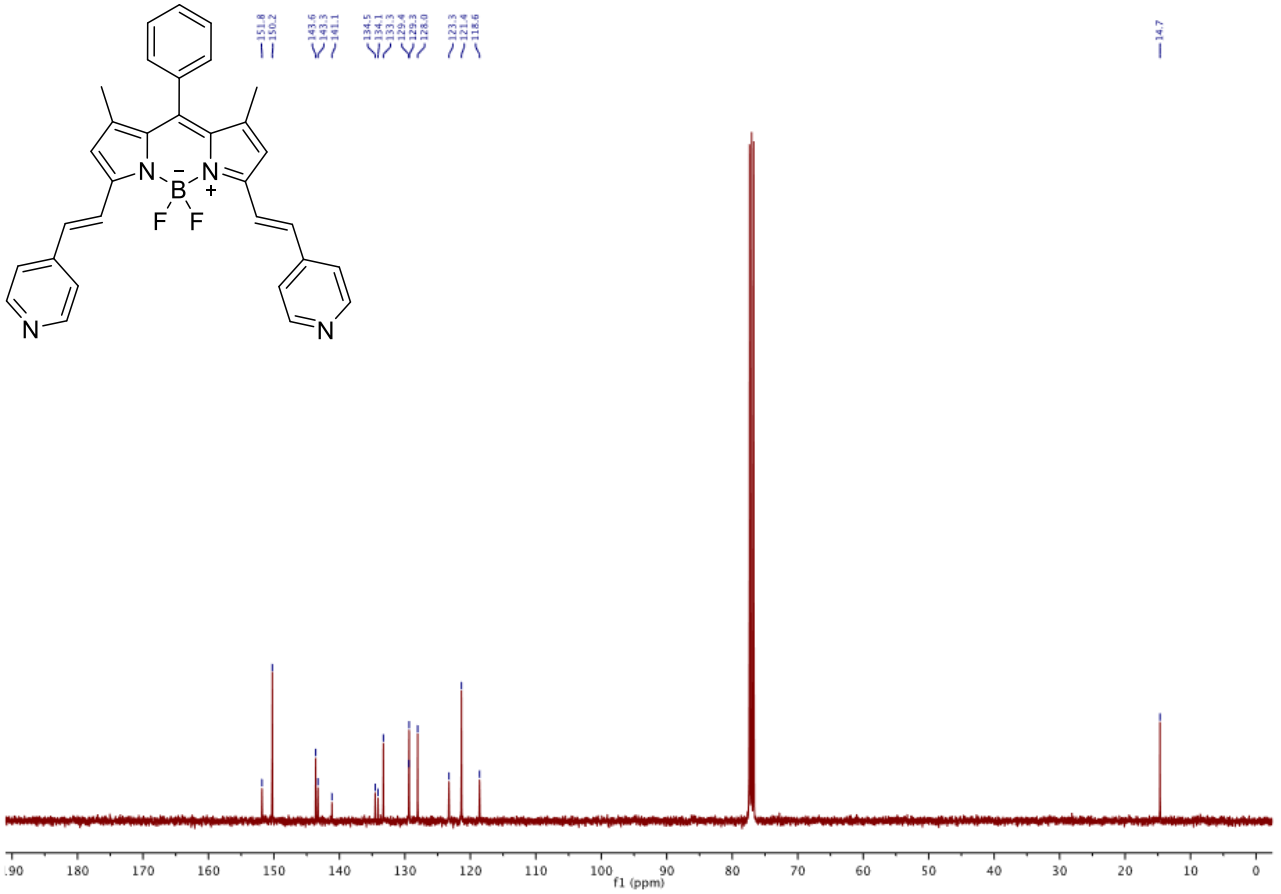

Figure A. 12. ^{13}C NMR spectrum of compound 6 in $CDCl_3$.

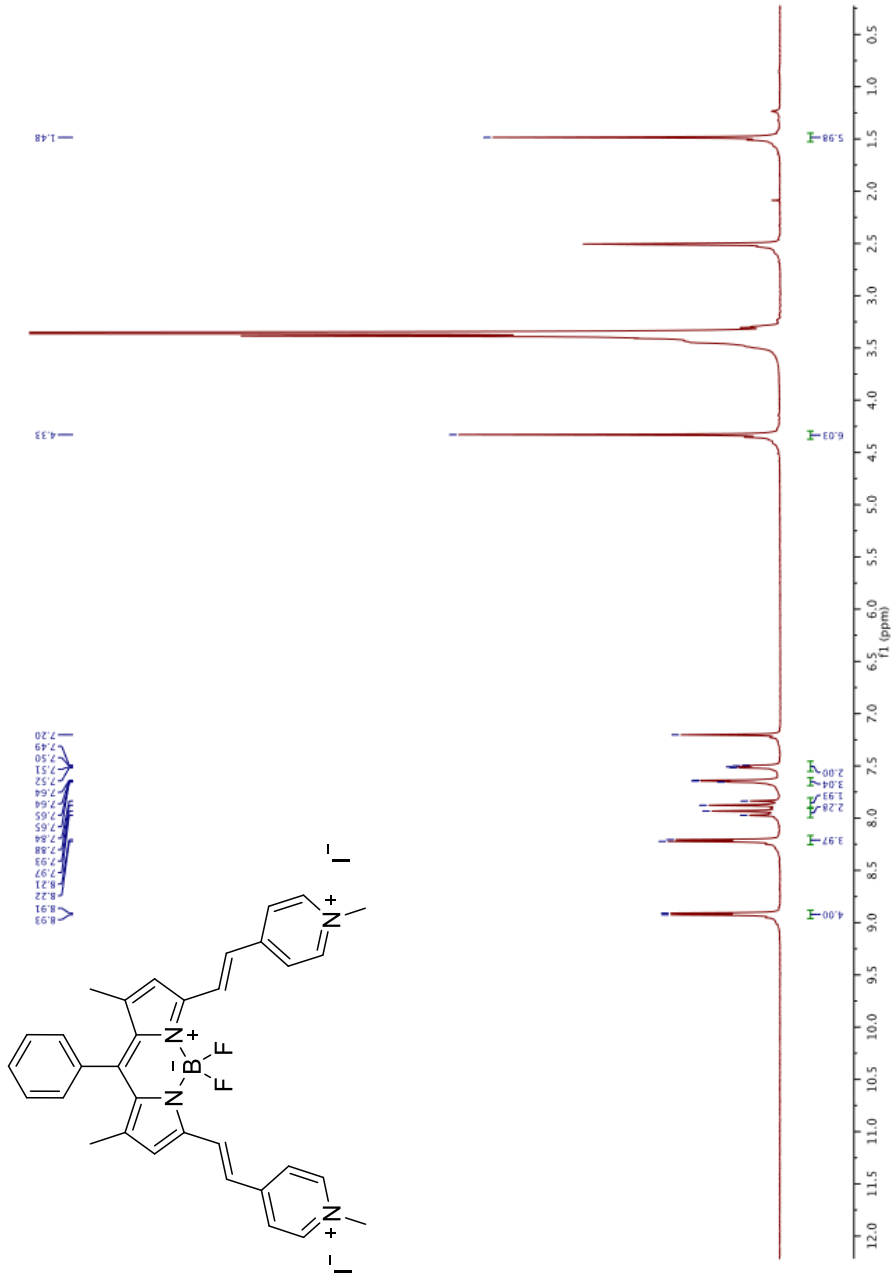

Figure A. 13. ^{1}H NMR spectrum of compound BOD-H in DMSO.

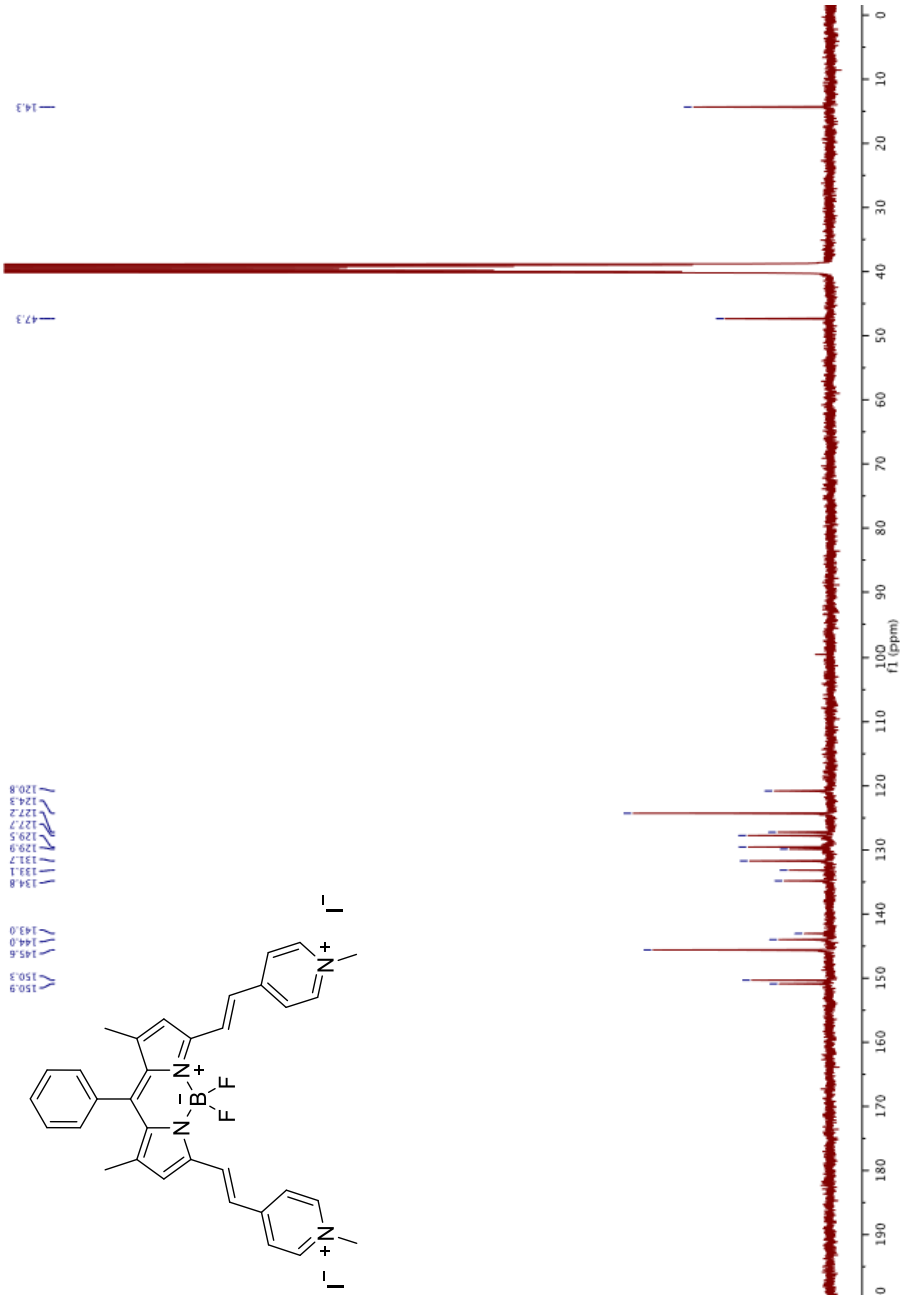

Figure A. 14. ^{13}C NMR spectrum of compound BOD-H in DMSO.

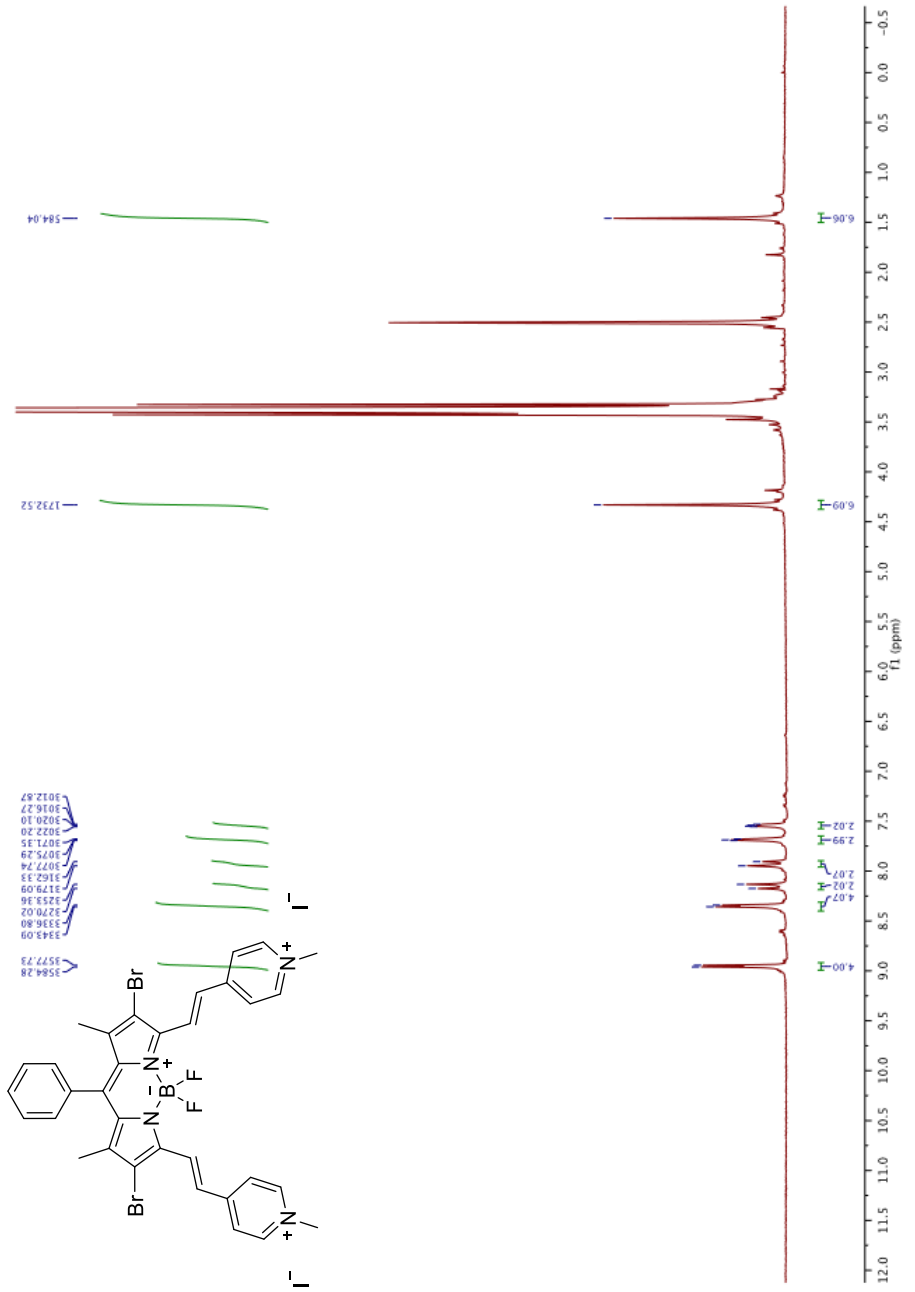

Figure A. 15. ^{1}H NMR spectrum of compound BOD-Br in DMSO.

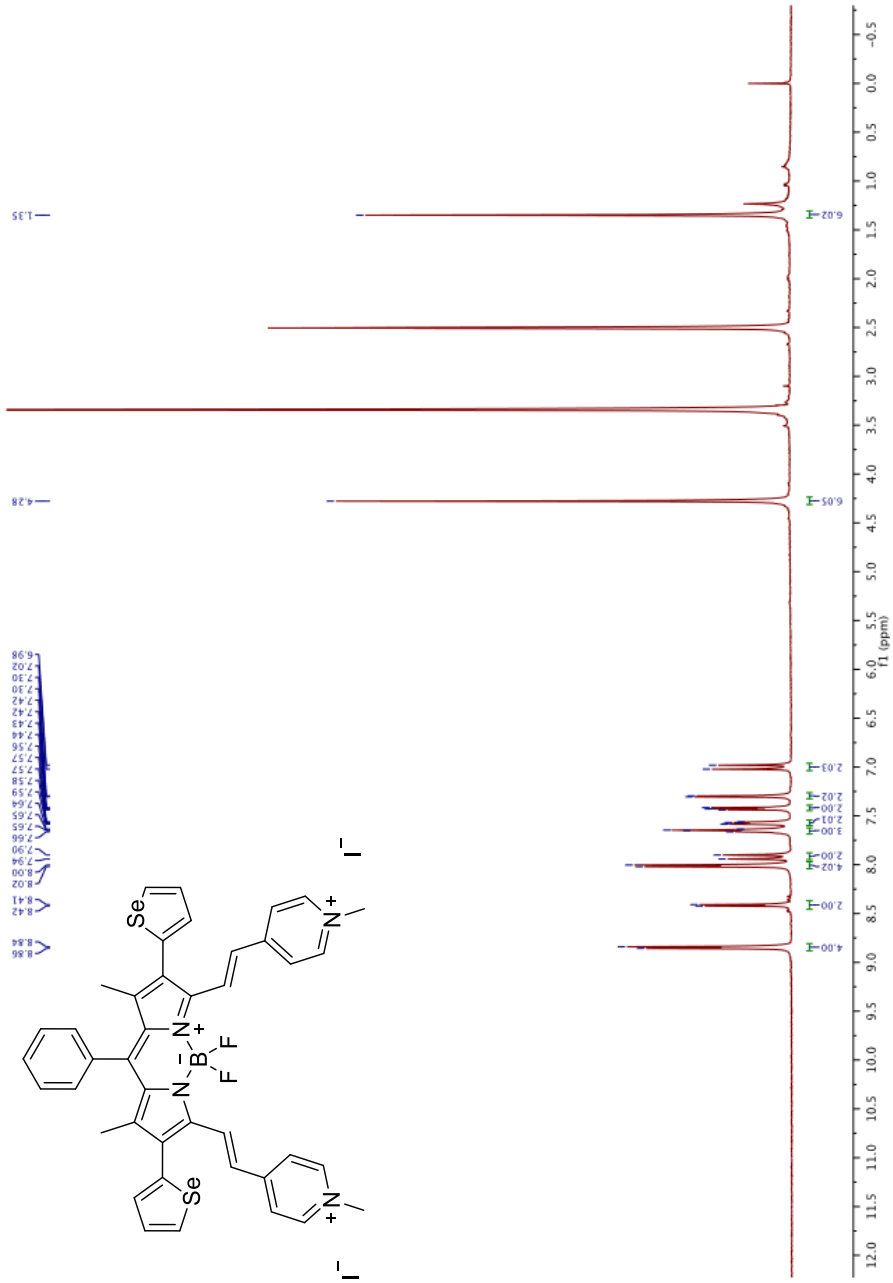

Figure A. 16. ^{1}H NMR spectrum of compound BOD-Se in DMSO.

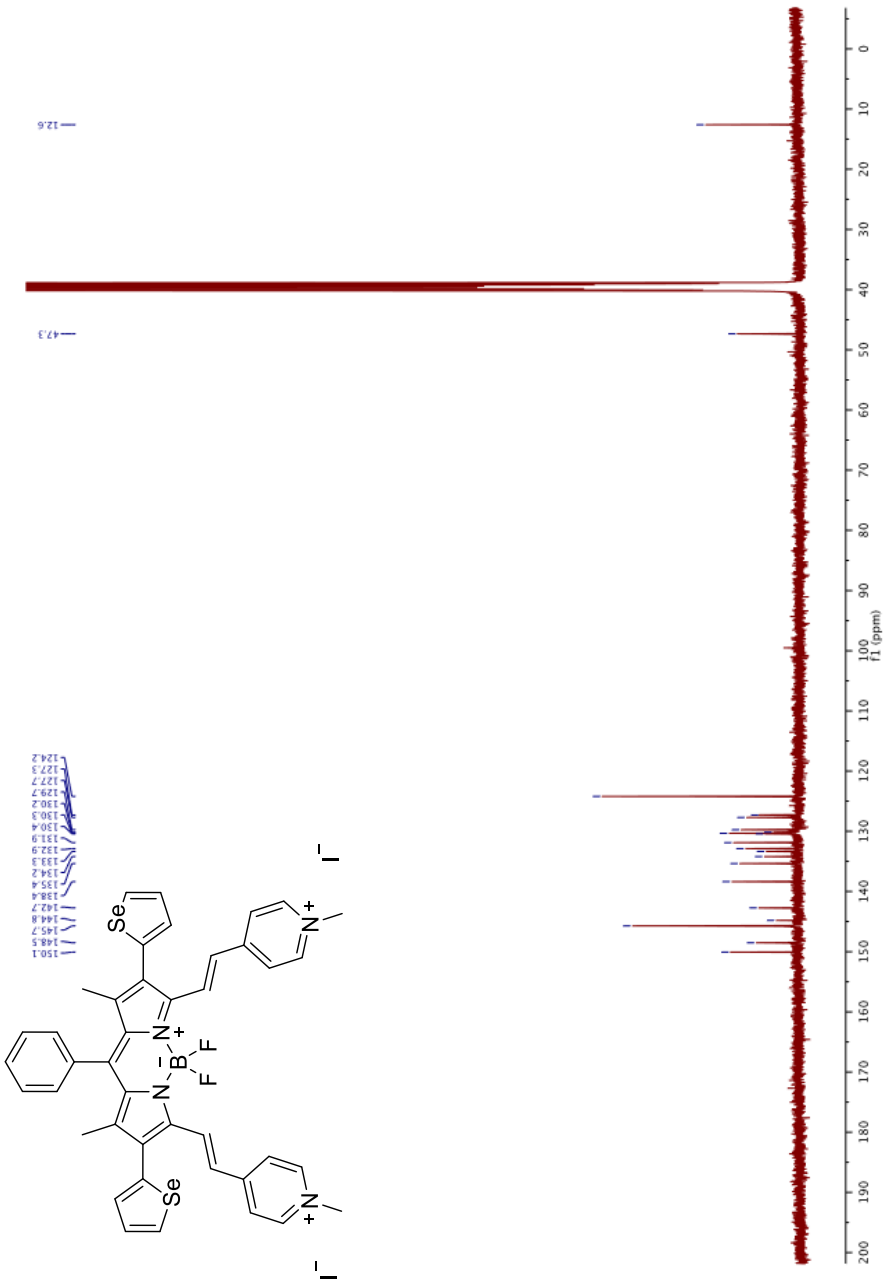

Figure A. 17. ^{13}C NMR spectrum of compound BOD-Se in DMSO.

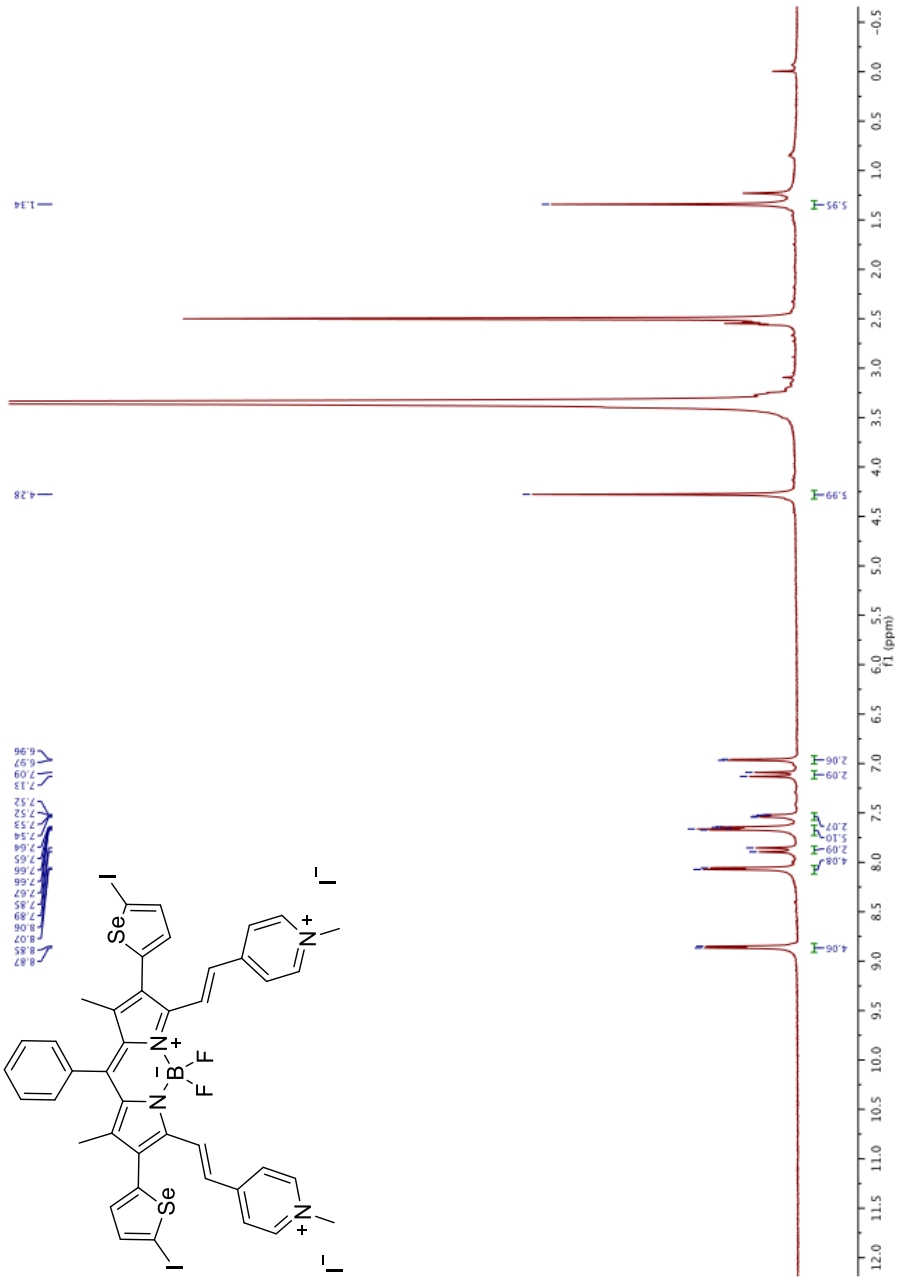

Figure A. 18. ^{1}H NMR spectrum of compound BOD-Se-I in DMSO.

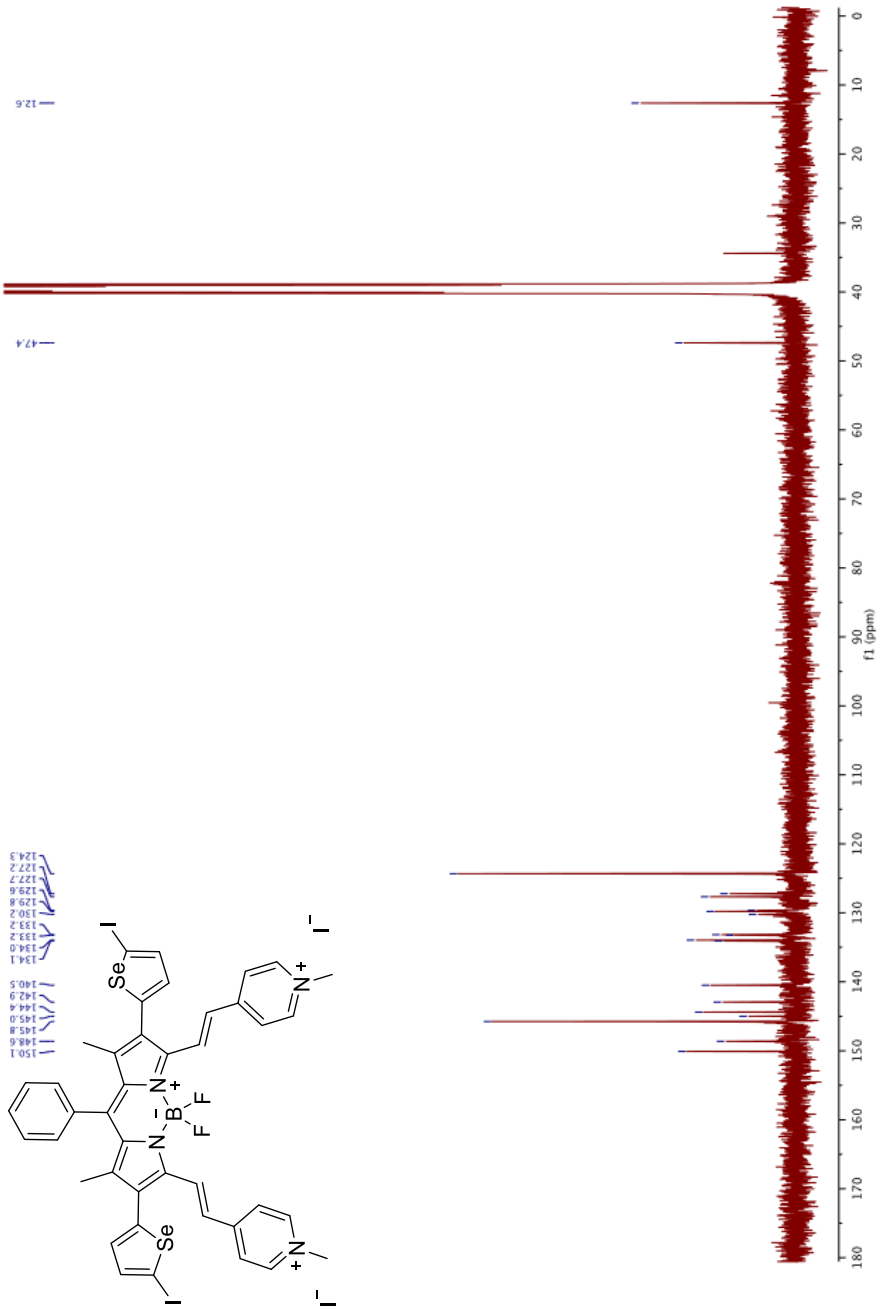

Figure A. 19. ^{13}C NMR spectrum of compound BOD-Se-I in DMSO.

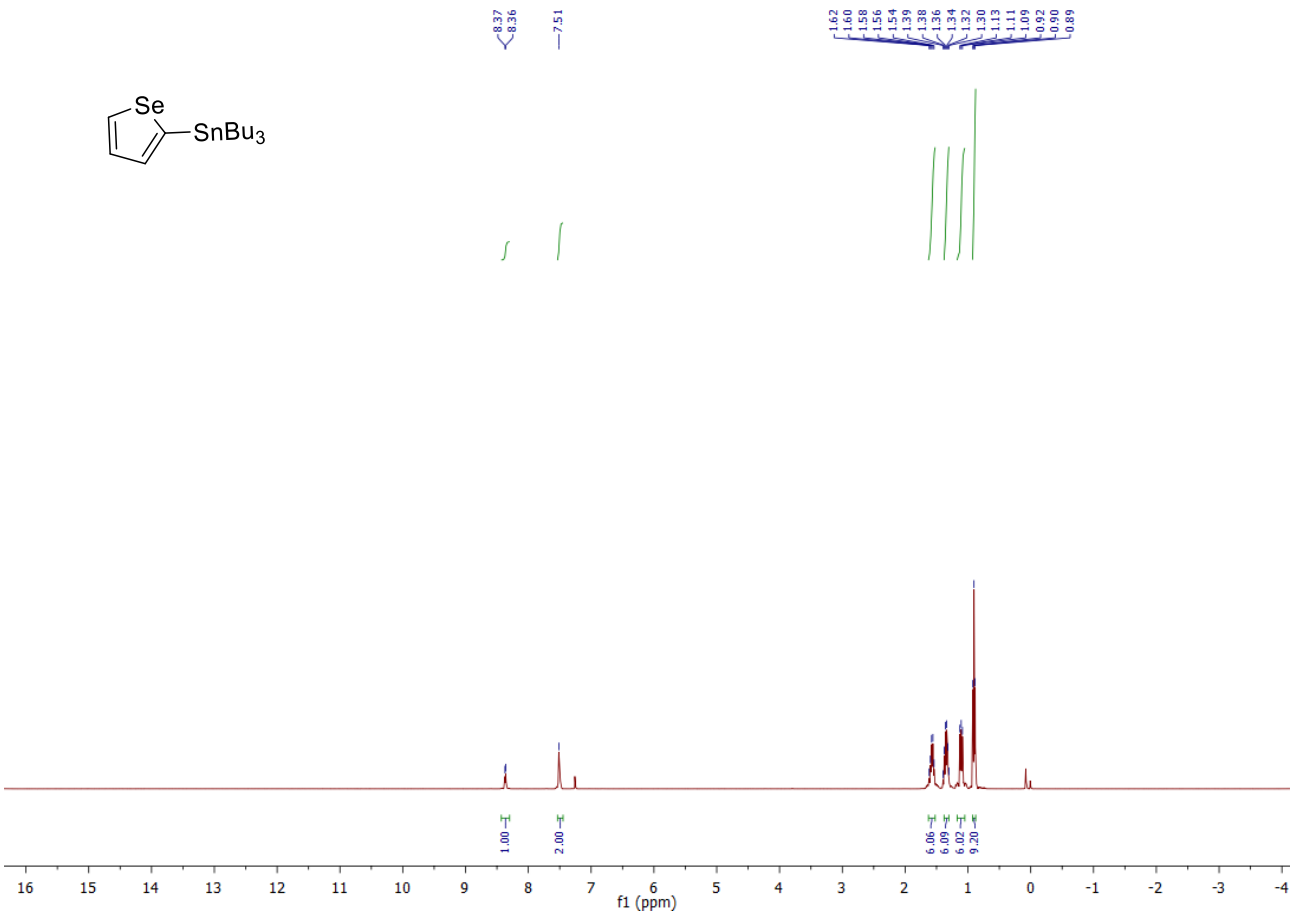

Figure A. 20. ^{1}H NMR spectrum of compound a in $CDCl_3$.

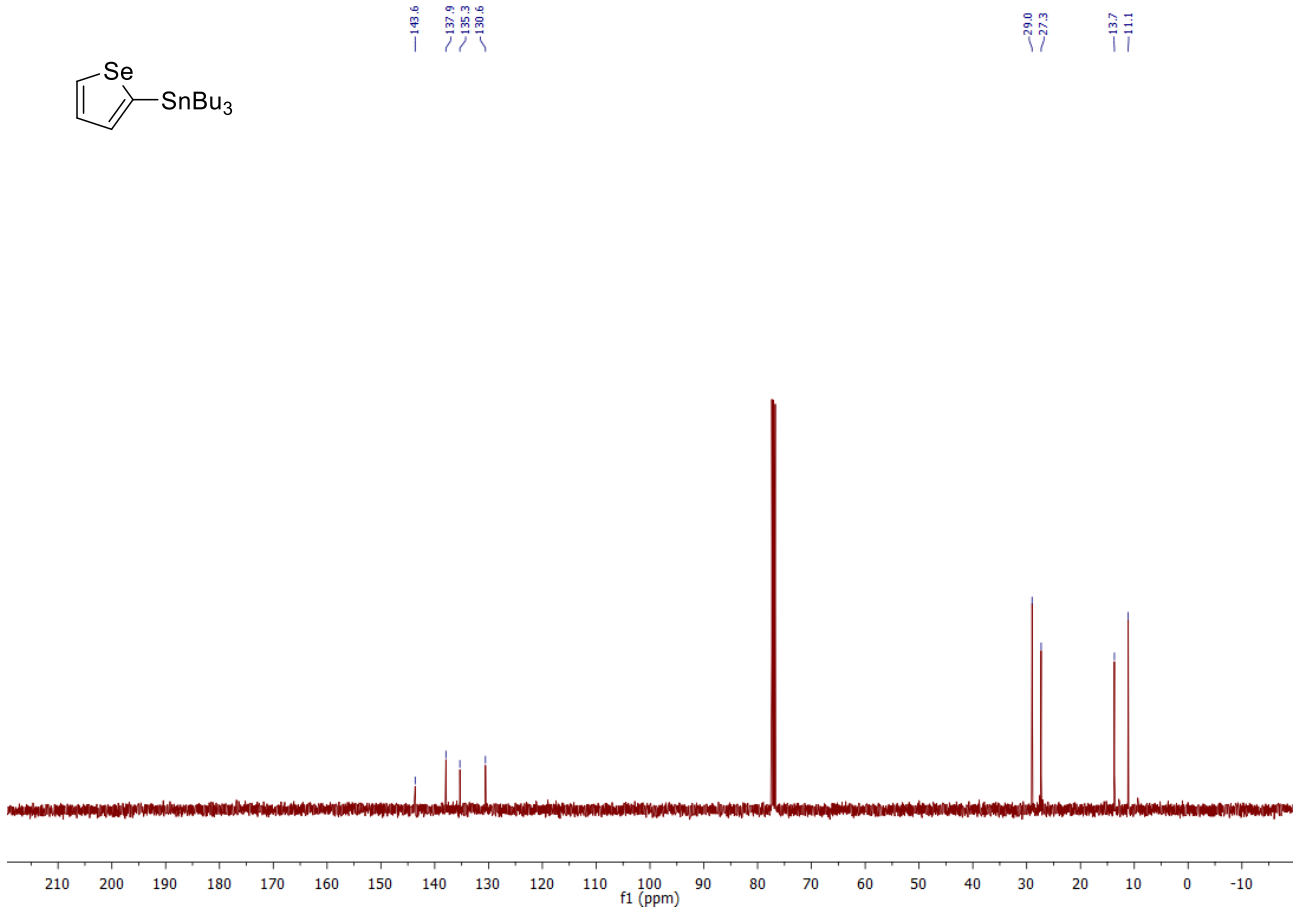

Figure A. 21. ^{13}C NMR spectrum of compound a in $CDCl_3$.

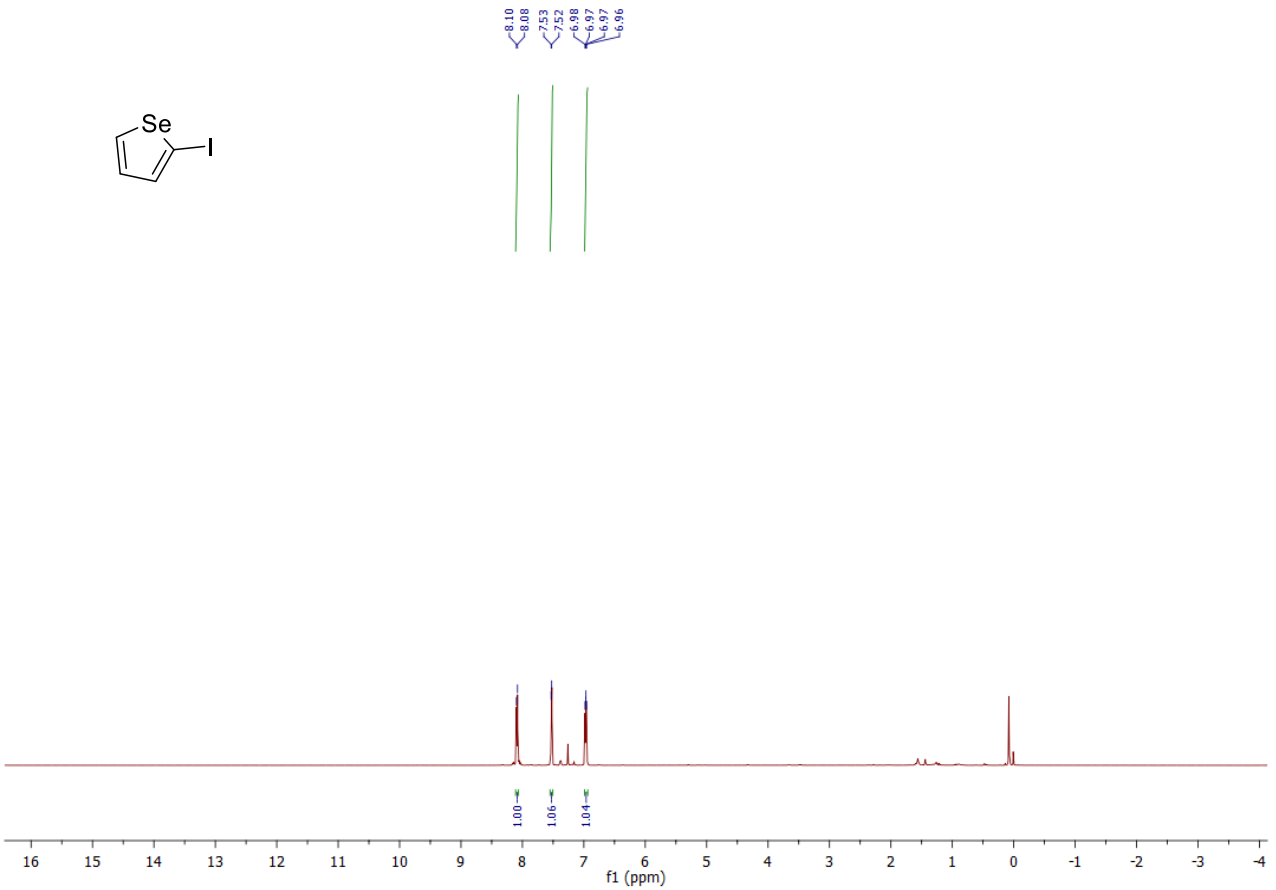

Figure A. 22. ^{1}H NMR spectrum of compound b in $CDCl_3$.

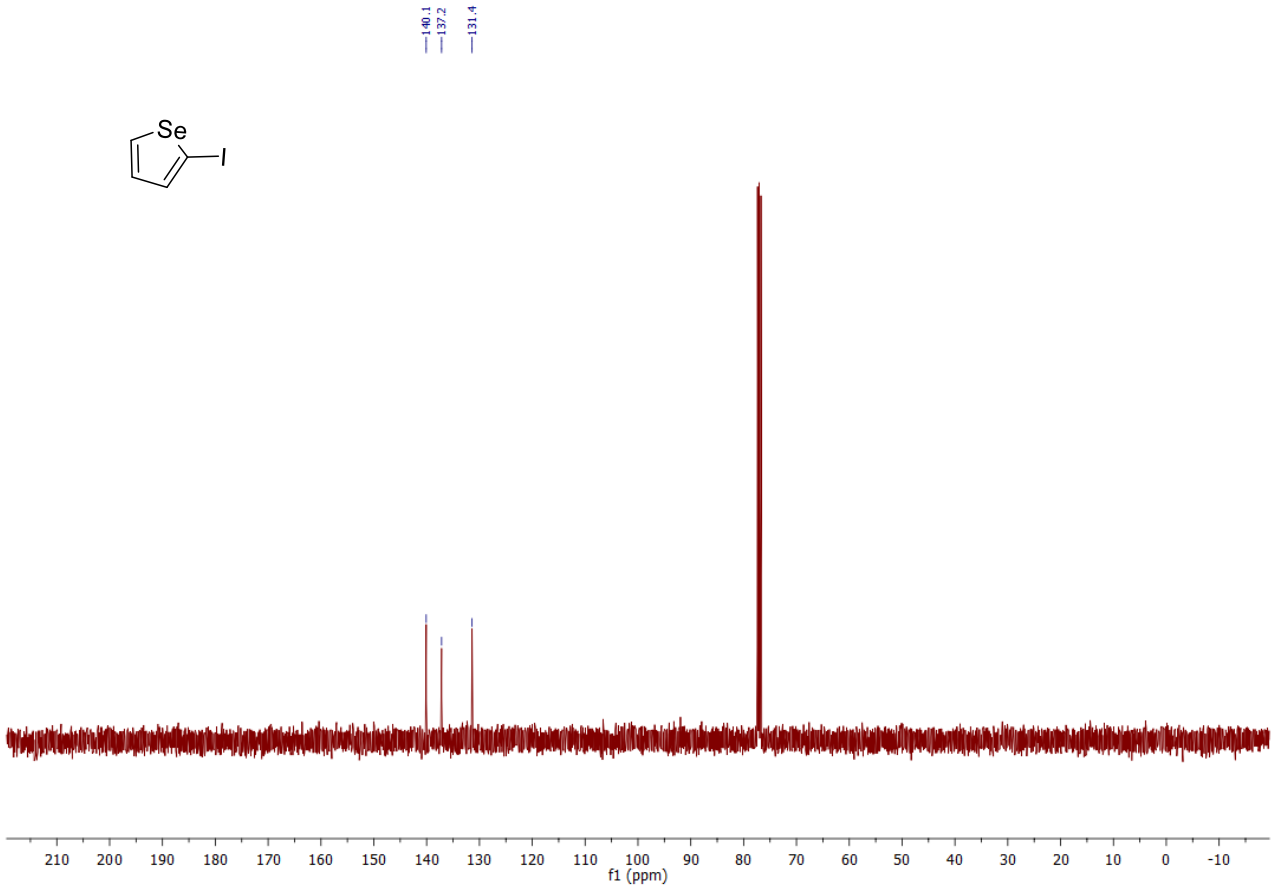

Figure A. 23. ^{13}C NMR spectrum of compound b in $CDCl_3$.

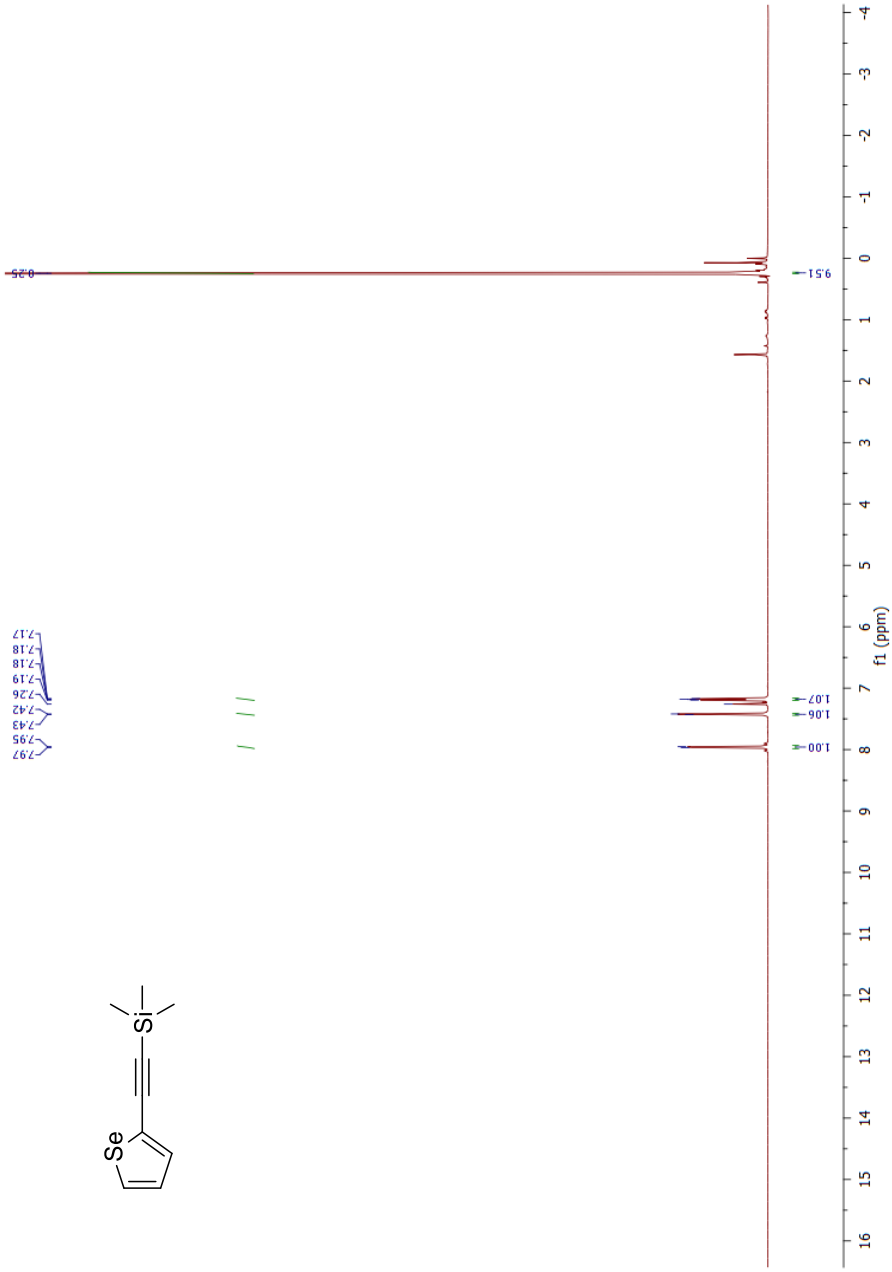

Figure A. 24. ^{1}H NMR spectrum of compound c in $CDCl_3$.

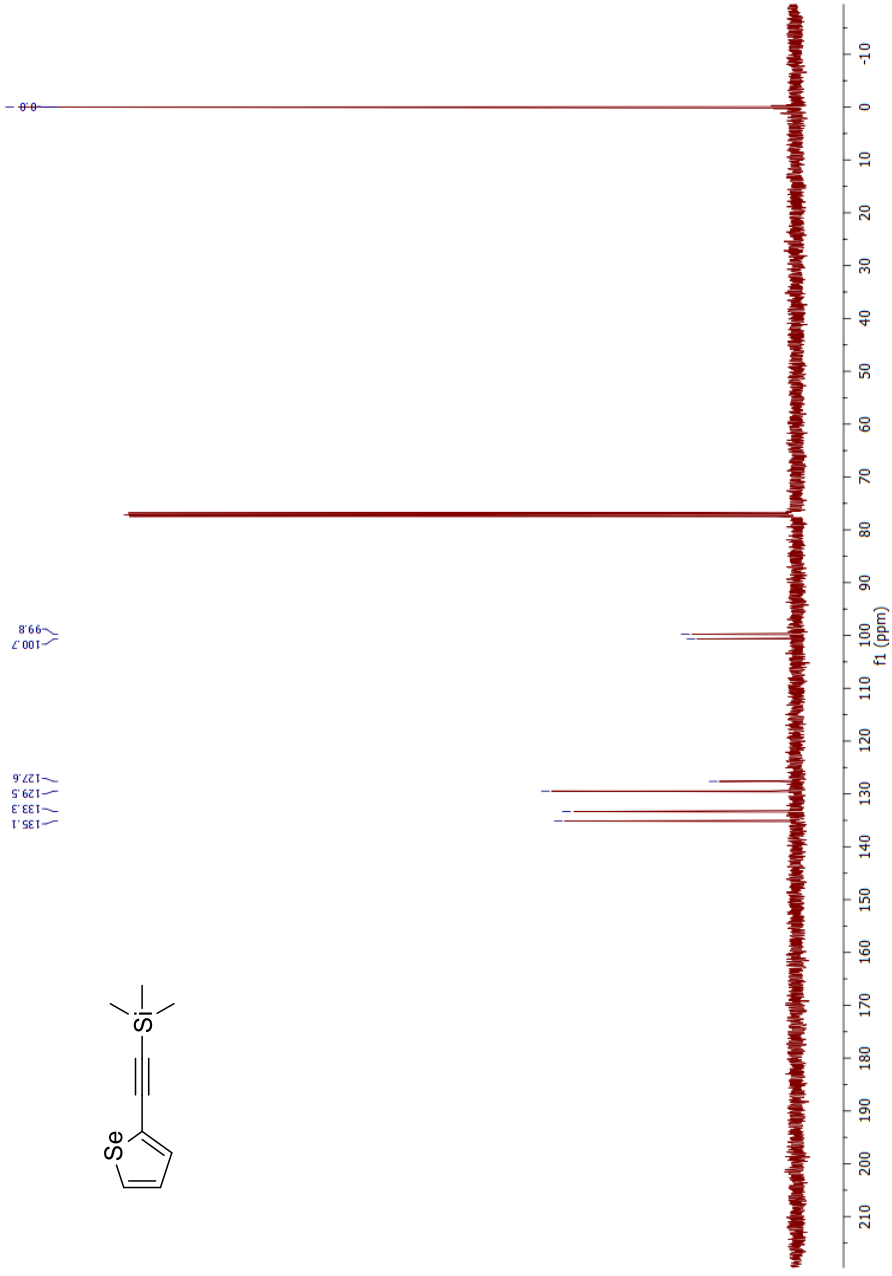

Figure A. 25. ^{13}C NMR spectrum of compound c in $CDCl_3$.

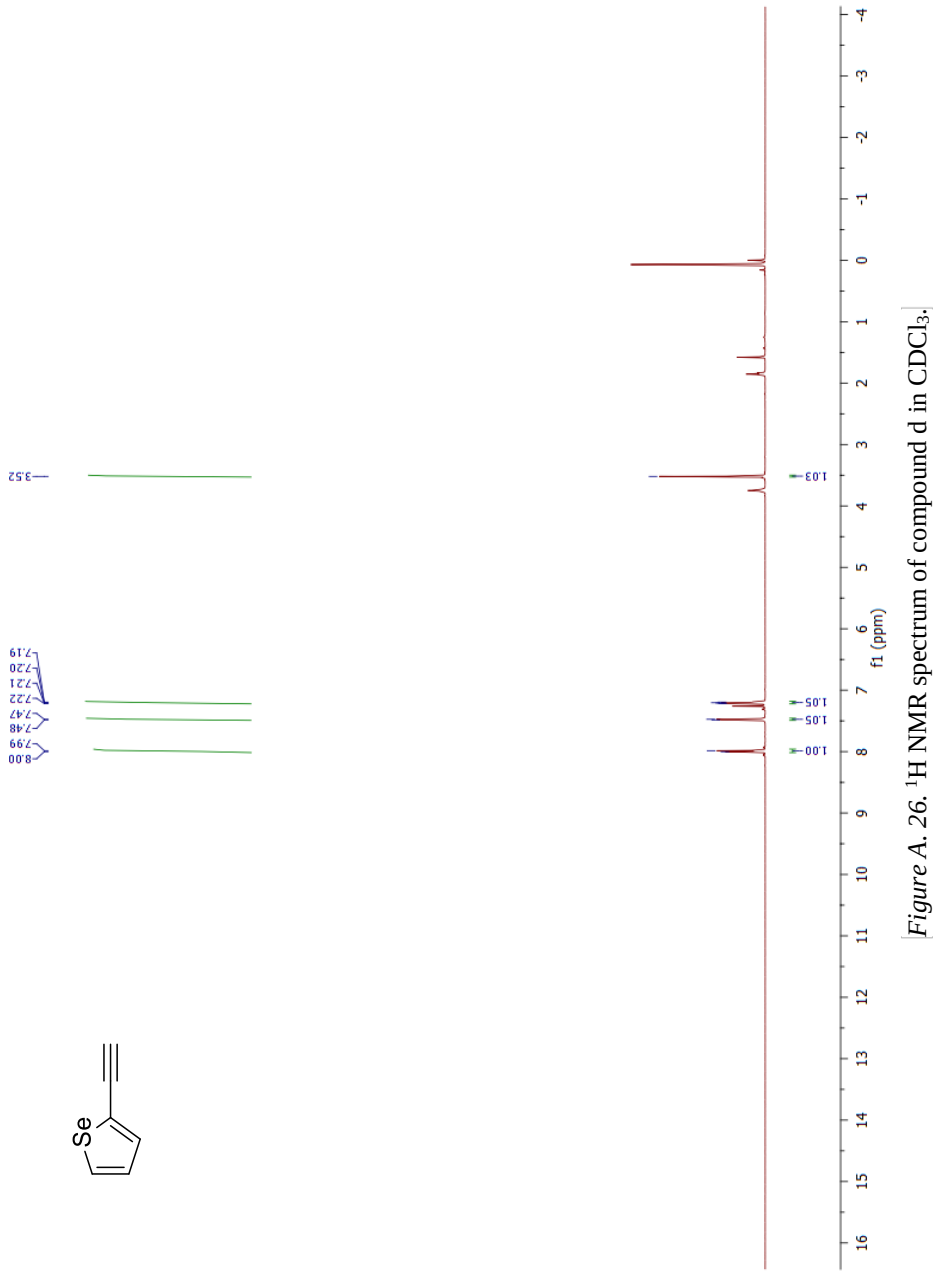

Figure A. 26. ^{1}H NMR spectrum of compound d in $CDCl_3$.

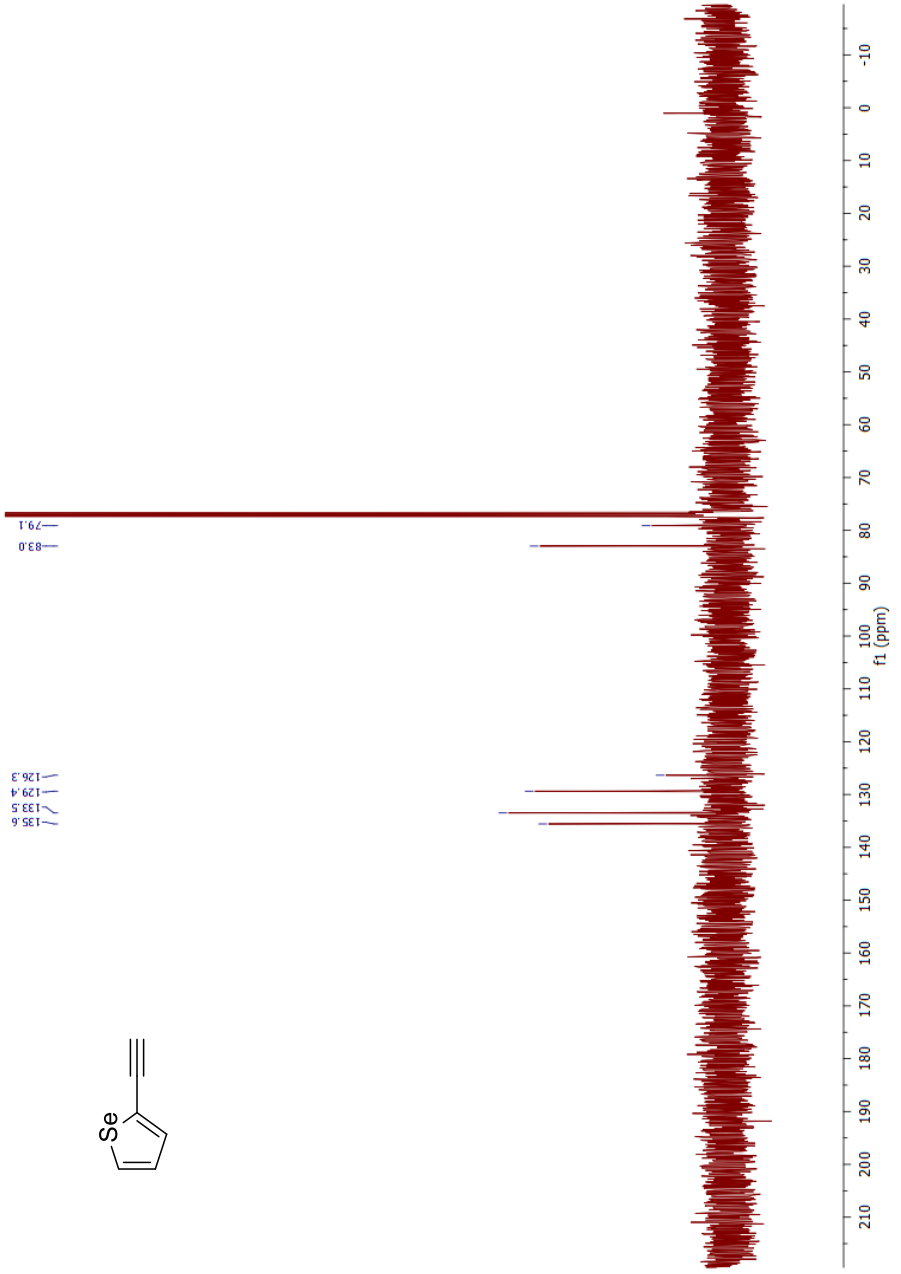

Figure A. 27. ^{13}C NMR spectrum of compound d in $CDCl_3$.

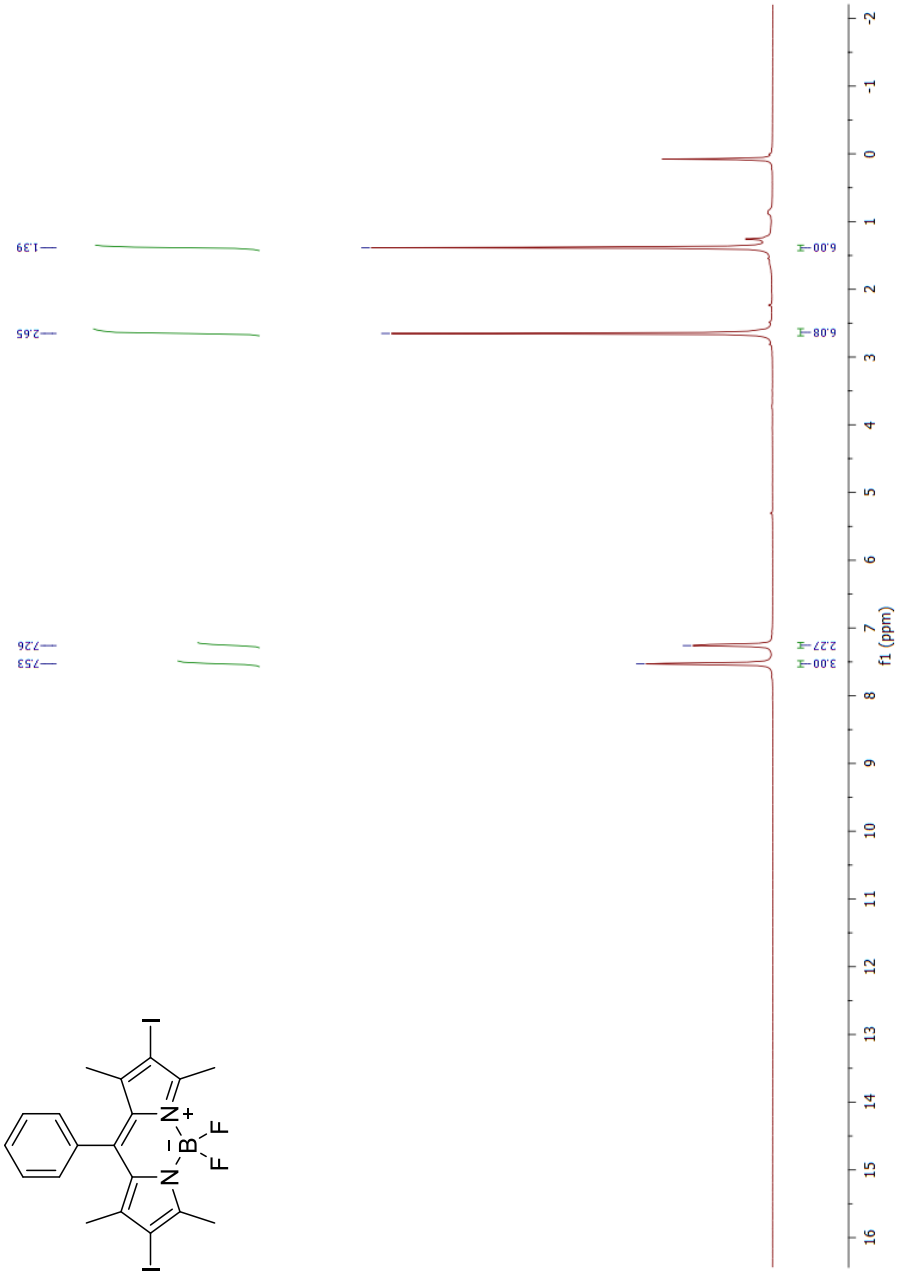

Figure A. 28. ^{1}H NMR spectrum of compound 7 in $CDCl_3$.

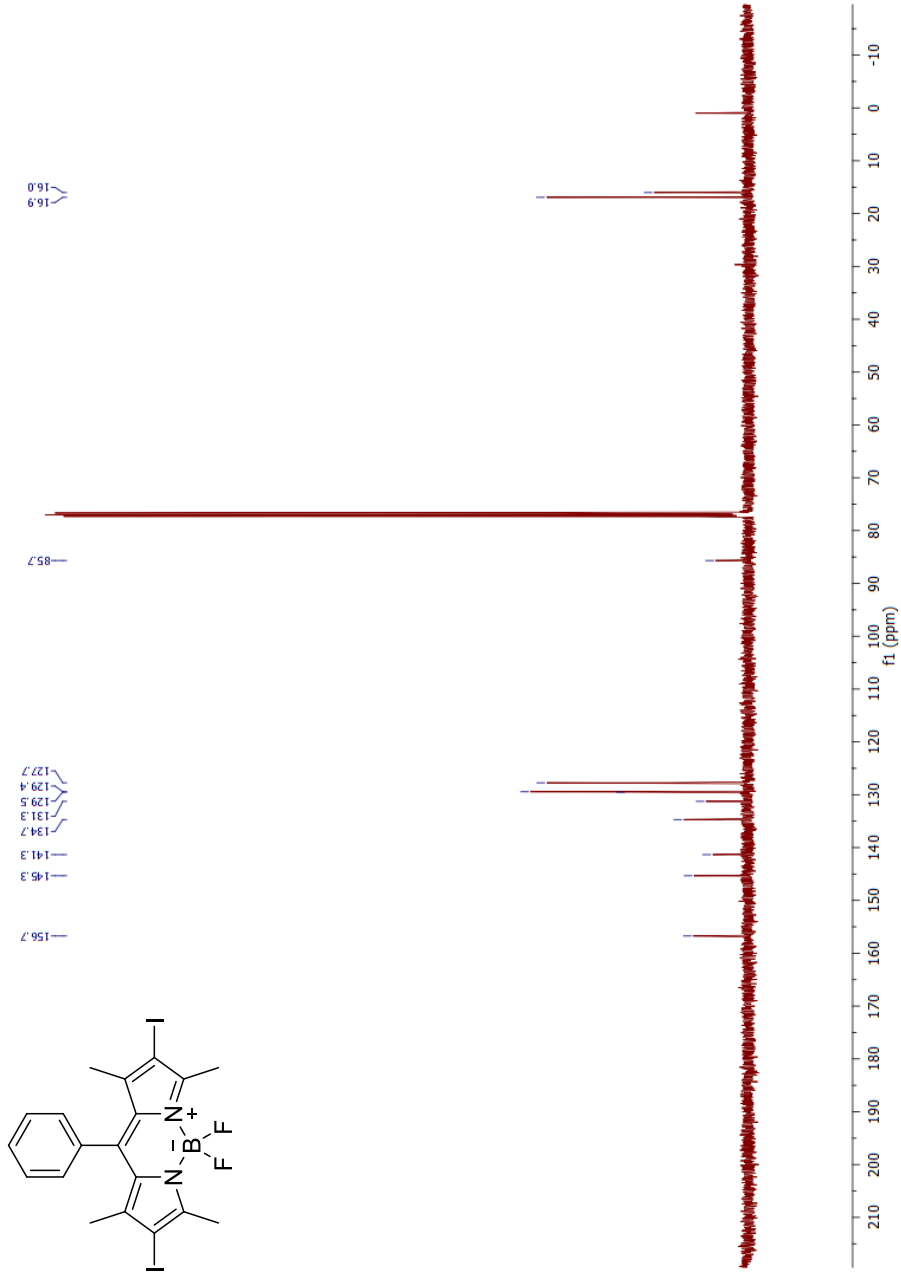

Figure A. 29. ^{13}C NMR spectrum of compound 7 in $CDCl_3$.

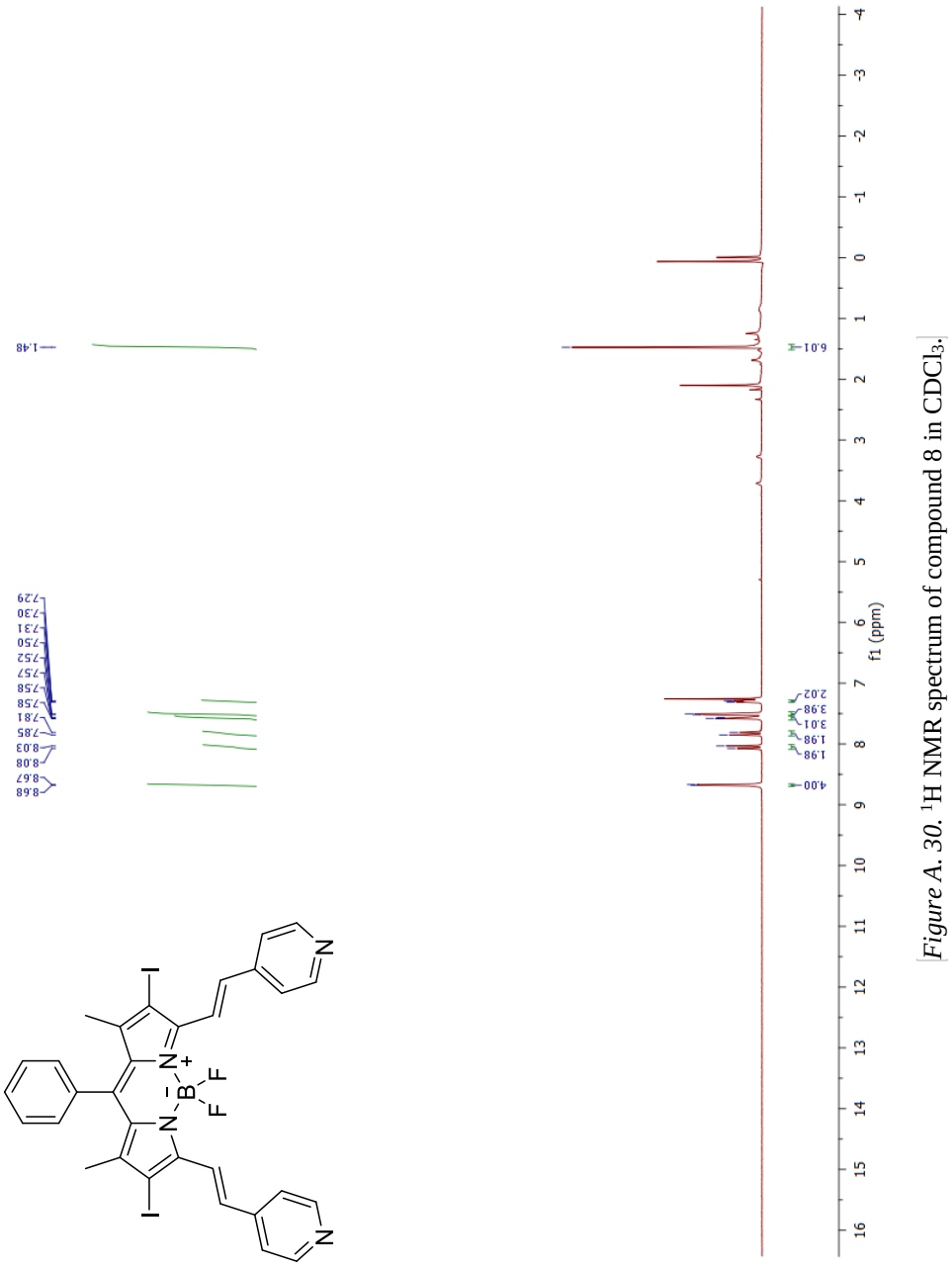

Figure A. 30. ^{1}H NMR spectrum of compound 8 in $CDCl_3$.

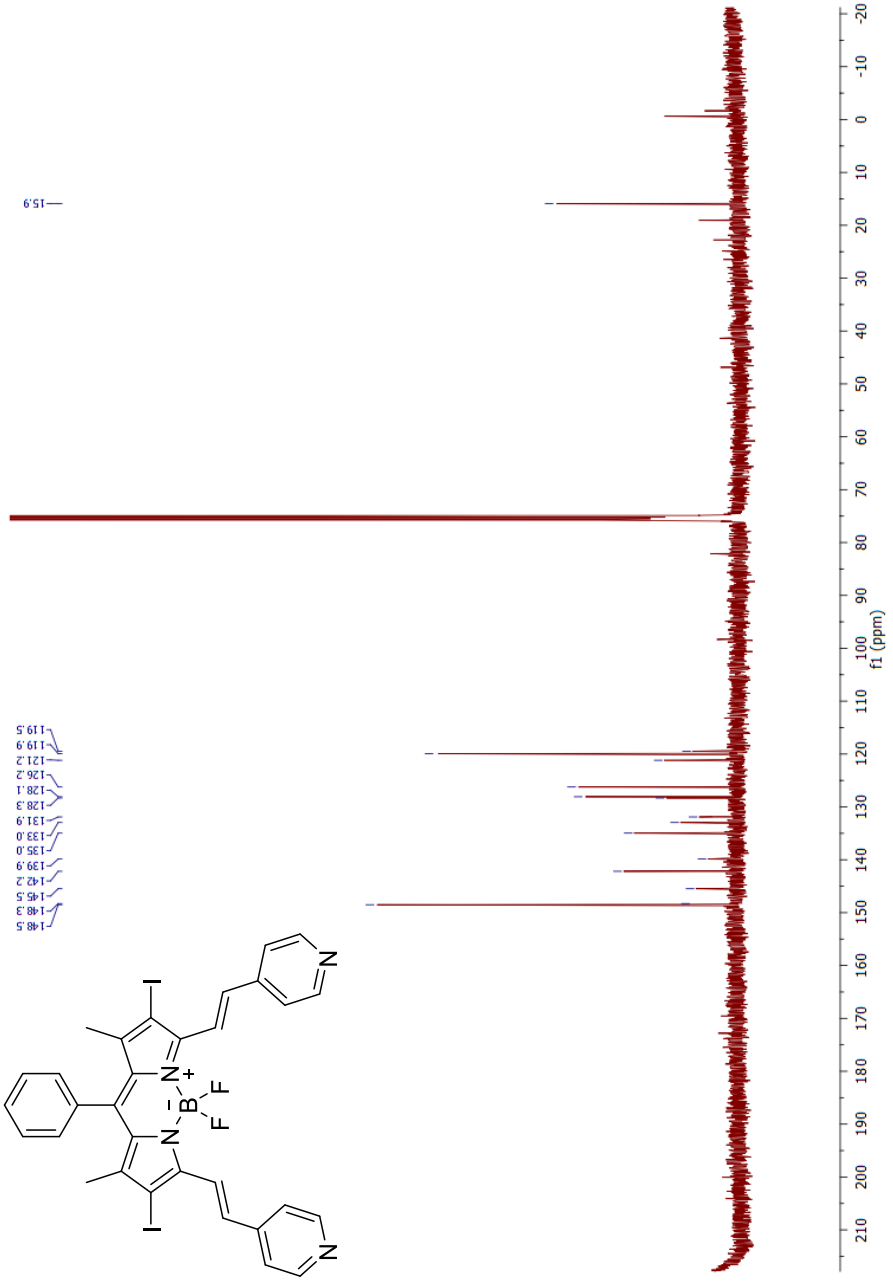

Figure A. 31. ^{13}C NMR spectrum of compound 8 in $CDCl_3$.

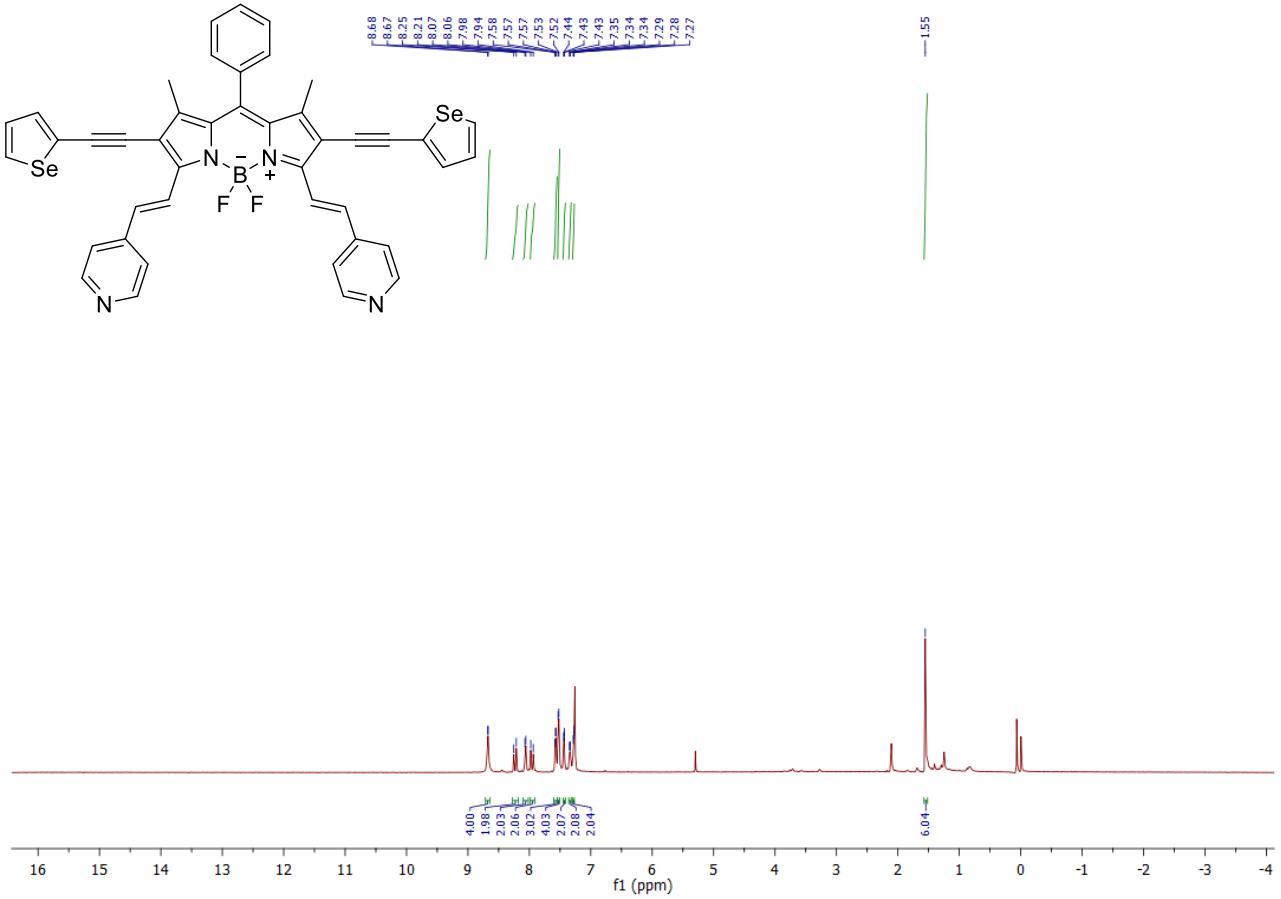

Figure A. 32. ^{1}H NMR spectrum of compound 9 in $CDCl_3$.

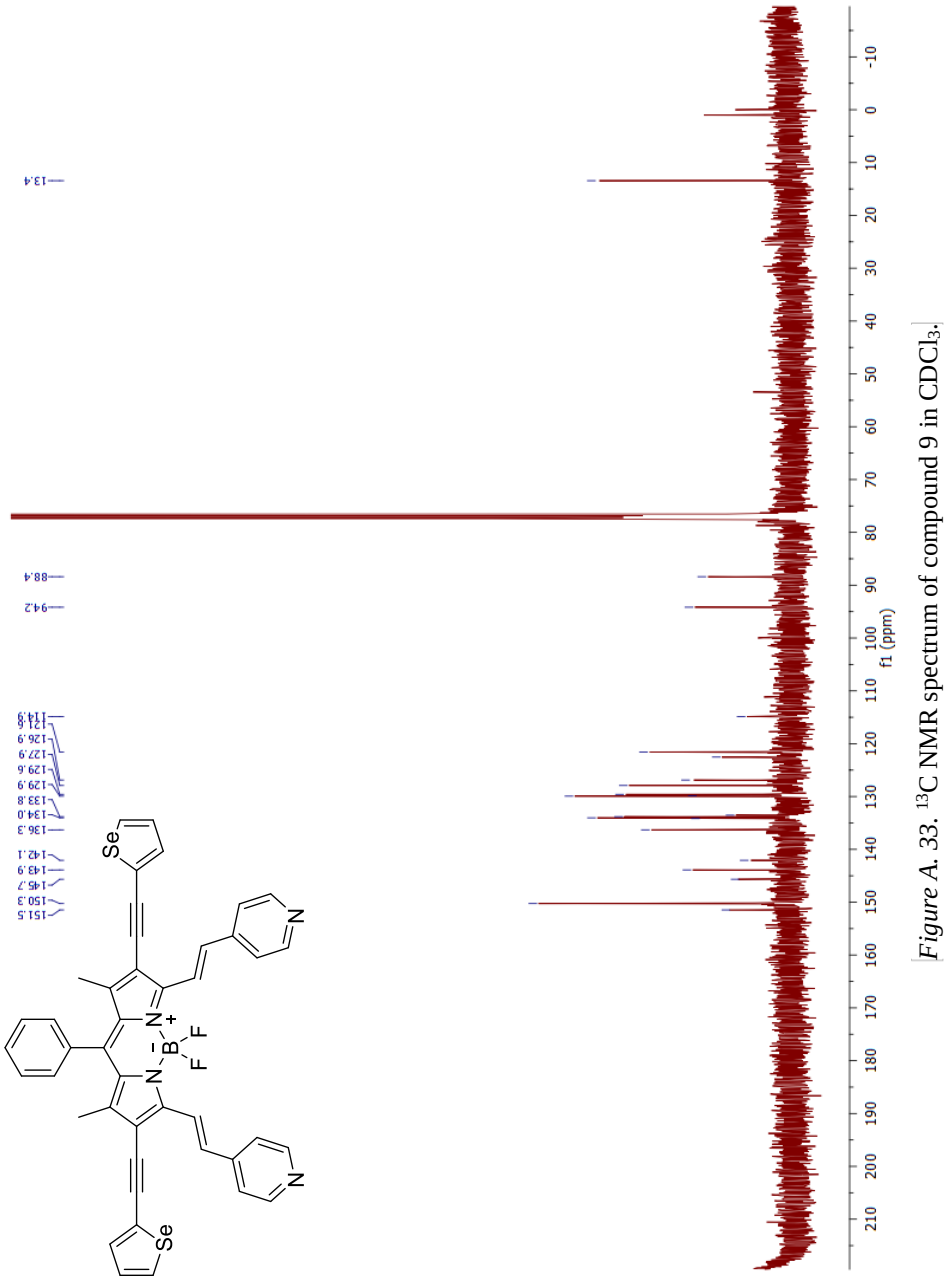

Figure A. 33. ^{13}C NMR spectrum of compound 9 in $CDCl_3$.

B. HRMS SPECTRA

Each compound analyzed by WATERS Synapt G1 High Resolution Mass Spectrometer.

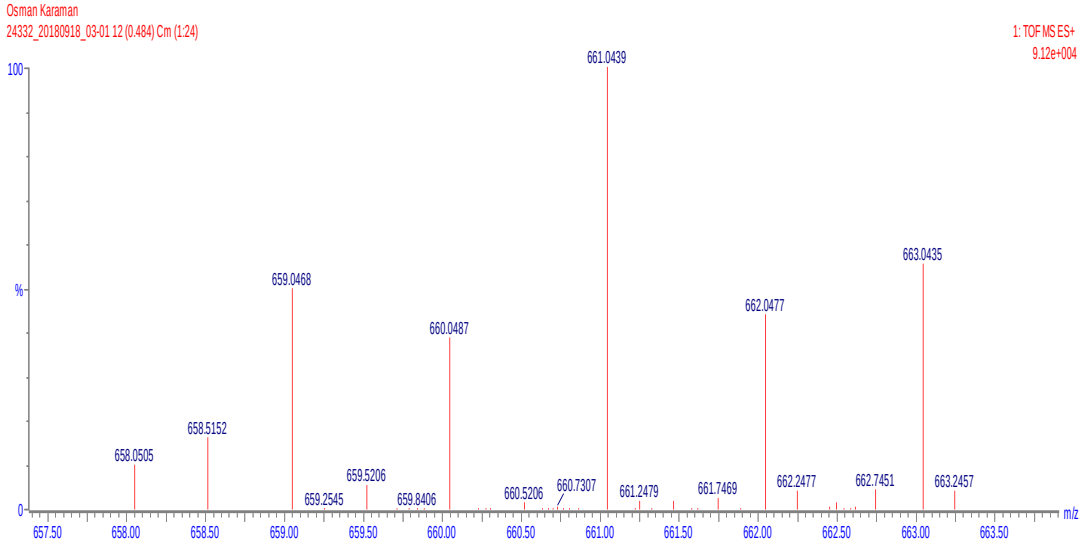

Figure B. 1. HRMS spectrum of compound 3.

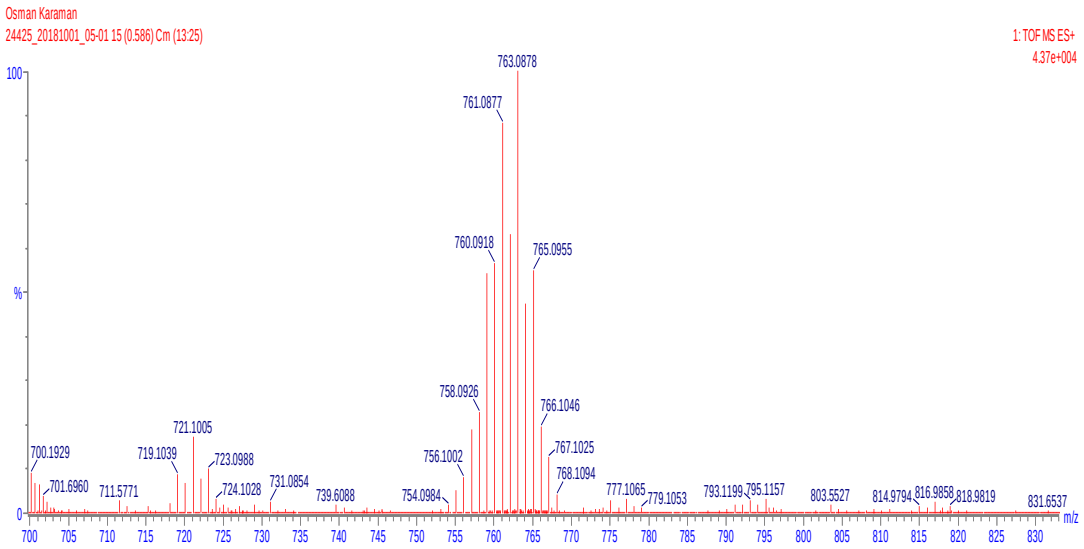

Figure B. 2 HRMS spectrum of compound 4.

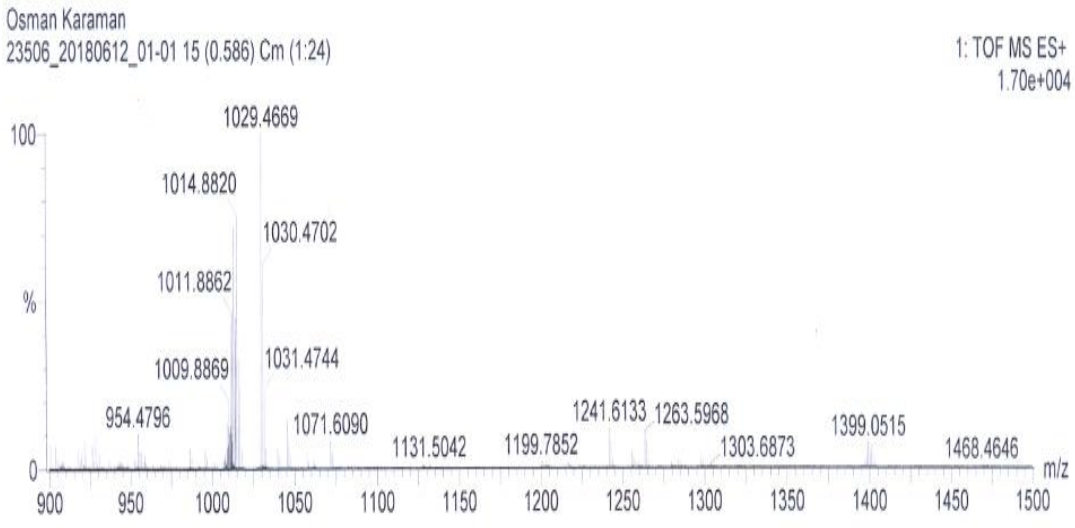

Figure B. 3. HRMS spectrum of compound 5.

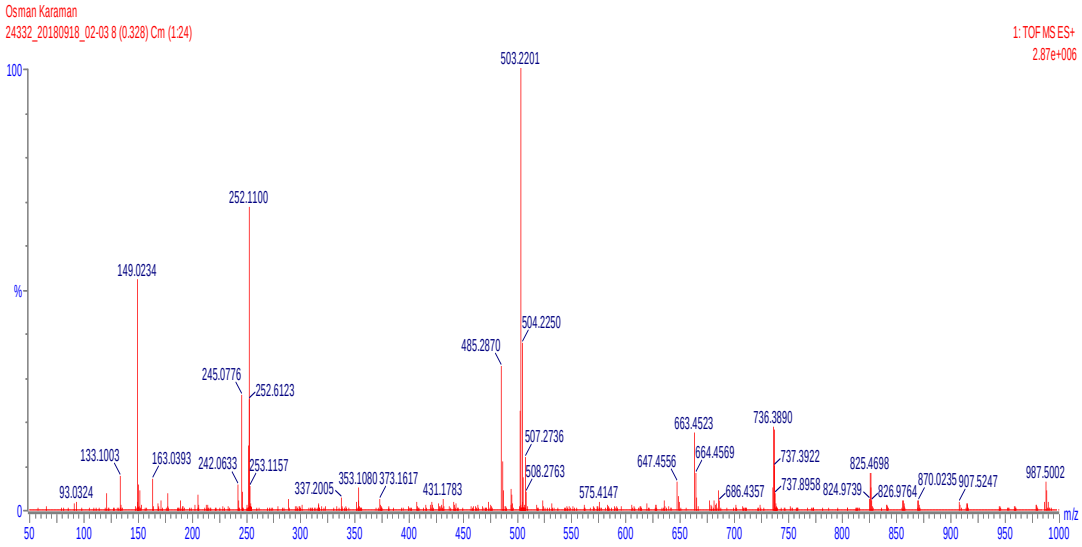

Figure B. 4. HRMS spectrum of compound 6.

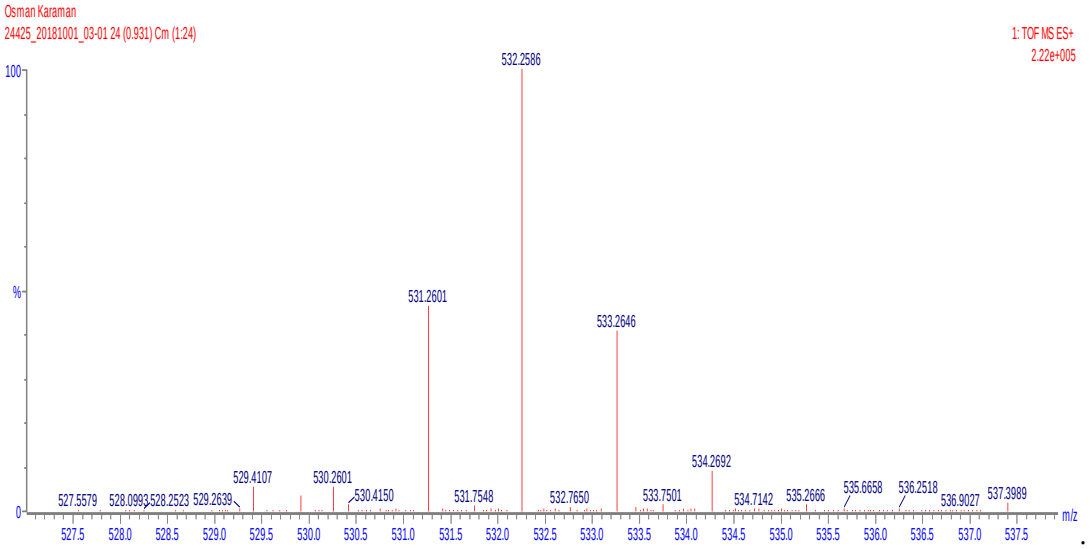

Figure B. 5. HRMS spectrum of compound BOD-H

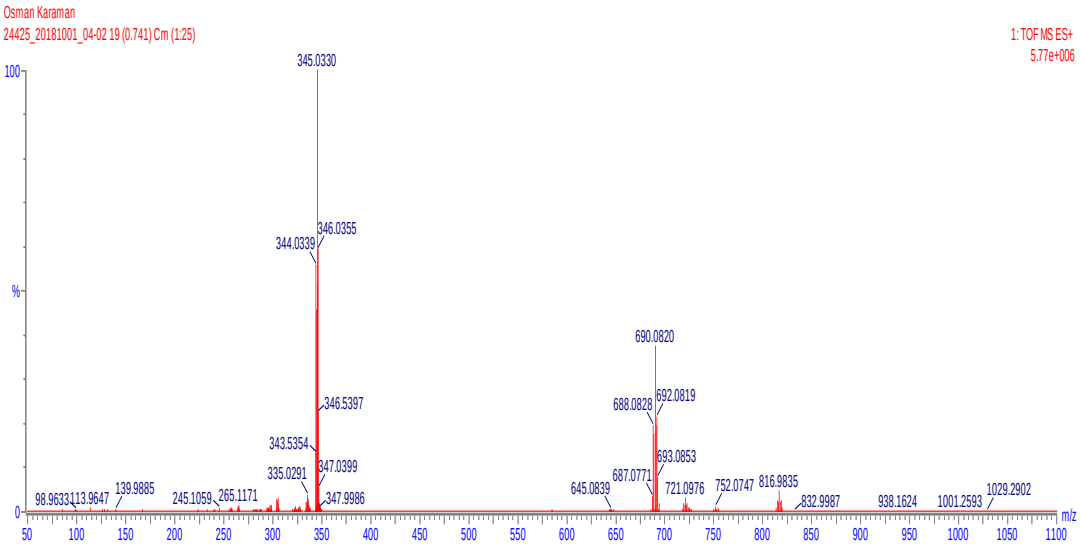

Figure B. 6. HRMS spectrum of compound BOD-Br.

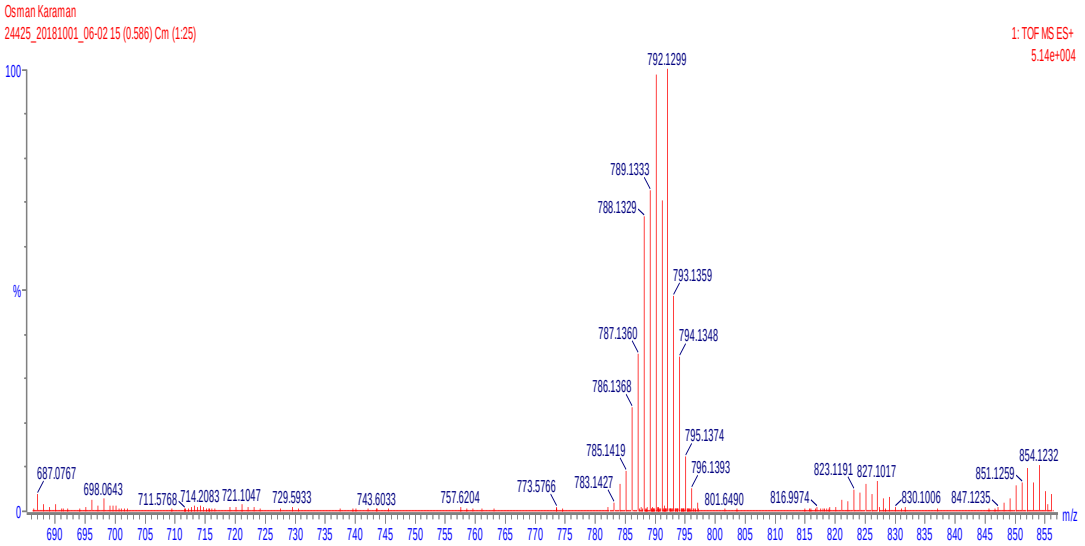

Figure B. 7. HRMS spectrum of compound BOD-Se.

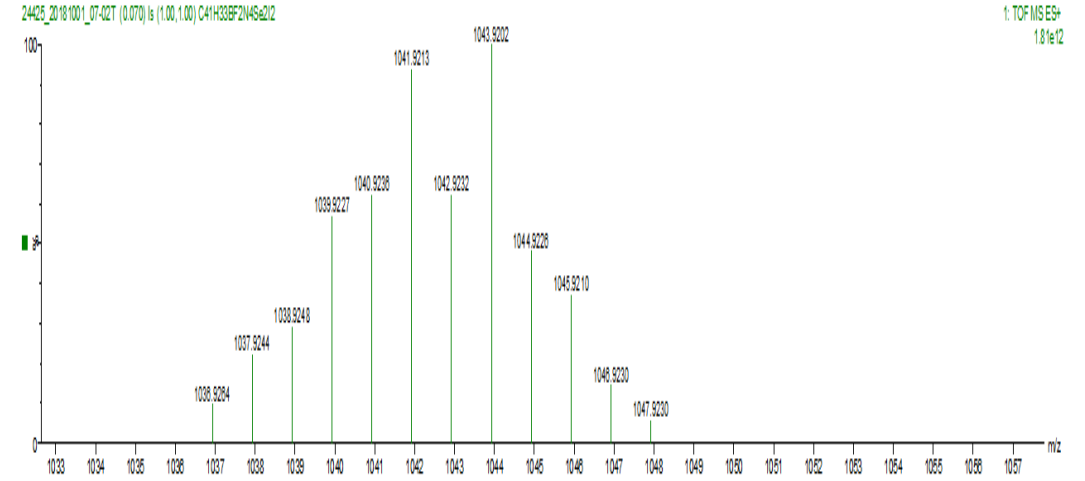

Figure B. 8. HRMS spectrum of compound BOD-Se-I.